

 National Library  
of Canada

Bibliothèque nationale  
du Canada

Canadian Theses Service

Service des thèses canadiennes

Ottawa, Canada  
K1A 0N4

## NOTICE

The quality of this microform is heavily dependent upon the quality of the original thesis submitted for microfilming. Every effort has been made to ensure the highest quality of reproduction possible.

If pages are missing, contact the university which granted the degree.

Some pages may have indistinct print especially if the original pages were typed with a poor typewriter ribbon or if the university sent us an inferior photocopy.

Previously copyrighted materials (journal articles, published tests, etc.) are not filmed.

Reproduction in full or in part of this microform is governed by the Canadian Copyright Act, R.S.C. 1970, c. C-30.

## AVIS

La qualité de cette microforme dépend grandement de la qualité de la thèse soumise au microfilmage. Nous avons tout fait pour assurer une qualité supérieure de reproduction.

S'il manque des pages, veuillez communiquer avec l'université qui a conféré le grade.

La qualité d'impression de certaines pages peut laisser à désirer, surtout si les pages originales ont été dactylographiées à l'aide d'un ruban usé ou si l'université nous a fait parvenir une photocopie de qualité inférieure.

Les documents qui font déjà l'objet d'un droit d'auteur (articles de revue, tests publiés, etc.) ne sont pas microfilmés.

La reproduction, même partielle, de cette microforme est soumise à la Loi canadienne sur le droit d'auteur, SRC 1970, c. C-30.

THE UNIVERSITY OF ALBERTA  
GEOCHEMICAL AND ISOTOPIG STUDIES OF ULTRAMAFIC XENOLITHS FROM  
WEST KETTLE RIVER, SOUTHERN BRITISH COLUMBIA

BY  
XIANYU XUE

A THESIS SUBMITTED TO THE FACULTY OF GRADUATE STUDIES AND RESEARCH  
IN PARTIAL FULFILMENT OF THE REQUIREMENTS FOR THE DEGREE OF

MASTER OF SCIENCE  
DEPARTMENT OF GEOLOGY

EDMONTON, ALBERTA

FALL 1988

Permission has been granted to the National Library of Canada to microfilm this thesis and to lend or sell copies of the film.

The author (copyright owner) has reserved other publication rights, and neither the thesis nor extensive extracts from it may be printed or otherwise reproduced without his/her written permission.

L'autorisation a été accordée à la Bibliothèque nationale du Canada de microfilmer cette thèse et de prêter ou de vendre des exemplaires du film.

L'auteur (titulaire du droit d'auteur) se réserve les autres droits de publication; ni la thèse ni de longs extraits de celle-ci ne doivent être imprimés ou autrement reproduits sans son autorisation écrite.

ISBN 0-315-45753-8

THE UNIVERSITY OF ALBERTA

RELEASE FORM

NAME OF AUTHOR: Xianyu Xue

TITLE OF THESIS: Geochemical and isotopic studies of ultramafic xenoliths from West Kettle River, southern British Columbia.

DEGREE: Master of Science

YEAR THIS DEGREE GRANTED: Fall 1988

Permission is hereby granted to THE UNIVERSITY OF ALBERTA LIBRARY to reproduce single copies of this thesis and to lend or sell such copies for private, scholarly or scientific research purposes only.

The author reserves other publication rights, and neither the thesis nor extensive extracts from it may be printed or otherwise reproduced without the author's written permission.

Xue Xianyu

(Student's signature)

Dept of Geology  
Peking University  
Beijing P.R. China

(Student's permanent address)

Date: October 13, 1988

THE UNIVERSITY OF ALBERTA  
FACULTY OF GRADUATE STUDIES AND RESEARCH

The undersigned certify that they have read, and recommend to the Faculty of Graduate Studies and Research for acceptance, a thesis entitled Geochemical and Isotopic Studies of Ultramafic Xenoliths from West Kettle River, Southern British Columbia submitted by Xianyu Xue in partial fulfilment of the requirements for the degree of Master of Science.

*A. Baadsgaard*

Supervisor

*[Signature]*

*Reidar G. Trønnes*

*Michael [Signature]*

Date *October 6, 1988*

**Dedicated to the memory of Dr. C. M. Scarfe**

---

## Abstract

A systematic geochemical and isotopic study of ultramafic xenoliths from a Pliocene basaltoid flow at West Kettle River, southern British Columbia, has been attempted to increase our understanding of the nature and evolution of the upper mantle beneath this region.

The bulk chemical variations of the West Kettle River Group Iherzolites and harzburgites seem to be largely controlled by partial melting processes. Most of these xenoliths have lower  $\Sigma\text{FeO}$  than xenolith suites from Summit Lake, British Columbia and San Carlos, southwestern U.S.A., possibly a result of less interaction with migrating melts.

Nd and Sr isotopic ratios of the clinopyroxenes in all but one of these Iherzolites and harzburgites (0.51296-0.51335, 0.70223-0.70342) are similar to MORB. The clinopyroxenes in these Iherzolites have Nd model ages of 1.5 to 3.6 Ga and plot close to a reference Nd isochron (with an age of 0.75 Ga and initial  $\epsilon_{\text{Nd}}$  of +6) in the Sm-Nd isotope evolution diagram. These xenoliths were most likely derived from an oceanic lithospheric mantle that was accreted by Terrane I of the Canadian Cordillera in mid-Jurassic. Their Nd model ages and Nd isochron age may reflect global continental crustal formation and overlying oceanic crustal formation, respectively.

Recent mantle metasomatism, possibly caused by migrating silicate melts, is suggested by inter-mineral oxygen isotope disequilibrium in one Iherzolite and low Sm/Nd (< CHUR) of the clinopyroxenes in the harzburgites. Ancient mantle metasomatism is implied by the more enriched  $^{143}\text{Nd}/^{144}\text{Nd}$  (0.51273) of the clinopyroxene in one other Iherzolite. The whole rock Sr isotopes for most xenoliths have been markedly affected by external contamination, most likely ground water contamination. The effect of ground water contamination on the Nd isotopes is minor unless the xenoliths were severely weathered. Very recent mantle metasomatism is suggested by the whole rock Nd isotopes and REE patterns in some of these xenoliths.

The multiple mantle metasomatism may be related to the Miocene to Recent volcanism in this region. Depleted isotopic compositions of the inferred metasomatic agents testify to the involvement of a MORB-like mantle component in their sources.



## Acknowledgements

I wish to express my deep gratitude to late Dr. C. M. Scarfe, my supervisor, for his supervision, encouragement and financial support through most of my study. Sincere thanks are also extended to Dr. H. Baadsgaard, my co-supervisor, whose efforts and enthusiasm were largely responsible for the success of the Sr - Nd isotopic analyses for the ultramafic xenoliths in this study, and who took up the responsibility for the review of this thesis at the final stage. Dr. A. J. Irving is thanked for collaboration in the major and trace element analyses at the Department of Geological Sciences, University of Washington. Dr. K. Muehlenbachs is acknowledged for the oxygen isotope analysis. Dr. P. Cavell, Dr. J. Wijbrans, Mr. W. Day and Mr. A. Stelmach are thanked for their help at various stages of the isotope analyses. Assistance from Mr. D. Tomlinson during the probe analysis is appreciated.

Dr. C. M. Scarfe, D. Canil, D. Sykes, S. Talman are thanked for assistance in the sample collection. Discussions with colleagues, notably, D. Canil, M. Sun, K. Wei and S. Talman have been very helpful and are gratefully acknowledged. D. Canil and M. Sun are also thanked for comments on part of Chapters VI and VIII. Dr. R. G. Tronnes is acknowledged for help during the final thesis preparation.

I would also like to thank my parents and brothers, whose encouragement and love made my study more enjoyable.

Financial support during the study was provided by a scholarship from the Chinese State Commission of Education and the Department of Geology teaching and research assistantships.

## Table of Contents

Chapter	Page
I. Introduction.....	1
II. Geological Setting.....	2
1. Tectonic setting .....	2
2. Host basalt and mantle xenoliths.....	5
III. Sample Descriptions.....	7
IV. Analytical methods.....	10
1. Sample preparation.....	10
2. Major and trace element analyses.....	10
3. Sr and Nd isotope analysis.....	13
4. Oxygen isotope analysis.....	13
V. Major and trace element geochemistry.....	15
1. Host basalt.....	15
2. Major element variation.....	18
3. First-series transition elements.....	22
4. REE abundances.....	26
5. Sr abundances.....	34
VI. Sr and Nd isotope geochemistry.....	36
1. Sr and Nd isotopic results.....	36
2. Problem of inter-mineral isotope equilibrium.....	41
3. Sources of secondary phases.....	42
VII. Oxygen isotope geochemistry.....	47
VIII. Discussion.....	53
1. Chemical variations of the upper mantle beneath West Kettle River.....	53
2. Evolution of the upper mantle beneath West Kettle River.....	52
3. Constraints on the source characteristics of volcanism in south-central	

British Columbia.....	69
IX. Summary and Conclusions.....	74
1. Mineralogical and chemical heterogeneity of the upper mantle.....	74
2. Timing of mantle depletion and enrichment.....	74
3. Evolution of the upper mantle and magmatism in south-central British Columbia.....	75
X. Bibliography.....	77
XI. Appendix I: Sample preparation.....	85
1. Whole rock powders.....	85
2. Clinopyroxenes.....	86
3. Basalt powder.....	86
XII. Appendix II: Procedures for major and trace element analyses with ICAP-AES.....	88
1. Major element analysis.....	88
2. Trace element analysis (excluding REE and Y).....	88
3. REE and Y analysis.....	90
XIII. Appendix III: Procedures for Rb-Sr and Sm-Nd isotope analyses.....	92
1. Sample decomposition.....	92
2. Ion-exchange separation.....	93
3. Mass spectrometry.....	95
4. Reagents and blanks.....	95
XIV. Appendix IV: Microprobe analyses of xenolith minerals.....	99

## List of Tables

Table	Page
1. Modal compositions of ultramafic xenoliths from West Kettle River .....	8
2. Chemical composition and normative mineralogy of West Kettle River host basaltoids .....	16
3. Trace element data for West Kettle River host basaltoids .....	17
4. Bulk chemical analysis for ultramafic xenoliths from West Kettle River .....	19
5. Trace element (excluding REE and Y) data for ultramafic xenoliths from West Kettle River.....	24
6. REE and Y concentrations in whole rock ultramafic xenoliths from West Kettle River.....	27
7. Mass balance calculations for Sr, Nd and Sm in ultramafic xenoliths from West Kettle River.....	31
8. Nd and Sr isotopic compositions of the whole rock ultramafic xenoliths and host basalt from West Kettle River .....	37
9. Nd and Sr isotopic compositions of the clinopyroxenes and olivines in ultramafic xenoliths from West Kettle River .....	38
10. Sr partition coefficients calculated for ultramafic xenoliths from south-central British Columbia .....	43
11. Oxygen isotope data for ultramafic xenoliths from West Kettle River .....	48
12. Compositions of the fertile West Kettle River lherzolites compared to those estimated for the primitive upper mantle in the literature .....	54
13. Mantle source compositions calculated from the compositions of the West Kettle River xenoliths and various melts, assuming a batch melting model.....	57
14. Nd and Sr model ages for ultramafic xenoliths from West Kettle River .....	63
15. $^{87}\text{Sr}/^{86}\text{Sr}$ measurements of N.B.S. SRM 987 strontium standard .....	96

16.  $^{143}\text{Nd}/^{144}\text{Nd}$  measurements of La Jolla neodymium standard ..... 96

17. Sm, Nd and Sr total blanks ..... 98

18. Reagent blanks ..... 98

19. Repeated probe analyses of standard diopside ..... 99

20. Probe data for West Kettle River ultramafic xenolith minerals ..... 100

## List of Figures

Figure	Page
1. Five geologic and physiographic belts in the Canadian Cordillera .....	3
2. Distribution of late Miocene to Recent volcanics and ultramafic xenolith occurrences in the Canadian Cordillera .....	4
3. Comparison of REE data obtained by ICAP-AES with those by INAA and replications of the ICAP-AES results .....	12
4. Bulk concentrations of various oxides plotted versus bulk Mg/(Mg+Fe) of the West Kettle River ultramafic xenoliths.....	20
5. Bulk concentrations of various oxides plotted versus bulk MgO of the West Kettle River ultramafic xenoliths.....	21
6. Transition element and Ca abundances, normalized to the estimated primitive upper mantle values, for West Kettle River ultramafic xenoliths and host basanitoid.....	25
7. Chondrite-normalized REE abundances in ultramafic xenoliths and host basanitoid from West Kettle River.....	28
8. Chondrite-normalized Yb, La, La/Yb versus CaO and Y versus Yb for the bulk lherzolites and harzburgites from West Kettle River.....	29
9. Mass balance for Sr, Nd and Sm in ultramafic xenoliths from West Kettle River.....	32
10. Sr versus CaO for bulk lherzolites and harzburgites from West Kettle River .....	35
11. Nd - Sr isotope diagram for clinopyroxenes and whole rocks of ultramafic xenoliths and host basanitoid from West Kettle River.....	39
12. Comparison of the $^{143}\text{Nd}/^{144}\text{Nd}$ , Sm/Nd, $^{87}\text{Sr}/^{86}\text{Sr}$ and Sr/Nd ratios between the whole rocks and clinopyroxenes for ultramafic xenoliths from West Kettle River.....	40

13. Comparison of $\delta^{18}\text{O}$ data for West Kettle River ultramafic xenoliths with the range of the reported $\delta^{18}\text{O}$ values for continental alkalic basalt-hosted ultramafic xenoliths worldwide.....	49
14. Plot of $\delta^{18}\text{O}_{\text{ol}}$ (‰ SMOW) versus $\delta^{18}\text{O}_{\text{cpx}}$ (‰ SMOW), $\delta^{18}\text{O}_{\text{ol}}$ (‰ SMOW) versus $\delta^{18}\text{O}_{\text{opx}}$ (‰ SMOW) and $\delta^{18}\text{O}_{\text{cpx}}$ (‰ SMOW) versus $\delta^{18}\text{O}_{\text{opx}}$ (‰ SMOW), for ultramafic xenoliths from West Kettle River.....	51
15. Plot of clinopyroxene-olivine $\delta^{18}\text{O}$ fractionation ( $10^3 \ln \alpha_{\text{cpx-ol}}$ ) as a function of temperature for ultramafic xenoliths from West Kettle River.....	52
16. Total Fe as FeO versus MgO for Group I peridotites from West Kettle River, in comparison with those from Summit Lake, Tariat Depression, San Carlos and Alligator Lake.....	55
17. Ca/Al (wt.) versus bulk Mg/(Mg+Fe) for ultramafic xenoliths from West Kettle River.....	60
18. Variations of CaO and Al <sub>2</sub> O <sub>3</sub> concentrations as a function of temperature (or degrees of partial melting) for the melts produced from melting of peridotites at 10 Kb and 20 Kb.....	61
19. Sm-Nd evolution diagram for clinopyroxenes and whole rocks of ultramafic xenoliths from West Kettle River.....	64
20. Total Fe as FeO of whole rocks and constituent minerals versus bulk MgO for ultramafic xenoliths from West Kettle River.....	65
21. Nd-Sr isotope diagram for clinopyroxenes and whole rocks of ultramafic xenoliths from south-central British Columbia.....	72
22. Nd-Sr isotope diagram for ultramafic xenolith clinopyroxenes and Miocene to Recent volcanics from south-central British Columbia.....	73
23. Relationship between sample weight and SiO <sub>2</sub> content for trace element analysis with ICAP-AES.....	89

## I. Introduction

Ultramafic xenoliths hosted by alkaline basalts and kimberlites, widely accepted as fragments of the upper mantle, are among the limited types of occurrence of mantle rocks at the Earth's surface (Frey, 1984). Petrological, geochemical, isotopic and experimental studies of these rocks have yielded direct information on the details of the constitution and processes in the upper mantle (BVSP, 1981). Their wide occurrence in a variety of tectonic settings enable characterization of the upper mantle both in individual localities and on a global scale. The intimate spatial and temporal relationships between these mantle xenoliths and the mantle-derived melts also present an opportunity to study the melt generation processes and their source characteristics (eg., Hawkesworth et al., 1983; Menzies, 1983).

This thesis reports major and trace element concentrations along with Nd, Sr and O isotopic ratios of ultramafic xenoliths from a Pliocene basaltic flow at West Kettle River, southern British Columbia. Previous petrographic and mineral chemical studies of the West Kettle River mantle xenoliths (Fujii and Scarfe, 1982a; Ross, 1983) have yielded important information on the constitution and geotherm of the upper mantle beneath this area. However, a systematic geochemical and isotopic investigation of these xenoliths is lacking, but is essential in understanding the chemical structure and evolution of the upper mantle (Sun, 1985).

This project was an extension of the earlier petrographic and mineral chemical work (Fujii and Scarfe, 1982a), and was aimed at better understanding of the composition and processes of the upper mantle beneath West Kettle River. Information resulting from this study also bears on the tectonic evolution of the Canadian Cordillera and constrains the source characteristics of the Miocene to Recent volcanism in south-central British Columbia.

---



## II. Geological Setting

### 1. Tectonic setting

West Kettle River (49°47'N, 119°4'W) is located near the boundary between the Omineca Crystalline Belt and the Intermontane Belt in southern British Columbia (Fig. 1). The Omineca Crystalline Belt is mainly composed of highly deformed and variably metamorphosed (to high grade) mid-Proterozoic to mid-Paleozoic miogeoclinal sedimentary rocks, and Paleozoic and lower Mesozoic volcanogenic and pelitic rocks, with local occurrence of Precambrian crystalline basement. The Intermontane Belt is made up largely of upper Paleozoic to mid-Mesozoic marine volcanic and sedimentary rocks and mid-Mesozoic to upper Tertiary marine and nonmarine sedimentary and volcanic rocks, which were deformed at various times from early Mesozoic to Neogene, and were cut by comagmatic intrusions (Coney et al., 1980; Monger et al., 1982).

The tectonic history of this region is characterized by accretion of Terrane I, one of the two super terranes in the Canadian Cordillera, during the mid-Mesozoic. The Intermontane Belt constitutes the bulk of Terrane I oceanic crust. The Omineca Crystalline Belt represents a tectonic welt from the collision of Terrane I with the North American continent (Monger et al., 1982). It is uncertain how much of the mantle portion of the oceanic lithosphere has been attached to the overlying crust in Terrane I and accreted to the North American continent (Smith, 1986). Following the terrane accretion, the processes associated with subduction and accretion continued into mid-Tertiary time.

The tectonic situation from Miocene to the present has been very constant and is dominated by interaction of the North American continent with the Pacific plates and the Juan de Fuca and Explorer plates (Fig. 2) (Souther, 1977). Extensional tectonic environments dominate the region of the Omineca Crystalline Belt and the Intermontane Belt (Souther, 1977). An upflow in the mantle is inferred beneath this region (Gough, 1986). The Juan de Fuca and Explorer plates are deduced to have been subducting under the Vancouver Island (Riddihough and Hyndman, 1976; Milne et al., 1978), but the subducted plate appears to be thin and loses its identity before it reaches the Intermontane Belt (Gough, 1986).

The volcanics from the Miocene to the late Pliocene in this region are featured by

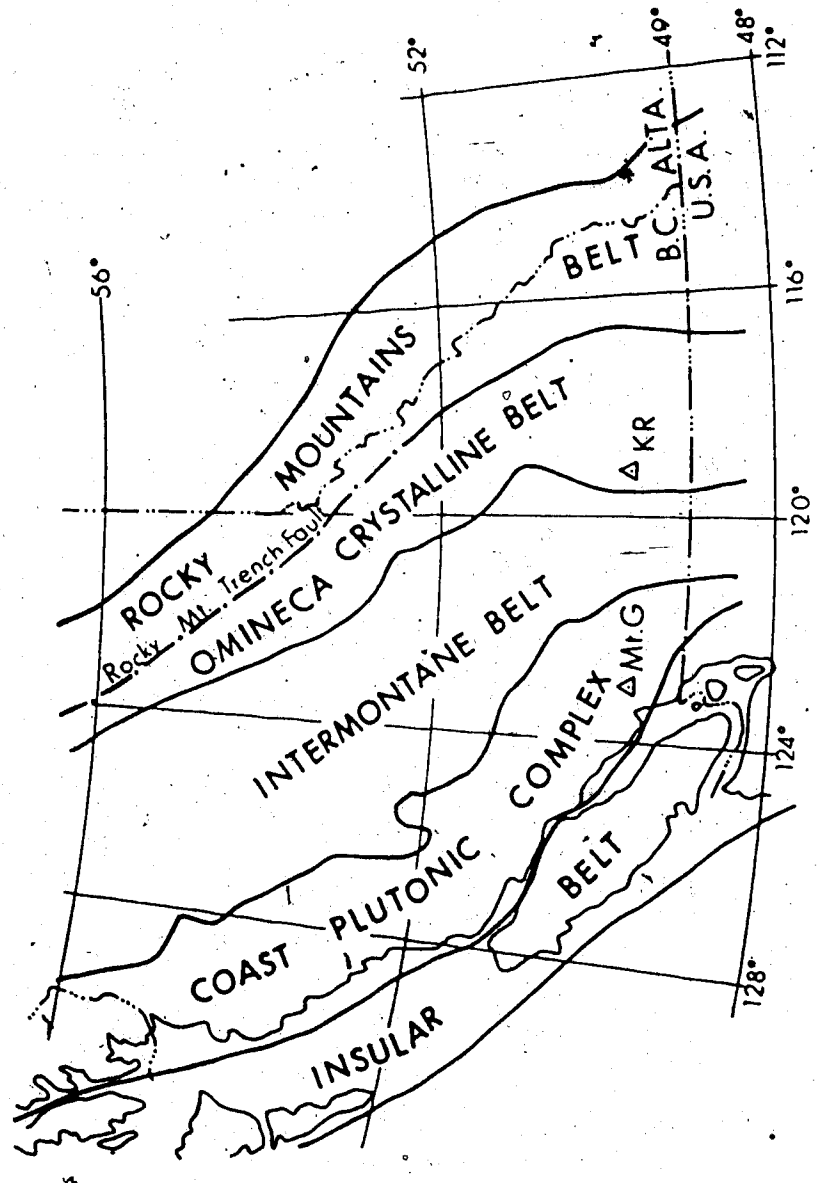


Fig. 1. Five geologic and physiographic belts in the Canadian Cordillera (adapted from Gough, 1986).

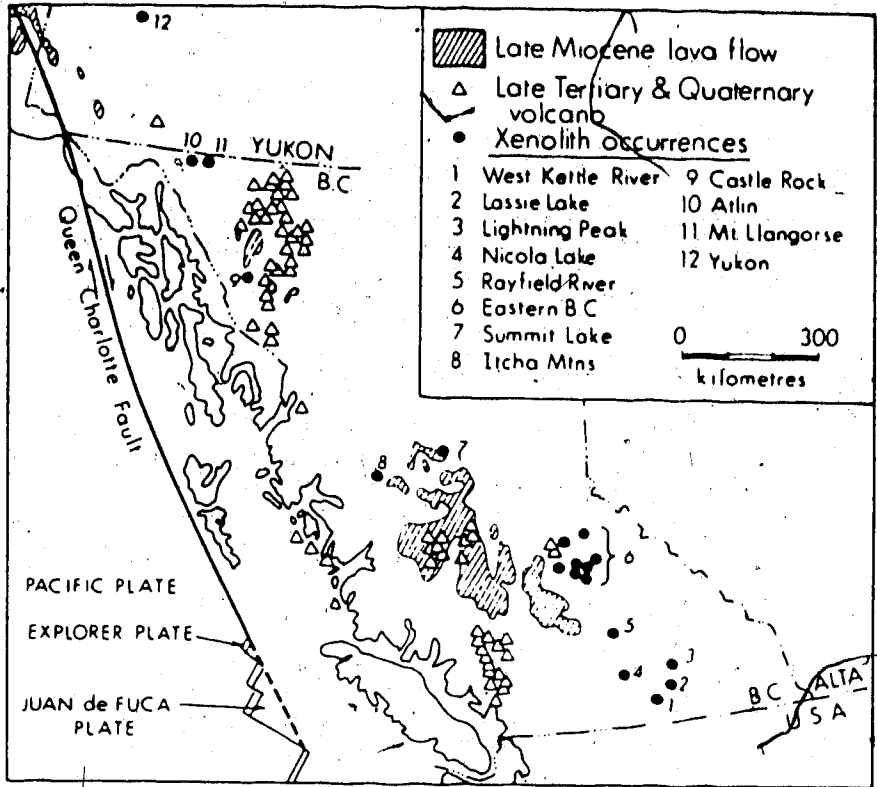


Fig. 2. Late Miocene to Recent volcanics distributions and ultramafic xenolith occurrences in the Canadian Cordillera (compiled from Souther, 1977; Canil et al., 1987).

eruption of large quantities of plateau basalts (Fig. 2) (Bevier, 1983). Late Pliocene and Quaternary volcanic activities are mainly sporadic eruptions of highly varied lavas from many central vents (Fig. 2), most of which belong to the alkaline olivine suite (Souther, 1977, Nicholls et al., 1982).

Many of these late Pliocene and Quaternary volcanic flows and cones, including the West Kettle River lava, contain xenoliths of ultramafic rocks, gabbro, granite and granulite, and xenocrysts of plagioclase, augite and hypersthene (eg. Nicholls et al., 1982; Fujii and Scarfe, 1982a). All of these xenolith localities occur along a northwest-trending belt (Fig. 2), which parallels a thinning of the lithosphere beneath southern British Columbia (Nicholls et al., 1982).

## 2. Host basalt and mantle xenoliths

The K-Ar dates of the West Kettle River basalts fall in the range 2.5-5 Ma (Ross, 1983). There are four lava flows stacked concordantly and separated by rubbly horizons about 10 cm thick. No weathering surfaces were detected, indicating the lack of a significant time lag between each flow. The first three flows are each approximately 2 m thick and belong to calc-alkaline series subalkaline basalts (Sun, 1985). The top flow has a thickness of 11 m and possesses well developed columnar joints. The average width of the columns is 50 cm. This flow is a basanitoid (nomenclature of Macdonald and Katsura, 1964) (Fujii and Scarfe, 1982a) and is the only one that contains mantle xenoliths.

The host basalt is fine-grained and contains euhedral olivine phenocrysts (10%) and euhedral or anhedral clinopyroxene phenocrysts (2%) in an intergranular groundmass of plagioclase, clinopyroxene, olivine and titanomagnetite (Fujii and Scarfe, 1982a). Xenocrysts of olivine, orthopyroxene and clinopyroxene are also present, some of which may represent disaggregated ultramafic xenoliths. The megacrysts are mostly augite and are of small size (< 3 cm).

Xenoliths are concentrated in the lower middle portion of the host lava flow and constitute about 0.5 % (by volume) of the flow (Fujii and Scarfe, 1982a). They are mostly subangular and range from 1-20 cm in diameter, with an average of 5 cm. The xenolith population includes both gabbroic and granitic rocks of crustal origin and ultramafic rocks of mantle origin. Both Cr-diopside-bearing Group I and augite-bearing Group II ultramafic xenoliths (see nomenclatures of Frey and Prinz,

1978; Wilshire and Shervais, 1975) are present. The Group I xenoliths dominate the xenolith population and include spinel lherzolite (76%), websterite, olivine websterite (19%) and dunite, harzburgite (5%) (Fujii and Scarfe, 1982a). The textures of these xenoliths are typically protogranular, but some are porphyroclastic or equilgranular. Heterogeneous Group I xenoliths characterized by patches or bands of websterites or olivine websterites in host dunites or lherzolites are common. The Group II xenoliths comprise wehrilite and clinopyroxenite, which sometimes occur as bands in Group I lherzolites. Hydrous mineral-bearing ultramafic xenoliths are absent from this locality.

### III. Sample descriptions

Nine Group I xenoliths from West Kettle River were selected for determination of major and trace element concentrations as well as Sr and Nd isotopic compositions. These xenoliths range from 10 - 20 cm in diameter. Modal compositions of these xenoliths are listed in Table 1.

The six lherzolites (KR-35, KR-141, KR-4001, KR-4002, KR-4003, KR-4005 and KR-4016) are very similar in modes and textures. They contain 10-15% clinopyroxene, 20-35% orthopyroxene, 50-65% olivine and 1-3% spinel (Table 1) and all exhibit coarse-grained, protogranular texture with some triple point junctions. Olivine and orthopyroxene grains are approximately 2 mm and contain well-developed kink bands. Clinopyroxenes are slightly smaller (1-2 mm). Red-brown spinels occur either interstitially or within other minerals. Reaction with host basalts is common at the contact between the xenoliths and the host basalts. Glassy veins containing plagioclase and olivine microlites were observed in lherzolite KR-4005. This possibly results from penetration by the host basalt, or incipient melting of the xenoliths on heating by the host basalt. Lherzolite KR-4003 is distinct in its abundant fluid inclusions, which cut through the grain boundaries. Similar fluid inclusions, though also present, are far less abundant in the other lherzolites.

The two harzburgites (KR-4000, KR-37) contain 70% olivine, 25% orthopyroxene, 3-5% clinopyroxene and 2-3% spinel (Table 1). They are both coarse-grained with 3 - 5 mm olivine and orthopyroxene grains and 0.1 - 1 mm clinopyroxene and red-brown spinel grains. Spinels occur either interstitially or as inclusions in other minerals. Well-developed kink bands were observed in the olivine and orthopyroxene grains. The textures for both harzburgites are xenomorphic-protogranular with some triple junctions.

The olivine websterite (KR-3020B) is a portion of a composite Type I xenolith and has a sharp contact with the host lherzolite (KR-3020). It is composed of coarse-grained clinopyroxene and orthopyroxene (1 - 4 mm) and smaller grains of olivine and spinel (0.1 - 2 mm). The texture of this sample is protogranular and some of the olivines are kinked. The spinels occur as interstitial crystals or inclusions in pyroxenes. The host lherzolite (KR-3020) was not analyzed for its bulk chemical and

Table 1. Modal compositions of ultramafic xenoliths from West Kettle River.

Sample No.	Type	Name	Method <sup>†</sup>	Modal Mineralogy			
				Oi	Opx	Cpx	Sp
KR-35	I	Spinel Lherzolite	1	55	25	15	5
			2	61.0	25.3	12.3	3.7
KR-37	I	Spinel Harzburgite	1	70	23	5	2
			2	70.3	24.2	4.4	1.1
KR-141	I	Spinel Lherzolite	1	55	28	15	2
			2	56.3	30.2	11.4	2.0
KR-4000	I	Spinel Harzburgite	1	70	25	3	2
			3			2.4	
KR-4001	I	Spinel Lherzolite	1	60	25	13	2
			3			12.4	
KR-4002	I	Spinel Lherzolite	1	65	20	13	2
			3			14.9	
KR-4003	I	Spinel Lherzolite	1	55	28	15	2
			3			14.9	
KR-4005	I	Spinel Lherzolite	1	55	27	15	3
			2	48.3	33.9	14.4	2.5
KR-4016	I	Spinel Lherzolite	1	55	30	13	2
			2	53.2	32.0	11.7	1.4
KR-3020B	I	Spinel Olivine Websterite	1	10	47	35	8
			2	9.2	42.4	39.4	8.8
KR-3003	I	Spinel Lherzolite	1	30	43	6	1
KR-3017	I	Spinel Lherzolite	1	60	30	8	2

<sup>†</sup> Methods 1: Visual estimations from thin sections. Errors are about  $\pm 2-3\%$  for spinels, clinopyroxenes and  $\pm 5-10\%$  for olivines, orthopyroxenes;

2: Mass balance calculations based on major element analysis ( $\text{SiO}_2$ , CaO,  $\text{Al}_2\text{O}_3$ , MgO). Errors are  $< \pm 1\%$  for clinopyroxenes, spinels and  $\pm 2-3\%$  for olivines, clinopyroxenes;

3: Calculated clinopyroxene modes from the CaO contents and the relationship:  $\text{Cpx} = -0.825 + 4.6433 \text{ CaO}$ , obtained from the xenoliths with mass balance calculation data. These results reasonably agree with the visual estimations.

Modes from method 2, when available, are employed in later calculations; Otherwise those from method 1 are to be used.

Sr, Nd isotope compositions. It is similarly coarse-grained as the olivine websterite (KR-3020B) and has a protogranular texture containing kinked olivines. This lherzolite has an uneven mineral distribution and grades into dunite at the contact with the olivine websterite (KR-3020B).

Two other lherzolites (KR-3003, KR-3017) were selected for the determination of oxygen isotopes in their constituent minerals only. They are both coarse-grained and have a protogranular texture with kink bands in olivines. Their modal compositions are listed in Table 1.

Except for sample KR-37, all these xenoliths are very fresh. Sample KR-37 was chosen to test the weathering effect on mantle xenoliths. It is fragile, with a yellow surface on the olivine grains and white-yellowish veinlets pervading grain boundaries and fracture surfaces. Although very fresh, the rest of the samples also contain a small amount of similar white-yellowish veinlets along fracture surfaces, and in case of KR-4000, along the grain boundaries too.



#### IV. Analytical Methods

##### 1. Sample preparation

Whole rock xenolith samples were separated from the core of the xenoliths and any fractured and weathered surfaces removed. The samples were cleaned in distilled (or Nanopure) water and ultrapure acetone and reduced in a Plattner steel mortar to essentially monomineralic sizes. After split, ten to twenty grams of sample was laid out, further reduced in the steel mortar to pass 40 mesh and then finely ground in an agate mortar.

Clinopyroxene separates used for Sr and Nd isotope analyses were preconcentrated using a Franz magnetic separator and picked under a binocular microscope two to three times. The minerals were then cleaned ultrasonically in 2.5 N HCl for 20 minutes, rinsed with distilled water and dried. Following two more examinations, these minerals were reduced to pass 80 mesh and reexamined twice. Finally, they were cleaned with 2.5 N HCl again for 10 minutes, rinsed with distilled water and dried, and then finely ground in an agate mortar. The clinopyroxenes are believed to be at least 99.95% pure.

Olivine, orthopyroxene and clinopyroxene separates for oxygen isotope analysis were prepared similarly, but were not subjected to acid leaching. Because of its resistance to reaction, olivine was washed in alcohol following the grinding. Only the fine portion suspended in alcohol was used for oxygen isotope analysis.

The host basalt sample was ground in a shatterbox of a tungsten carbide mill.

Detailed description of the sample preparation procedures is given in Appendix I.

##### 2. Major and trace element analyses

Major and trace elements were determined by inductively-coupled argon plasma atomic-emission spectrometry (ICAP-AES) at the Department of Geological Sciences, University of Washington.

Samples were first dried in the oven prior to decomposition. The major and trace elements were determined in three groups.

(1) Major Elements ( Si, Mg, Fe, Ti, Al, Ca, Mn and Cr)

The lithium metaborate fusion technique was employed for the sample decomposition. Fe, Ti, Al, Ca, Mn and Cr were determined on a nitric acid solution

containing La internal standard and the results corrected against the USGS standard PCC-1. Mg and Si were measured in a more diluted nitric acid solution containing Y internal standard and the results corrected against a basalt sample (BHVO) of known composition (Irving, unpubl. data).

(2) Trace elements (Ni, Co, Sr, V, Cr, Mn, K and Ti)

Samples were digested in a mixture of concentrated HF, HNO<sub>3</sub> and HClO<sub>4</sub> and unattacked spinel filtered and fused with NaOH. The sample solutions for the ICAP-AES runs were in HCl containing Lu internal standard. A portion of the solution was spiked with the elements to be analyzed. The trace element concentrations were determined by analyzing the blank, the unspiked solution and the spiked solution.

Based on the replicate analyses, the errors are estimated to be about 1-5% for Cr, Sr, V and Sc, about 10-15% for Ti, Ni and Co and up to 200% for K. Ti and Cr concentrations determined in this way are within the error limits of those obtained by major element analysis. Sr concentrations determined from ICAP-AES and isotope dilution (ID) are within the error limits of each other.

(3) Y and rare earth elements (REE)

Sample decompositions were similar to those for the other trace elements. Y and REE were preconcentrated quantitatively by cation exchange separations as described by Crock et al. (1986). The samples were run in nitric acid solutions containing Cd internal standard.

The accuracy of the REE analysis by ICAP-AES is shown by comparison with the INAA (instrumental neutron activation analysis) data for HL86-O, a Hawaiian basalt (Irving, unpubl. data) and UM-11, an ultramafic xenolith from San Carlos (BVSP, 1981), as well as by comparison with the Sm and Nd ID results for the samples in this study (Fig. 3). Reproducibility of these analyses can be attested by replicate analyses of samples KRBWC-1, KR-37 and KR-141 (Fig. 3). It is shown in Fig. 3 that the REE data by ICAP-AES are excellent for the basaltic samples and, with the exception of Ce, Sm and Nd, are also reasonably good for the ultramafic samples. The Ce, Nd and Sm results are erratic for the ultramafic samples of the lowest concentrations (e.g., KR-141). This may be ascribed to the low signal/background ratios for these elements in the ICAP-AES runs. As a result, in the REE pattern diagram (Fig. 7a-c), the Sm and Nd ID data for the ultramafic xenoliths are used and Ce is plotted only when its

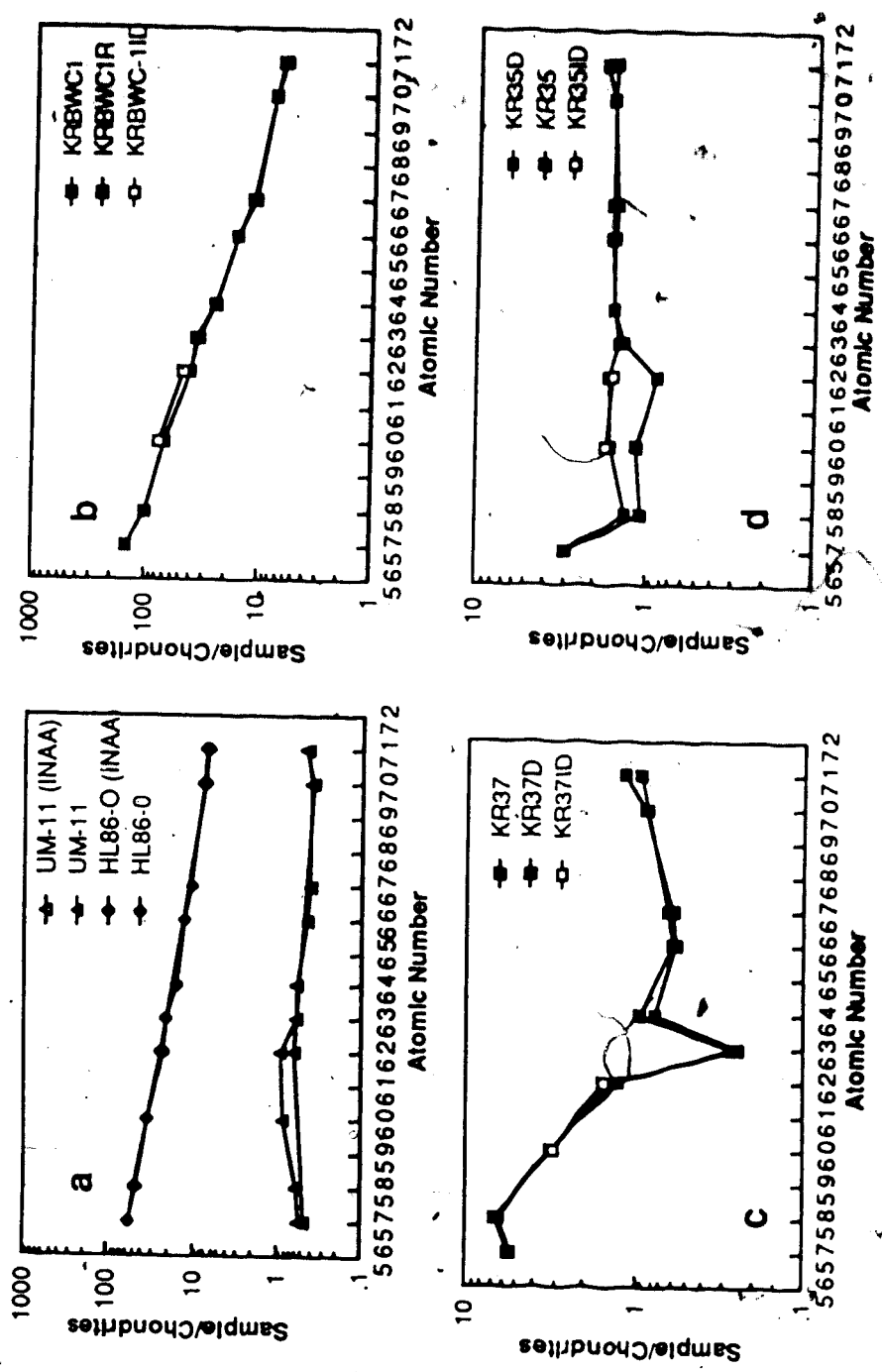


Fig. 3 (a) Comparison of the ICAP-AES results with the INAA data for HL86-O, a Hawaiian basalt (Irving, unpubl. data) and UM-11, an ultramafic xenolith from San Carlos (BVSP, 1981); (b)-(d): Replications of ICAP-AES data for the host basalt (KRBWC-1) and ultramafic xenoliths (KR-37, KR-141) from West Kettle River. Also shown are the Sm and Nd data by isotope dilution. (See the text for discussion). R or D = duplicate; ID = isotope dilution. 57: La; 58: Ce; 60: Nd; 62: Sm; 63: Eu; 64: Gd; 66: Dy; 67: Ho; 70: Yb; 71: Lu.

concentration exceeds 2 ppm.

Detailed accounts of the procedures for major and trace element analyses are presented in Appendix II.

### 3. Sr and Nd isotope analysis

Samples were digested with a mixture of concentrated HF and HNO<sub>3</sub>. Initial Sr separation was achieved by Ba(NO<sub>3</sub>)<sub>2</sub> co-precipitation, followed by purification through two cation exchange columns. Sm and Nd were first separated by ammonia precipitation, then further purified through four cation exchange columns.

All the Nd and most of the Sr isotope ratios (IR's) were determined on a VG 354 mass spectrometer. Most of the Sr, Sm and Nd ID's and some of the Sr-IR's were determined on a Micromass 30 mass spectrometer. The <sup>87</sup>Sr/<sup>86</sup>Sr ratios obtained from both IR's and ID's measured on either of the mass spectrometers are within error of one another. All <sup>143</sup>Nd/<sup>144</sup>Nd ratios were normalized to <sup>144</sup>Nd/<sup>146</sup>Nd = 0.7219 and <sup>87</sup>Sr/<sup>86</sup>Sr to <sup>86</sup>Sr/<sup>88</sup>Sr = 0.1194.

Precision and reproducibility were established throughout the entire study from repeated analyses of the N.B.S. SRM 987 standard for <sup>87</sup>Sr/<sup>86</sup>Sr and the La Jolla standard for <sup>143</sup>Nd/<sup>144</sup>Nd. Eight analyses of the La Jolla standard on the VG 354 mass spectrometer gave a weighted mean for <sup>143</sup>Nd/<sup>144</sup>Nd of 0.511855 ± 2 (2 σ). Six analyses of the N.B.S. SRM 987 standard on the VG 354 mass spectrometer defined a weighted mean for <sup>87</sup>Sr/<sup>86</sup>Sr of 0.71025 ± 3 (2 σ). No corrections against these standards were attempted for the <sup>87</sup>Sr/<sup>86</sup>Sr and <sup>143</sup>Nd/<sup>144</sup>Nd measurements.

The average Sr blank throughout this study is 4.03 ng. The average Sm and Nd blanks, prior to September 30, 1988, were 0.84 ng and 11.20 ng respectively. Subsequent purification of MLA reagent reduced the Sm blank to 0.09 ng and the Nd blank to 1.26 ng. Because the isotopic compositions of blank Sr, Sm and Nd is close to that of the samples, the blanks for Sr, Sm and Nd are considered insignificant and blank corrections therefore not made. Detailed procedures for the Sr and Nd isotope analyses are described in Appendix III.

### 4. Oxygen isotope analysis

Oxygen was extracted using the BrF<sub>5</sub> technique (Clayton and Mayeda, 1963) at

650°C. The  $^{18}\text{O}/^{16}\text{O}$  ratios in the  $\text{CO}_2$  were measured on a VG 602D Micromass mass spectrometer. All the results are reported in permil (‰) relative to SMOW standard. The  $\delta^{18}\text{O}$  value of the NBS-28 quartz standard is 9.6 at the Department of Geology, University of Alberta laboratory. Measurements are estimated to be precise within  $\pm 0.14\%$  based on previous replicate analyses. The differences in  $\delta^{18}\text{O}$  between coexisting minerals are reported as  $\Delta_{x-y}$ , where:

$$\Delta_{x-y} = \delta^{18}\text{O}_x - \delta^{18}\text{O}_y = 1000 \ln \alpha_{x-y}$$

## V. Major and Trace Element Geochemistry

### 1. Host basalt

One West Kettle River host basanitoid sample (KRBWC-1) was analyzed for major and trace element contents. Rare earth elements (REE) of the West Kettle River basanitoid were not previously determined. The results for major and the other trace element concentrations in KRBWC-1 generally agree with the available data (Fuji and Scarfe, 1982a; Sun, 1985) (Tables 2, 3). The West Kettle River basanitoid is very similar, in major element contents, to the San Carlos basanites, which also contain ultramafic xenoliths (Table 2). The highly fractionated REE pattern of the West Kettle River basanitoid (KRBWC-1) (Fig. 7a) is typical of highly alkalic, silica-undersaturated basalts and indicates that it has originated in the garnet ilherzollite stability field (Kay and Gast, 1973). Compared with the San Carlos basanites, the West Kettle River basanitoid has lower heavy REE (HREE), but higher light REE (LREE) (Table 3). As a result, its REE pattern ( $La/Yb = 28.8$ ) is more fractionated than that of the San Carlos basanites ( $La/Yb = 14.2-19.2$ ). This may be interpreted as derivation of the West Kettle River basanitoid by lower degree of partial melting (Kay and Gast, 1973; Roy et al., 1975).

The  $Mg/(Mg+\Sigma Fe)$  ratios (0.55-0.57) and Ni, Cr contents (153-270; 233-383) of the West Kettle River basanitoid, similar to those of the San Carlos basanites, are lower than the estimated values for primary magmas (Irving and Green, 1976; Frey et al., 1978; Hart and Davis, 1978; Sun and Hanson, 1978; Wass, 1980). It may therefore have experienced fractionation of olivine at high pressure (Frey and Prinz, 1978). The forsterite content of the equilibrium olivine for the West Kettle River basanitoid magma can be estimated to be between  $Fo_{82} - Fo_{86}$ . The minimum value is obtained by assuming that all the Fe has been present as FeO in the magma and the maximum value calculated by using the measured  $Fe_2O_3/FeO$  ratio (Frey and Prinz, 1978). The partition coefficient of Fe/Mg between the melt and olivine used in these calculations is from Roeder and Emslie (1970). If a  $Fe_2O_3/FeO$  ratio of 0.2 is assumed, as suggested for the Victorian basanite magmas (Irving and Green, 1976), the equilibrium olivine would have a forsterite content of  $Fo_{84}$  (Frey and Prinz, 1978). This value agrees with the composition of the olivine phenocrysts

Table 2. Chemical composition and normative mineralogy of West Kettle River host basanitoid in comparison with those of the San Carlos basanites.

	West Kettle River				San Carlos	
	KRBWC-1	KRB	WKR4B	KR35B	PA-53B	PA-17
SiO <sub>2</sub>	42.91	44.5	45.01	44.83	44.68	44.61
TiO <sub>2</sub>	3.09	3.12	2.94	2.57	2.84	2.73
Al <sub>2</sub> O <sub>3</sub>	14.38	14.1	14.65	14.60	14.20	14.15
Cr <sub>2</sub> O <sub>3</sub>	0.03	0.08			0.03*	--
Fe <sub>2</sub> O <sub>3</sub>	13.09		13.45	14.50		
Fe <sub>2</sub> O <sub>3</sub>		3.73			4.72	6.66
FeO		8.52			7.85	6.38
MnO	0.18	0.21	0.18	0.19	0.18	0.20
MgO	8.83	9.50	8.53	8.44	8.82	8.62
CaO	9.43	9.55	9.29	9.20	8.30	8.15
BaO	0.05					
SrO	0.11					
Na <sub>2</sub> O	3.94	4.20	3.46	3.43	4.13	4.38
K <sub>2</sub> O	1.84	1.65	1.64	1.44	2.73	2.70
P <sub>2</sub> O <sub>5</sub>	1.02	0.79	0.85	0.80	0.97	0.95
LOI	0.84				0.35	0.29
Total	99.74	99.95	100.00	100.00	100.77	100.80
100Mg/ (Mg+ΣFe)	0.572	0.588	0.557	0.549	0.565	0.554
100Mg/ (Mg+Fe <sup>2+</sup> )	0.650	0.665	0.636	0.634	0.667	0.707
or	11.13	9.75	9.82	8.63	16.1	15.9
ab	11.52	12.92	16.51	17.05	13.2	15.3
an	16.48	14.75	19.86	20.48	12.1	11.0
ne	12.22	12.25	7.13	6.71	14.3	14.4
di	15.09	22.00	17.28	16.79	18.2	18.6
ol	15.02	15.04	19.11	20.65	15.3	12.1
mt	5.48	5.41	2.63	2.84	4.9	7.0
il	6.00	5.93	5.66	4.95	3.9	3.8
ap	2.42	1.83	2.00	2.88	2.0	2.0

Data for KRBWC-1 from this study by ICAP-AES; Data for KRB from Fujii and Scarfe (1982); Data for WKR4B and WKR35B from Sun (1985); Data for PA-53B and PA-17 from Frey and Prinz (1978). Mg/(Mg+Fe<sup>2+</sup>) ratios for all West Kettle River basalts are calculated from Fe<sup>3+</sup>/Fe<sup>2+</sup> of KRB. Fe<sub>2</sub>O<sub>3</sub>\* = total Fe as Fe<sub>2</sub>O<sub>3</sub>.

Table 3. Trace element data for West Kettle River host basanitoids in comparison with San Carlos basanites (in ppm).

	West Kettle River			San Carlos	
	KRBWC-1	WKR4B	KR35B	PA-53B	PA-17
Sc	20			22.2	22.7
V	246	216	220		
Cr	233	231	383	303	189
Co	56			48	48
Ni	153	164	270	265	195
Cu	88				
Zn	107				
Ba	460	470	397		
Sr	911	914	803		
Li	18				
Zr	202	319	281		
Y	25	25	24		
Be	3.2				
Nb		66	56		
Rb		29	26		
La	44.850			32.6	38.5
Ce	80.149			82	67
Nd	40.442			37	33
Sm	7.874			7.85	7.17
Eu	2.557			2.23	2.28
Gd	6.354				
Tb				1.1	1.1
Dy	5.161				
Hb	0.810			1.1	1.1
Yb	1.560			2.3	2.0
Lu	0.201			0.38	0.30
La/Yb	28.8			14.2	19.2

Data sources as for major elements in Table 2; KRBWC-1 by ICAP-AES from this study.



in the West Kettle River basanitoid (Fujii and Scarfe, 1982a).

## 2. Major element variations

### (1) Oxides vs. $Mg/(Mg+\Sigma Fe)$

Major element concentrations of the West Kettle River xenolith whole rocks are reported in Table 4. The bulk compositional variations of ultramafic xenoliths can be evaluated by oxides vs.  $Mg/(Mg+\Sigma Fe)$  relationships, because the  $Mg/(Mg+\Sigma Fe)$  ratio is a sensitive indicator of mafic mineral/silicate liquid fractionation (Frey and Prinz, 1978). The bulk  $Al_2O_3$ , CaO and  $TiO_2$  of the West Kettle River lherzolites and harzburgites decrease systematically with increasing  $Mg/(Mg+\Sigma Fe)$  (Fig. 4). Such a variation is typical of spinel lherzolite and harzburgite xenoliths worldwide and is considered to result from mafic mineral/melt equilibrium processes (partial melting or fractional crystallization) (Frey and Prinz, 1978; Preß et al., 1986). However, the correlation coefficients for these trends are generally low (0.88 - 0.95) and there are only weak correlations between  $\Sigma FeO$ ,  $SiO_2$ ,  $Cr_2O_3$ , NiO and  $Mg/(Mg+\Sigma Fe)$  for these West Kettle River xenoliths (Fig. 4). The poor correlations may be partly due to the sampling problem resulting from coarse grain size, restricted sample size, and to the errors in  $Mg/(Mg+Fe^{2+})$  introduced by the presence of  $Fe^{3+}$ . Slight source heterogeneity, multi-stage melting/crystallization, or interaction of some of these xenoliths with migrating melts may also have been responsible for the data scattering.

KR-3020B, an olivine websterite in a composite Group I xenolith, has a  $Mg/(Mg+\Sigma Fe)$  value within the range for the harzburgites and lherzolites (Fig. 4). Its mineral composition is indistinguishable from that of the host lherzolite (KR-3020) (Appendix IV). As expected from its modal composition, KR-3020B has distinctly higher CaO,  $Al_2O_3$ ,  $Cr_2O_3$  and lower NiO and FeO than the lines defined by the lherzolites and harzburgites (Fig. 4). A direct genetic linkage of sample KR-3020B with the lherzolites and harzburgites does not seem likely. Similar major element patterns have been documented for websterite bands in composite Group I xenoliths from other localities (eg. Frey and Prinz, 1978; Kempton et al., 1984). They very likely represent precipitates from silicate melts in the upper mantle (Irving, 1980; Frey and Prinz, 1978).

Table 4. Bulk chemical analysis for ultramafic xenoliths from West Kettle River (wt.%).

Sample	KR-35	KR-37	KR-141	KR-4000	KR-4001
SiO <sub>2</sub>	43.62	44.23	44.50	42.95	44.92
TiO <sub>2</sub>	0.12	0.01	0.08	0.05	0.08
Al <sub>2</sub> O <sub>3</sub>	3.71	1.81	3.18	1.55	3.51
Cr <sub>2</sub> O <sub>3</sub>	0.44	0.38	0.48	0.26	0.43
FeO*	8.53	8.12	8.15	8.65	7.80
NiO	0.28	0.29	0.26	0.31	0.24
CoO	0.01	0.01	0.01	0.02	0.01
MnO	0.14	0.13	0.13	0.13	0.13
MgO	39.52	43.58	39.82	45.47	37.75
CaO	2.68	1.14	2.58	0.69	3.38
Na <sub>2</sub> O	0.08	0.00	0.10	0.08	0.00
K <sub>2</sub> O	0.02	0.00	0.02	0.09	0.00
Total	99.15	99.70	99.31	100.24	98.25
100Mg/ (Mg+ΣFe)	89.20	90.54	89.70	90.36	89.61

Sample	KR-4002	KR-4003	KR-4005	KR-4016	KR-3020B
SiO <sub>2</sub>	44.74	44.80	44.85	43.88	46.88
TiO <sub>2</sub>	0.11	0.17	0.15	0.11	0.20
Al <sub>2</sub> O <sub>3</sub>	3.58	4.26	4.02	3.09	9.49
Cr <sub>2</sub> O <sub>3</sub>	0.42	0.40	0.39	0.36	0.96
FeO*	7.98	8.03	8.05	8.07	5.67
NiO	0.25	0.23	0.25	0.26	0.16
CoO	0.01	0.01	0.01	0.01	0.01
MnO	0.13	0.14	0.14	0.13	0.12
MgO	39.08	37.50	37.86	39.97	26.39
CaO	2.84	3.46	3.36	2.72	8.56
Na <sub>2</sub> O	0.00	0.20	0.14	0.00	0.76
K <sub>2</sub> O	0.02	0.09	0.08	0.06	0.20
Total	99.16	99.29	99.30	98.66	99.40
100Mg/ (Mg+ΣFe)	89.72	89.27	89.34	89.82	89.24

Note: FeO\* = Total Fe as FeO; Data by ICAP-AES;

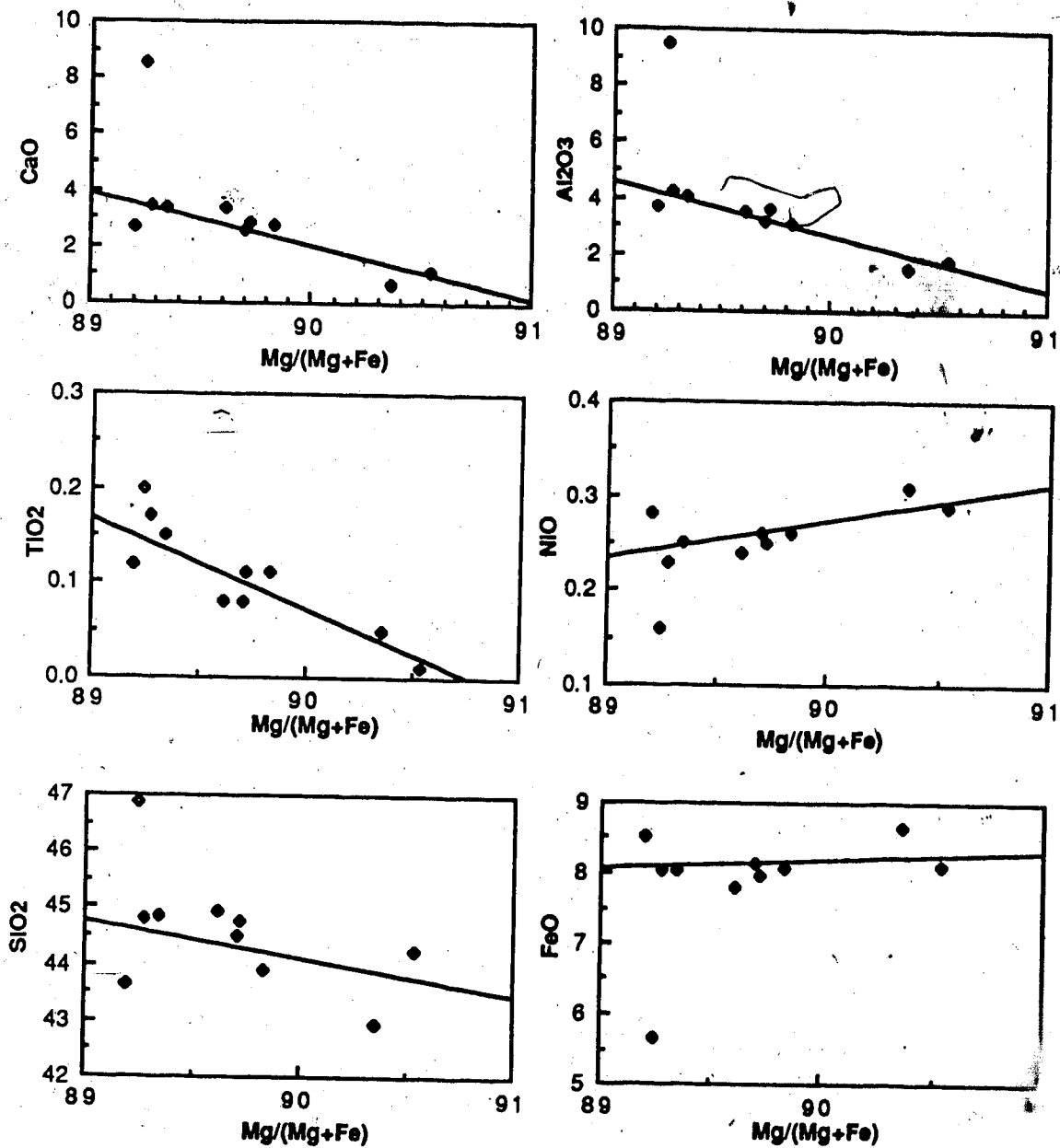


Fig. 4. Bulk concentrations of various oxides plotted versus bulk Mg/(Mg+Fe) of West Kettle River ultramafic xenoliths. Lines are calculated from least squares regressions of the lherzolites and harzburgites. The olivine websterite plots off the lines in most of these diagrams. Open diamond: olivine websterite (KR-3020B); Solid diamond: lherzolite or harzburgite.

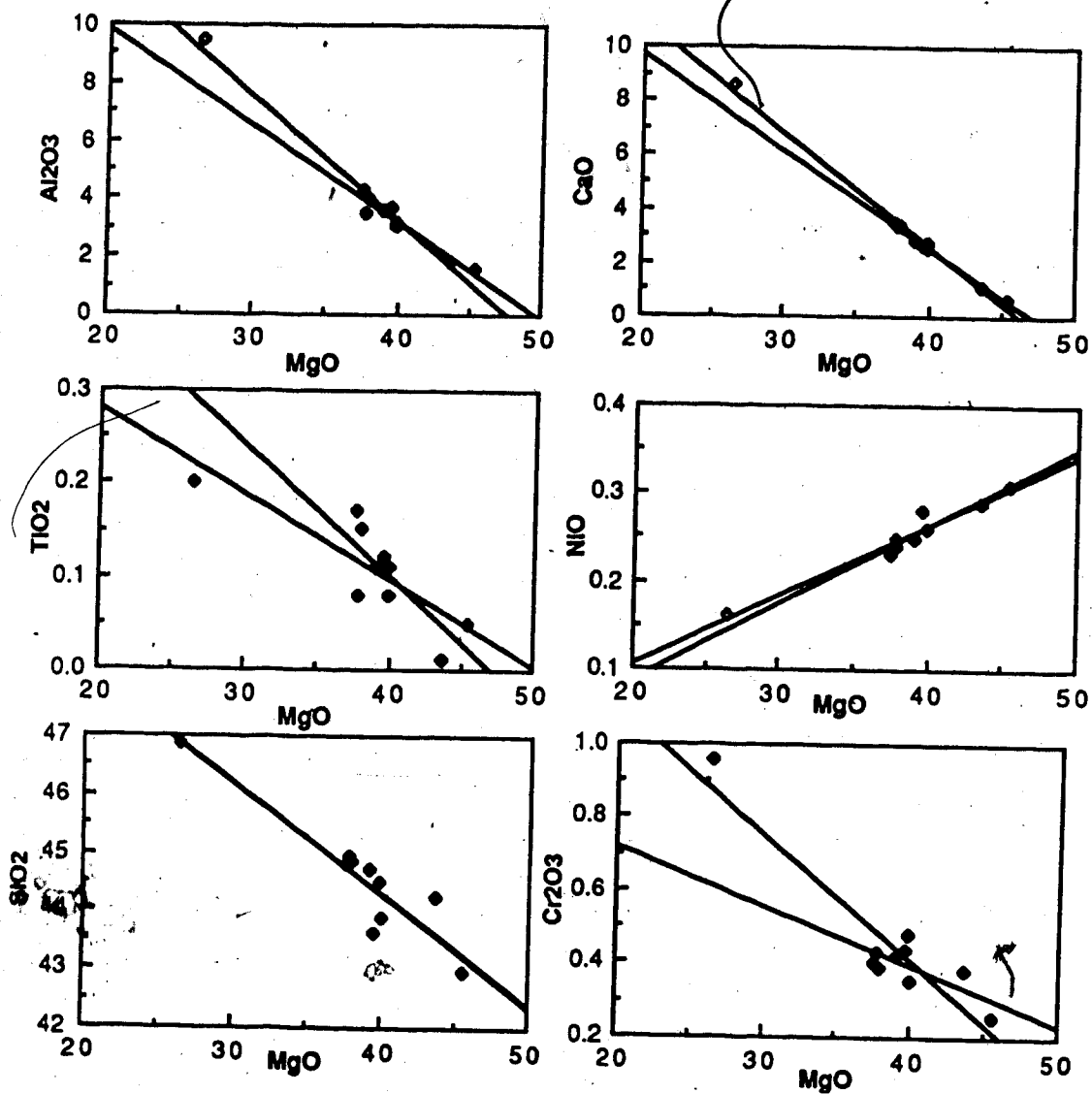


Fig. 5. Bulk concentrations of various oxides plotted versus bulk MgO of the West Kettle River ultramafic xenoliths. The two lines are calculated from least squares regressions of the West Kettle River ultramafic xenoliths with and without the websterite. Symbols as in Fig. 4.

## (2) Oxides vs. MgO

Another type of correlation diagram, commonly employed in the interpretation of chemical variations in mantle xenoliths, is the oxide vs. MgO plot. Systematic variations of CaO, Al<sub>2</sub>O<sub>3</sub>, FeO, NiO, SiO<sub>2</sub> with MgO for bulk spinel peridotites have been compiled both for xenolith suites from single localities elsewhere (e.g. BVSP, 1981; Nickel and Green, 1984; Preß et al., 1986) and for mantle xenoliths worldwide taken as a whole (Maaloe and Aoki, 1977; Palme and Nickel, 1985). These systematic trends, in combination with constraints from the meteoritic data, have often been used to extrapolate the primitive upper mantle compositions (eg. Jagoutz et al., 1979; Palme and Nickel, 1985; Hart and Zindler, 1986). Not unlike xenoliths elsewhere, the West Kettle River harzburgites and lherzolites display strong linear correlations between Al<sub>2</sub>O<sub>3</sub>, CaO, NiO and MgO (Fig. 5). SiO<sub>2</sub>, Cr<sub>2</sub>O<sub>3</sub>, TiO<sub>2</sub> in these xenoliths are only loosely correlated with MgO (Fig. 5). Interestingly, in most of these oxide vs. MgO diagrams, the olivine websterite (KR-3020B), when taken together with the lherzolites and harzburgites, falls on reasonably good trends with correlation coefficients similar or even higher than the corresponding lines calculated from lherzolites and harzburgites alone (Fig. 5). These two trends, however, are mostly not in accord with each other (Fig. 5). As discussed earlier, the websterite is not derived from the same process as the harzburgites and lherzolites. The apparent coherence of their compositions warns against modeling of the primitive upper mantle composition based on the oxide-MgO correlations without independent evidence for a genetic relationship (eg. correlation of the oxides with Mg/(Mg+ΣFe)). Compositions of the primitive mantle derived this way might be biased by the samples of different origin. A similar argument has been made by Preß et al. (1986) based on three clinopyroxene-rich lherzolites from Mongolia. It should be noted that both the West Kettle River olivine websterite and the Mongolia clinopyroxene-rich lherzolites (Preß et al., 1986) have significantly lower ΣFeO than the lines defined by the other lherzolites and harzburgites (not plotted).

## 3. First-series transition elements

This group of elements (Sc, Ti, V, Cr, Mn, Fe, Co, Ni) and the adjacent element Ca are compatible to at least one of the major constituent minerals in ultramafic rocks.

The lower atomic number elements (Ca - Cr) are all to some extent accepted by clinopyroxene and to a lesser extent by orthopyroxene and almost completely rejected by olivine and can be conveniently named as pyroxene-compatible elements (Kurat et al., 1980). The higher atomic number elements (Mn - Ni) are compatible to all the major minerals in ultramafic xenoliths, more so in olivine, and can be called olivine-compatible elements (Kurat et al., 1980). As a result of their variable behavior, the first series transition element patterns are sensitive to partial melting and fractional crystallization processes and may provide us with some insight into the genesis of the ultramafic xenoliths.

Trace element abundances for the West Kettle River ultramafic xenoliths are reported in Table 5. Fig. 6 shows the transition element and Ca contents, normalized to the estimated primitive upper mantle compositions (Sun, 1982; Jagoutz et al., 1979), for the West Kettle River ultramafic xenoliths and host basanitoid. Three of the lherzolites (KR-4003, KR-4005, KR-4001) have nearly flat patterns with normalized values close to 1 (Fig. 6). From these fertile lherzolites to the more depleted harzburgites, the pyroxene-compatible element contents generally decrease and the olivine-compatible element contents either slightly increase (Ni) or remain essentially unchanged (Mn, Fe, Co) (Fig. 6).

A noteworthy feature of the transition element patterns for these lherzolites and harzburgites is the large variations in the pyroxene-compatible element contents (Ca, Sc, Ti, V), in contrast with the restricted values for the olivine-compatible elements (Mn, Fe, Co, Ni) (Fig. 6). This is typical of lherzolite and harzburgite xenoliths worldwide (eg. Frey and Green, 1974; Frey and Prinz, 1978). Quantitative modeling of the distribution of these elements, particularly Ca, Sc and Ni, during partial melting and fractional crystallization processes suggests that lherzolites and harzburgites represent partial melting residues, rather than fractional crystallization cumulates (Frey and Green, 1974; Frey and Prinz, 1978; Francis, 1987).

The general trend for the West Kettle River basanitoid (KRBWC-1) is a "W" shape with depletions of Cr and Ni (Fig. 6), which characterizes basalts in general (Allegre et al., 1968; Bougault and Hekinian, 1974; Kay and Hubbard, 1978). The transition element patterns of the depleted lherzolites and harzburgites are complementary to that of the basanitoid, in accord with the partition coefficients of

Table 5. Trace element (excluding REE) data (ppm) for ultramafic xenoliths from West Kettle River.

Sample	KR-35	KR-37	KR-141	KR-4000	KR-4001
Sr	62	12	32	66	10
Sc	14	8	13	5	16
V	67	38	60	21	70
Cr	3019	2381	3236	1902	2976
Co	107	103	95	106	90
Ni	2226	2350	2061	2420	1927
Sample	KR-4002	KR-4003	KR-4005	KR-4016	KR-3020B
Sr	16	49	53	22	44
Sc	13	18	18	16	38
V	62	81	79	70	167
Cr	2913	2730	2760	2693	6912
Co	89	92	100	102	73
Ni	1990	1843	2002	2099	1215

Data by ICAP-AES.

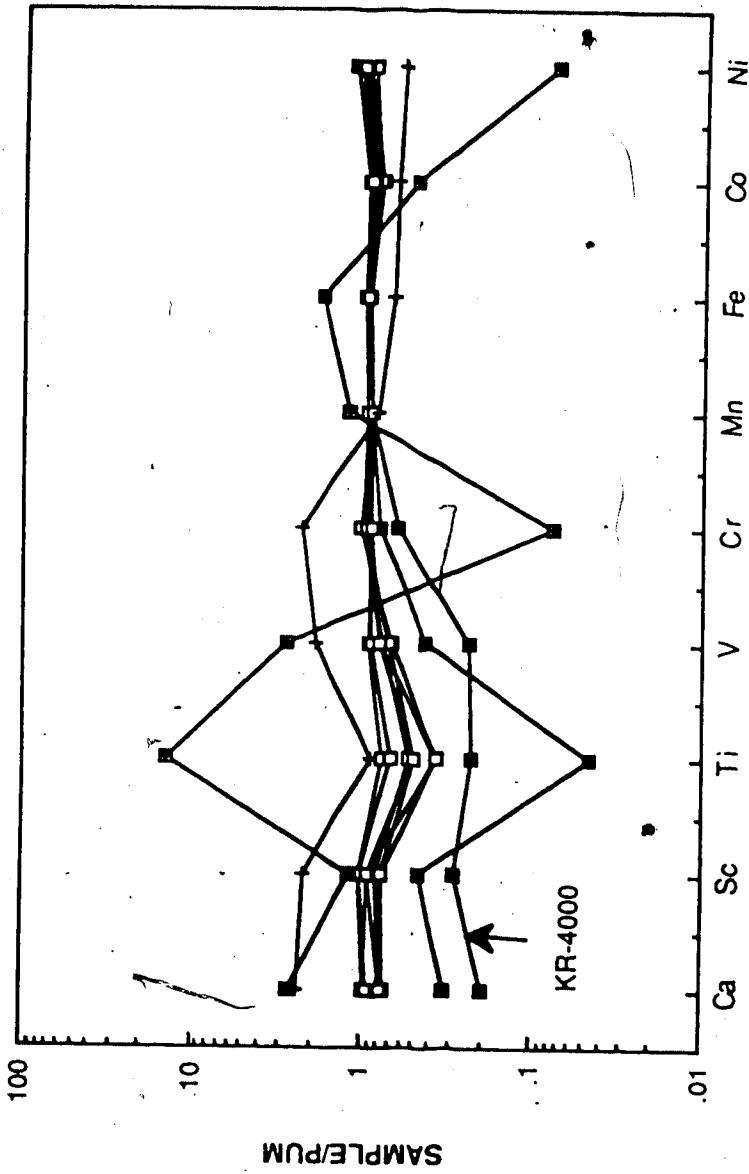


Fig. 6. Transition element and Ca abundances of West Kettle River ultramafic xenoliths and host basanitoid, normalized to the estimated primitive upper mantle values. The normalizing values for all the elements except Sc are from Sun (1982). The Sc value is from Jagoutz et al. (1979). Solid square: harzburgite; Open square: olivine websterite; cross with cross inside: host basalt.



these elements between mafic minerals and silicate liquids. For example, a Ti valley characterizes most of the depleted lherzolites and harzburgites and forms a mirror image to the highest Ti in the basalt (Fig. 6). This is due to the much greater incompatibility of Ti than the adjacent elements (Sc, V). Harzburgite KR-4000, however, lacks such a Ti valley (Fig. 6). Its Cr content is lower than the fertile lherzolite (Fig. 6), which cannot be explained by a simple partial melting model. The Fe content of this xenolith is also anomalously higher than the other xenoliths (Fig. 16). Equilibration of this xenolith with a silicate melt in the upper mantle may have resulted in these features.

The olivine websterite (KR-3020B) has a distinctly different transition element pattern from the basanitoid (Fig. 6) and thus is unlikely to represent a completely crystallized silicate melt within the upper mantle. The systematic shift of this xenolith from the lherzolites, to higher values for the pyroxene-compatible elements, and to lower values for the olivine-compatible elements (Fig. 6), is due to its higher modal proportion of clinopyroxene.

#### 4. REE abundances

##### (1) Bulk REE patterns

The bulk REE concentrations of the West Kettle River ultramafic xenoliths are presented in Table 6. Chondrite-normalized REE concentrations of these xenoliths are plotted in Fig. 7a - c. As observed for similar xenoliths elsewhere (Frey, 1984), the REE patterns of the West Kettle River lherzolites and harzburgites range from relative LREE depletion to LREE enrichment. The heavy REE (HREE) in these xenoliths have unfractionated distributions and their absolute abundances range from 0.15 to 0.35 ppm. Their LREE contents (0.15-1.70 ppm) are more variable than the HREE. The two harzburgites (KR-37, KR-4000) are most enriched in LREE. Harzburgite KR-37 is also peculiar in its strong negative Eu anomaly (Fig. 7c), which is not expected in spinel peridotite xenoliths (Frey, 1984). Four of the seven lherzolites (KR-141, KR-4001, KR-4002, KR-4016) are LREE depleted ( $La/Yb < \text{chondritic value}$ ) and are with or without relative La enrichment ( $La/Nd > \text{chondritic value}$ ) (Fig. 7a). Lherzolite KR-35 has a moderate LREE enrichment pattern (Fig. 7b) and two other lherzolites (KR-4003, KR-4005) have convex-upwards REE patterns with the highest chondrite-normalized values in Sm and Nd (Fig. 7b).

Table 6. REE and Y concentrations in ultramafic xenoliths from West Kettle River.

Sample	La	Ce	Nd	Sm	Eu	Gd	Dy	Ho	Yb	Lu	Y
KR-35	0.934	(1.067)	1.032	0.307	0.109	0.403	0.518	0.117	0.338	0.050	3.014
KR-37	1.699	5.346	1.861	0.309	0.020	0.241	0.192	0.045	0.178	0.031	1.220
KR-141	0.402	(0.492)	0.486	0.175	0.076	0.322	0.430	0.097	0.312	0.048	2.624
KR-4000	1.131	2.135	0.972	0.191	0.057	0.185	0.161	0.032	0.094	0.015	0.924
KR-4001	0.251	(0.689)	0.408	0.155	0.069	0.346	0.416	0.097	0.295	0.053	2.464
KR-4002	0.154	(0.506)	0.531	0.222	0.087	0.367	0.488	0.110	0.348	0.061	2.977
KR-4003	0.405	(0.796)	1.838	0.420	0.072	0.242	0.307	0.058	0.218	0.031	1.986
KR-4005	0.585	(1.357)	1.430	0.348	0.107	0.404	0.512	0.113	0.338	0.050	3.071
KR-4016	0.178	(0.643)	0.526	0.212	0.077	0.295	0.417	0.095	0.276	0.042	2.423
KR-3020B	1.090	2.564	1.811	0.544	0.201	0.743	1.068	0.256	0.760	0.120	6.548

All the REE and Y concentrations were analyzed by ICAP-AES, except for Sm and Nd, which were analyzed by isotope dilution; The Ce data in brackets are suspect due to their low counts in ICAP-AES (see discussion in Chapter III) and will not be plotted in the REE patterns (Fig. 7a - 7c).

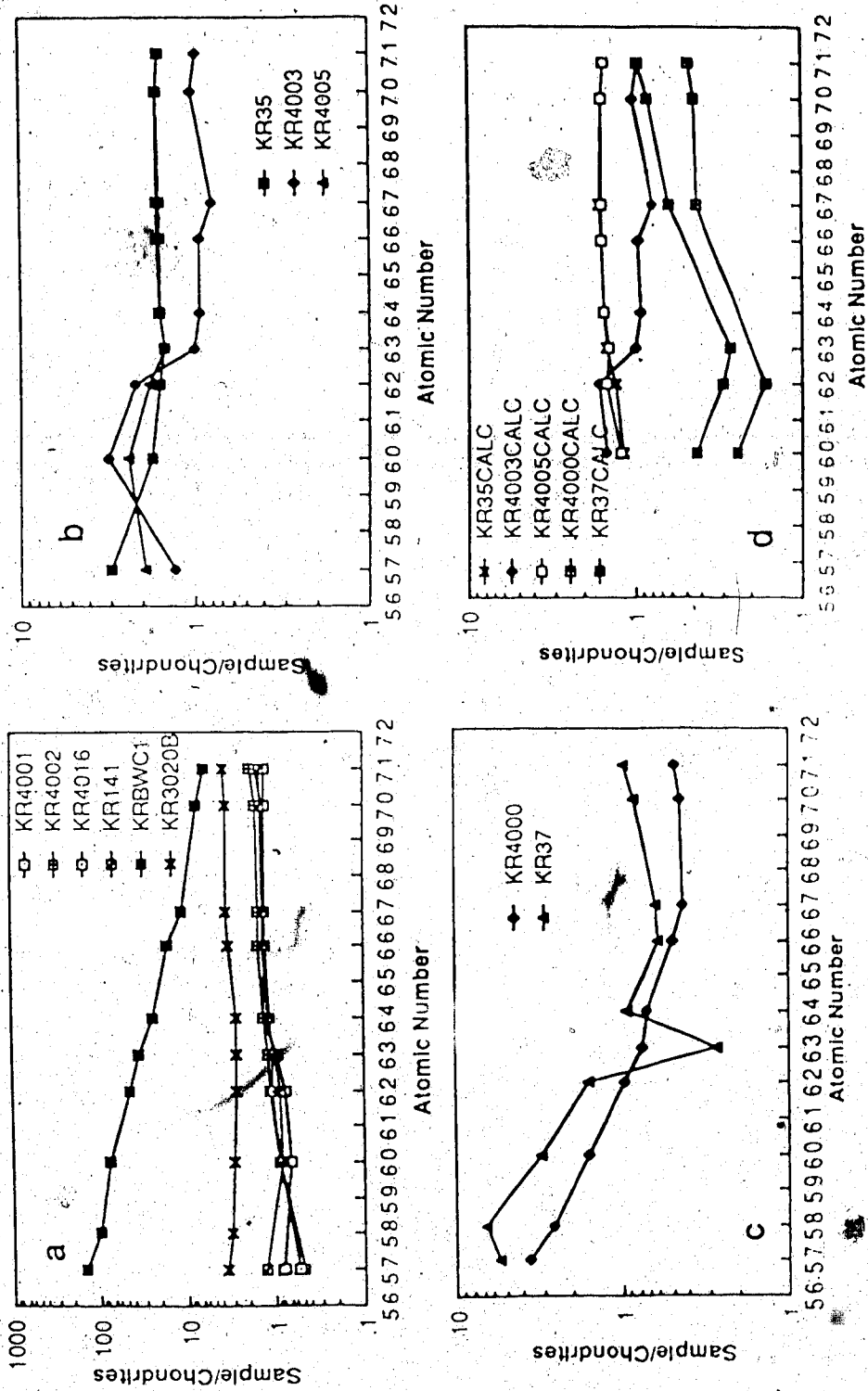


Fig. 7. (a)-(c) Chondrite-normalized REE abundances in ultramafic xenoliths and host basanitoid from West Kettle River. The normalizing values are from Boynton (1984); (d) Reconstructed clean whole rock REE patterns, using the measured HREE and calculated Sm and Nd abundances, for those ilmenites and harzburgites suffering from secondary contaminations (see text for discussion). For the atomic numbers of the REE, see Fig. 3.

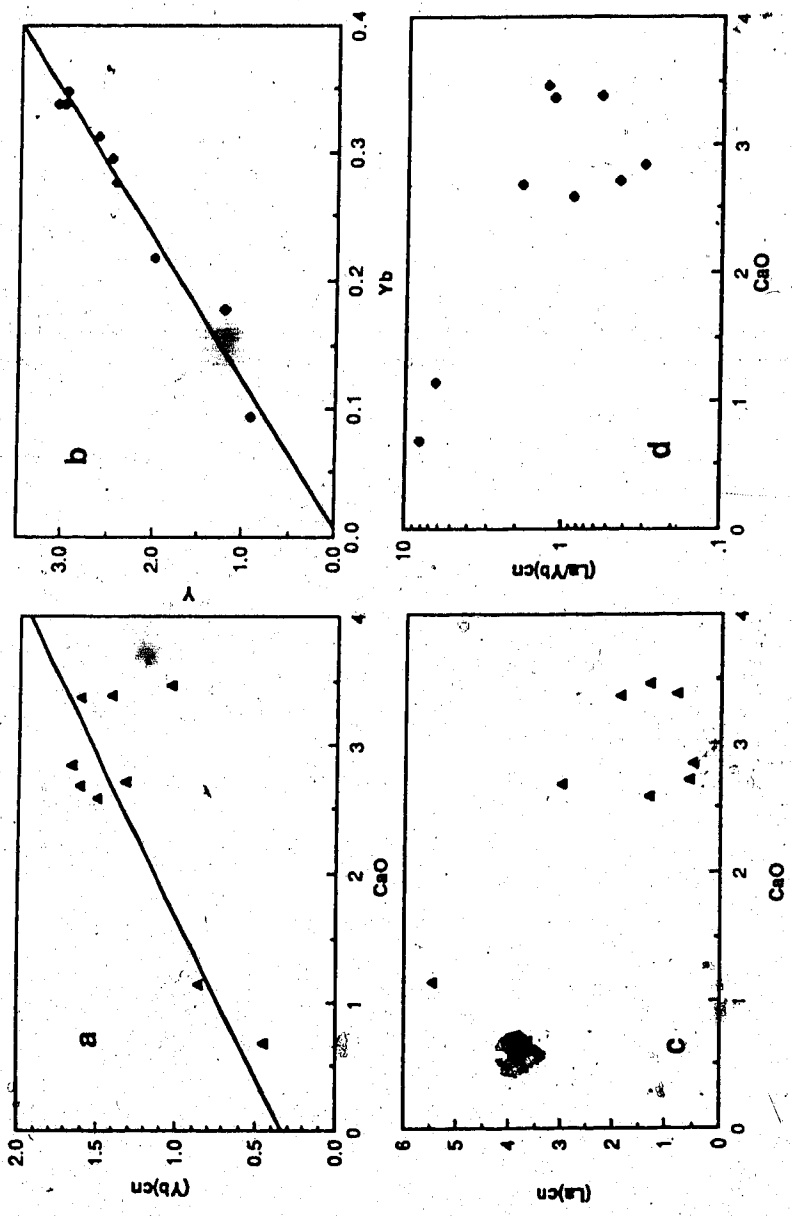


Fig. 8. (a), (c) and (d) Chondrite-normalized Yb (a), La (c) and La/Yb (d) versus CaO for the bulk ilherzolites and harzburgites from West Kettle River; (b) Y versus Yb for the bulk ilherzolites and harzburgites from West Kettle River.

Positive correlations exist between the HREE (eg. Yb) and CaO (proportional to modal clinopyroxene) for these lherzolites and harzburgites (Fig. 8a), suggesting that the HREE contents are controlled by the processes responsible for the major element variations. Y in these xenoliths behaves very similarly to the HREE (Fig. 8b). HREE and Y in lherzolite KR-4003 are, however, too low for its CaO contents when compared with the other lherzolites (Fig. 8a). Positive correlations between HREE and CaO have been recognized for most peridotite xenolith suites elsewhere (Frey, 1984). In addition, in many of these xenolith suites inverse correlations between the LREE and CaO have been documented (Frey, 1984). Similarly, among the West Kettle River lherzolites and harzburgites, the two harzburgites with the lowest CaO have by far the highest La and La/Yb (Fig. 8c, d). In principle, patterns of LREE depletion and positive correlation of LREE with CaO are expected for anhydrous peridotites, if they represent simply partial melting residues from a primitive lherzolite source (Frey and Green, 1974). The LREE enrichments and their inverse correlation with CaO for the harzburgites and some of the lherzolites from West Kettle River suggest that they have been affected by other processes (instead of partial melting) that had little effects on the major element and HREE abundances, but have significantly affected the LREE.

The olivine websterite KR-3020B has a flat REE pattern. Both its HREE and LREE contents are higher than those of the lherzolites (Fig. 7a). Similar REE patterns have also been documented for websterite xenoliths elsewhere (Frey, 1984). Such a REE pattern implies that KR-3020B does not represent a completely crystallized silicate magma, but may reflect crystal segregation from such a magma (Frey, 1984; Irving, 1980). As discussed earlier, this interpretation is also supported by the major element variations and transition element pattern of this websterite.

## (2) Mass balance calculations

It has been demonstrated that LREE of whole rock ultramafic xenoliths are susceptible to secondary contamination (eg. Jagoutz et al., 1980; Kurat et al., 1980; Stosch and Seck, 1980; Stosch et al., 1986; Zindler and Jagoutz, 1988). In order to assess the upper mantle processes, it is necessary to ascertain the location and origin of the LREE in these xenoliths. Only Sm and Nd were analyzed for the clinopyroxenes in the West Kettle River ultramafic xenoliths (Table 9). Mass balance calculations of Sm and Nd are presented in Table 7 and plotted in Fig. 9. The calculated values are derived from the modal compositions, concentrations in clinopyroxenes and partition

coefficients from Zindler and Jagoutz (1988), assuming chemical equilibrium between the coexisting minerals.

The discrepancies in the Sm and Nd concentrations between the measured whole rocks and the calculated whole rocks, when beyond statistical uncertainties (up to 20%) associated with the estimation of modal compositions and Nd isotope dilution analyses, could be ascribed to interstitial materials or inclusions in the xenolith whole rocks. These contaminant phases may have been derived from ground water, host basalt or mantle metasomatic fluids.

There is a general correlation between the bulk LREE enrichment and the proportion of Nd residing in the secondary phases. For the four lherzolites that display LREE depletion patterns, reasonable agreement is obtained between the calculated and measured whole rock Sm and Nd concentrations (Fig. 9). For the two harzburgites with strong LREE enrichment, about 80 - 85 % of the Sm and Nd are attributable to the secondary phases (Fig. 9). For lherzolites KR-4003 and KR-4005, that have convex upwards LREE patterns, about 50 % of the Nd resides in the secondary phases (Fig. 9). For lherzolite KR-35 that shows moderate LREE enrichment, there is also some indication of Sm and Nd in the secondary phases (Fig. 9). Therefore, the LREE enrichments of the bulk West Kettle River xenoliths are at least partly attributable to the secondary phases. The secondary phases may also be responsible for the slight La enrichment in KR-4001 and KR-141 (Fig. 7a).

Table 7. Mass balance calculations of Sr, Nd and Sm for ultramafic xenoliths from West Kettle River.

Sample	Calculated WR/Measured WR				
	Sr	Nd	Sm	Sm/Nd	Sr/Nd
KR-35	0.17	0.68	0.84	1.23	0.25
KR-37	0.22	0.14	0.19	1.35	1.60
KR-141	0.24	0.88	1.00	1.17	0.27
KR-4000	0.04	0.15	0.17	1.11	0.25
KR-4001	0.88	0.97	0.99	1.01	0.91
KR-4002	0.33	1.00	1.00	1.10	0.32
KR-4003	0.25	0.48	0.76	1.58	0.52
KR-4005	0.20	0.52	0.83	1.60	0.38
KR-4016	0.32	1.00	1.00	1.07	0.30

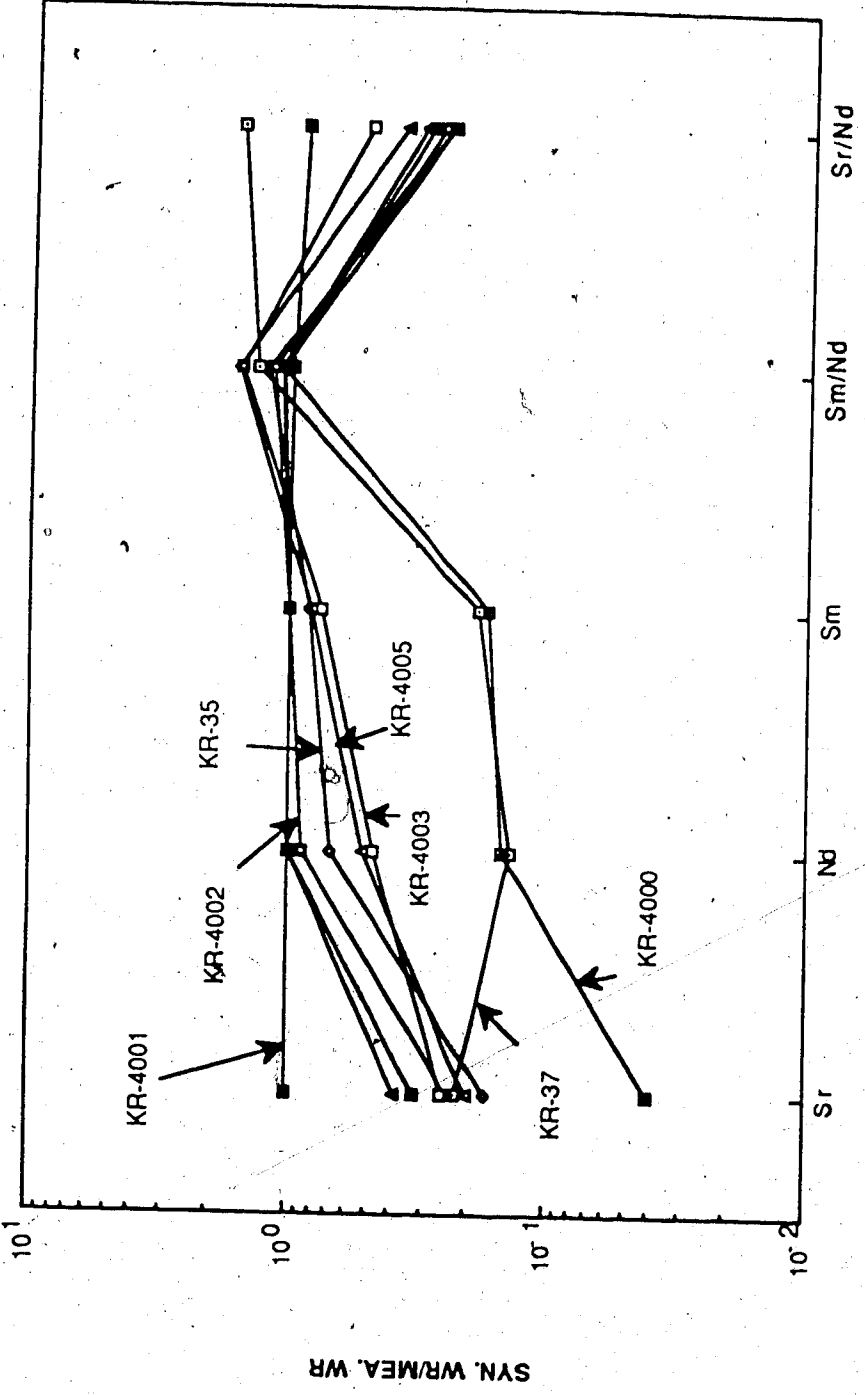


Fig. 9. Calculated whole rock concentrations divided by those of the measured whole rocks for Sr, Nd and Sm in ultramafic xenoliths from West Kettle River. Mass balance calculations were based on modal compositions, concentrations in clinopyroxenes and partition coefficients from Zindler and Jagoutz (1988), assuming elemental equilibrium between coexisting minerals.

The REE patterns of the xenolith whole rocks prior to these secondary processes ('uncontaminated' whole rocks) can be reconstructed by utilizing the measured whole rock HREE and the calculated Sm and Nd concentrations, and are shown in Fig. 7d. Although large errors are associated with the calculated Sm and Nd concentrations, the general pattern may be valid. The REE patterns of the 'uncontaminated' whole rock for all but one (KR-4003) of the lherzolites display LREE depletion. A convex-upwards LREE pattern is exhibited by the 'uncontaminated' whole rock of KR-4003 (Fig. 7d), implying that this sample has experienced LREE enrichment, which was followed by a LREE depletion event. The 'uncontaminated' whole rocks of the two harzburgites show concave-upwards REE patterns (Fig. 7d), suggesting that they have been metasomatized in the upper mantle after melt extraction. It should be emphasized that the ideal way to trace the upper mantle processes based on such 'contaminated' xenoliths is to analyze the REE concentrations in their constituent clinopyroxenes. If the above argument is valid, the REE patterns of the reconstructed 'uncontaminated' whole rocks should match those of the constituent clinopyroxenes.

The negative Eu anomaly of KR-37 seems to be a feature associated with the secondary phases and disappears in the 'uncontaminated' whole rock REE pattern (Fig. 7d). Sample KR-37 is severely weathered and was initially chosen to test the weathering effect on mantle xenoliths. The distinctive negative Eu anomaly and strong LREE enrichment of its whole rock may be largely associated with weathering. Studies of weathered granodiorites and shales have indicated that REE can be mobilized by ground water during weathering (Humphris, 1984; Schieber, 1986). Change in pH of the ground water (Nesbitt, 1979) and absorption by clay minerals in the weathered rocks (Aagaard, 1974; Dypvik and Brunfelt, 1976) may facilitate precipitation of the REE from the ground water. The REE patterns of the ground water precipitation are often inherited from the source rocks (Nesbitt, 1979; Dypvik and Brunfelt, 1976; Cullers et al., 1975). West Kettle River lavas were erupted through Precambrian gneisses (Monger et al., 1982), the REE in the grain boundary phases of KR-37 were possibly transported by ground water from these rocks. Since REE are generally low in the ground water (Keasler and Loveland, 1982), a prolonged exposure time to ground water and high water/rock ratio, as suggested by the severely weathered appearance of KR-37, may have been important for the significant addition of LREE (Humphris, 1984). The LREE enrichment for the other West Kettle River whole rock xenoliths



may not be due to ground water contamination, because they are all very fresh. Host basalt interaction or mantle metasomatism may be a possible explanation. Further discussion on the characteristics and sources of the secondary phases will be presented in the Nd-Sr isotope chapter (Chapter VI).

#### 5. Sr abundances

Sr is one of the large ion lithophile (LIL) elements, which are incompatible with all the major mineral phases in anhydrous ultramafic xenoliths. Fig. 10 indicates that the Sr concentrations in the West Kettle River whole rock xenoliths do not correlate with CaO. Similar to the LREE, the inconsistent variations of Sr with the major elements are very common for whole rock ultramafic xenoliths and can often be attributed to the secondary phases in these xenoliths (eg. Zindler and Jagoutz, 1988 and references cited therein). Sr mass balance calculations of the West Kettle River xenoliths (Table 7; Fig. 9) confirmed this inference: only one of the lherzolites (KR-4001) has the bulk of the Sr in its major mineral phases; the rest of the lherzolites and harzburgites contain over 60% of the Sr contents in the secondary phases. Obviously, for most of the West Kettle River xenoliths, the contribution from the secondary phases is more significant for Sr than for LREE.

Sr is the daughter element of the important Rb-Sr isotope system. The identification of the secondary phases will be further discussed in the Nd-Sr isotope chapter (Chapter VI).

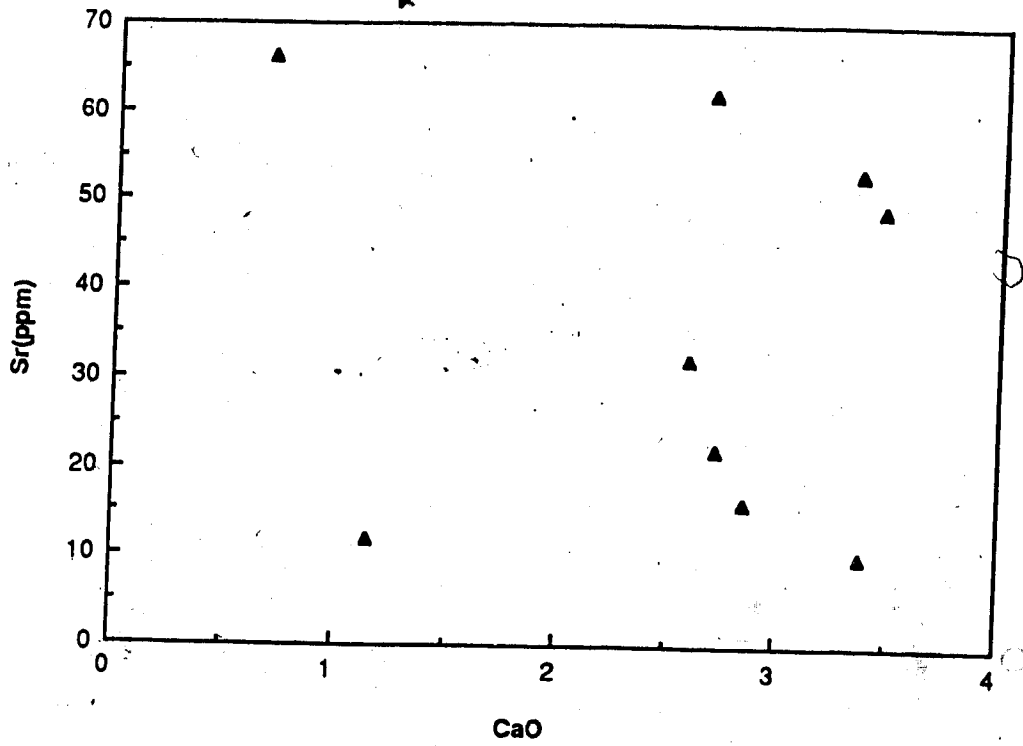


Fig. 10. Sr versus CaO for bulk lherzolites and harzburgites from West Kettle River.

## VI. Sr and Nd Isotope Geochemistry

### 1. Sr and Nd isotopic compositions

Sm, Nd, Sr concentrations and Nd, Sr isotopic ratios for the West Kettle River xenolith whole rocks and host basanitoid are reported in Table 8. Isotope results for the clinopyroxenes and olivines from these xenoliths are given in Table 9. Fig. 11 shows a plot of  $^{143}\text{Nd}/^{144}\text{Nd}$  vs.  $^{87}\text{Sr}/^{86}\text{Sr}$  for these samples.

The  $^{87}\text{Sr}/^{86}\text{Sr}$  of the xenolith clinopyroxenes range from 0.70223 - 0.70342 and are comparable to the previous data for Group I ultramafic xenoliths from West Kettle River (Sun, 1985). Their  $^{143}\text{Nd}/^{144}\text{Nd}$  range from 0.51273 - 0.51335. Except for lherzolite KR-4003, all these clinopyroxenes fall into the MORB range and are correlated along the mantle array in the  $^{143}\text{Nd}/^{144}\text{Nd}$  vs.  $^{87}\text{Sr}/^{86}\text{Sr}$  diagram (Fig. 11). KR-4003 clinopyroxene has the lowest  $^{143}\text{Nd}/^{144}\text{Nd}$  ratio (0.51273) and plots to the left of the mantle array (Fig. 11).

The  $^{87}\text{Sr}/^{86}\text{Sr}$  of the xenolith whole rocks range from 0.70349 - 0.70504 and  $^{143}\text{Nd}/^{144}\text{Nd}$  from 0.51104 - 0.51328. Only one lherzolite (KR-4001) has nearly identical  $^{87}\text{Sr}/^{86}\text{Sr}$  and  $^{143}\text{Nd}/^{144}\text{Nd}$  ratios between the whole rock and the clinopyroxene (Fig. 12a, c). The  $^{87}\text{Sr}/^{86}\text{Sr}$  of the whole rocks for most xenoliths are markedly higher than the corresponding clinopyroxenes (Fig. 12c) (also see Sun, 1985). With two exceptions (KR-37, KR-4003), the  $^{143}\text{Nd}/^{144}\text{Nd}$  ratios of the whole rocks are similar to, or slightly lower than, those of the constituent clinopyroxenes (Fig. 12a). The  $^{143}\text{Nd}/^{144}\text{Nd}$  ratio of the KR-37 whole rock is much lower than that of the corresponding clinopyroxene and the  $^{143}\text{Nd}/^{144}\text{Nd}$  ratio of the KR-4003 whole rock is higher than that for its constituent clinopyroxene (Fig. 12a). It has been shown from the mass balance calculations (see Chapter V) that significant amounts of Sr (for most of these xenoliths) and Sm, Nd (for some of them) are present in the secondary phases. The offsets in  $^{87}\text{Sr}/^{86}\text{Sr}$  and  $^{143}\text{Nd}/^{144}\text{Nd}$  ratios between the whole rocks and clinopyroxenes may therefore be attributable mainly to these secondary phases. Similar results have been observed for ultramafic xenoliths from many other localities (eg. Zindler and Jagoutz, 1988). Identification of the sources of such secondary phases is crucial in extracting information concerning the upper mantle processes from these xenolith whole rock data.

The host basalt has a  $^{87}\text{Sr}/^{86}\text{Sr}$  ratio of 0.70269, comparable to the previous

Table 8: Sm, Nd, Sr concentrations and Nd and Sr isotopic ratios for the ultramafic xenolith whole rocks and host basaltoid from West Kettle River.

Sample	Sm (ppm)	Nd (ppm)	$^{147}\text{Sm}/$ $^{144}\text{Nd}$	$^{143}\text{Nd}/$ $^{144}\text{Nd}$ <sup>3</sup>	$\epsilon_{\text{Nd}}$	Sr (ppm)	$^{87}\text{Sr}/$ $^{86}\text{Sr}$ <sup>3</sup>	
KR-35 WR	0.307	1.032	0.179	$0.512991 \pm 21$ <sup>2</sup>	6.03	64.27	$0.70408 \pm 6$ <sup>1</sup>	
				$0.512947 \pm 12$ <sup>2</sup>			62.99	$0.70403 \pm 7$
				$0.512949 \pm 26$ <sup>2</sup>				$0.70411 \pm 5$
								$0.70409 \pm 2$
KR-37 WR	$0.305$ <sup>2</sup>	$1.827$ <sup>2</sup>	$0.101$ <sup>2</sup>	$0.510999 \pm 16$ <sup>2</sup>	-31.09	11.52	$0.70448 \pm 7$ <sup>1</sup>	
	$0.309$ <sup>2</sup>	$1.861$ <sup>2</sup>	$0.100$ <sup>2</sup>	$0.511044 \pm 15$ <sup>2</sup>				
KR-141 WR	0.175	0.486	0.217	$0.513065 \pm 19$ <sup>2</sup>	8.33	33.15	$0.70426 \pm 5$	
				$0.513070 \pm 42$ <sup>2</sup>			$0.70427 \pm 6$	
KR-4000 WR	0.189	0.972	0.119	$0.513034 \pm 37$	7.72	65.76	$0.70504 \pm 1$	
	0.191					66.65	$0.70498 \pm 3$ <sup>1</sup>	
KR-4001 WR	0.155	0.408	0.229	$0.512953 \pm 47$	6.15	8.319	$0.70349 \pm 5$	
		0.483					$0.70368 \pm 6$	
KR-4002 WR	0.222	0.531	0.252	$0.513283 \pm 16$	12.58	16.16	$0.70391 \pm 2$	
	0.218	0.501	0.262					
KR-4003 WR	0.420	1.838	0.138	$0.513087 \pm 19$	8.76	47.26	$0.70398 \pm 1$	
							$0.70399 \pm 2$	
KR-4005 WR	0.348	1.430	0.147	$0.513002 \pm 48$	7.10	51.34	$0.70422 \pm 1$	
KR-4016 WR	0.212	0.526	0.243	$0.513175 \pm 23$	10.48	19.21	$0.70422 \pm 3$	
							$0.70381 \pm 3$	
KR-3020BWR	0.544	1.811	0.182	$0.513053 \pm 23$	7.78	44.1	$(0.70360 \pm 8)$	
				$0.513037 \pm 9$				
KRBWC-1	9.28345	3.917	0.124	$0.513080 \pm 14$	8.629	70.5	$0.70269 \pm 1$	
							$0.70268 \pm 2$	

<sup>1</sup> Ratios calculated from the isotope dilution analyses.

<sup>2</sup> Data obtained prior to Sept., 1987.

<sup>3</sup> Errors quoted are derived from  $2\sigma$  standard deviations.

Table 9: Sm, Nd, Sr concentrations and Nd and Sr isotope ratios for the clinopyroxenes and olivines in ultramafic xenoliths from West Kettle River.

Sample	Sm (ppm)	Nd (ppm)	$^{147}\text{Sm}/$ $^{144}\text{Nd}$	$^{143}\text{Nd}/$ $^{144}\text{Nd}^2$	$\epsilon_{\text{Nd}}$	Sr (ppm)	$^{87}\text{Sr}/$ $^{86}\text{Sr}^2$
KR-35 Cpx	2.015	5.639	0.216	0.513102 ± 16	9.05	88.82	0.70305 ± 8
KR-37 Cpx	1.186	5.592	0.128	0.512962 ± 17	6.32	56.53	0.70311 ± 3 0.70299 ± 3 <sup>1</sup>
KR-141 Cpx	1.515	3.687	0.248	0.513150 ± 31	9.99	68.24	0.70264 ± 1 0.70269 ± 3 <sup>1</sup> 0.70273 ± 4
KR-4000 Cpx	0.964	4.644	0.125	0.513104 ± 13	9.09	80.04	0.70289 ± 8
KR-4001 Cpx	1.135	2.996	0.229	0.513017 ± 12	7.39	55.82	0.70350 ± 9 0.70342 ± 2 <sup>1</sup>
KR-4002 Cpx	1.917	4.218	0.275	0.513353 ± 16	13.95	40.53	0.70223 ± 1 0.70229 ± 7 <sup>1</sup>
KR-4003 Cpx	2.059	5.739	0.217	0.512734 ± 42	1.87	77.83	0.70282 ± 7 0.70268 ± 5 <sup>1</sup>
KR-4005 Cpx	1.927	5.084	0.229	0.513145 ± 15	9.89	70.43	0.70258 ± 2 0.70256 ± 5 <sup>1</sup> 0.70269 ± 3 0.70261 ± 2
KR-4016 Cpx	1.923	4.560	0.255	0.513252 ± 14 0.513262 ± 13	12.17	51.37	0.70261 ± 9
KR-35 Ol-1 <sup>3</sup>			0.114				0.70439 ± 1
Ol-2 <sup>3</sup>			0.102				0.70438 ± 2
KR-37 Ol-1 <sup>3</sup>			0.983	0.511680 ± 18			0.70368 ± 1
Ol-2 <sup>3</sup>			0.967				0.70474 ± 1

<sup>1</sup> Ratios calculated from the isotope dilution analyses.

<sup>2</sup> Errors quoted are derived from 2-σ standard deviations.

<sup>3</sup> The olivines are crudely picked mineral concentrates with variable amounts of pyroxenes, which were removed after olivine dissolved with HCl. No acid leaching was applied to these olivines.

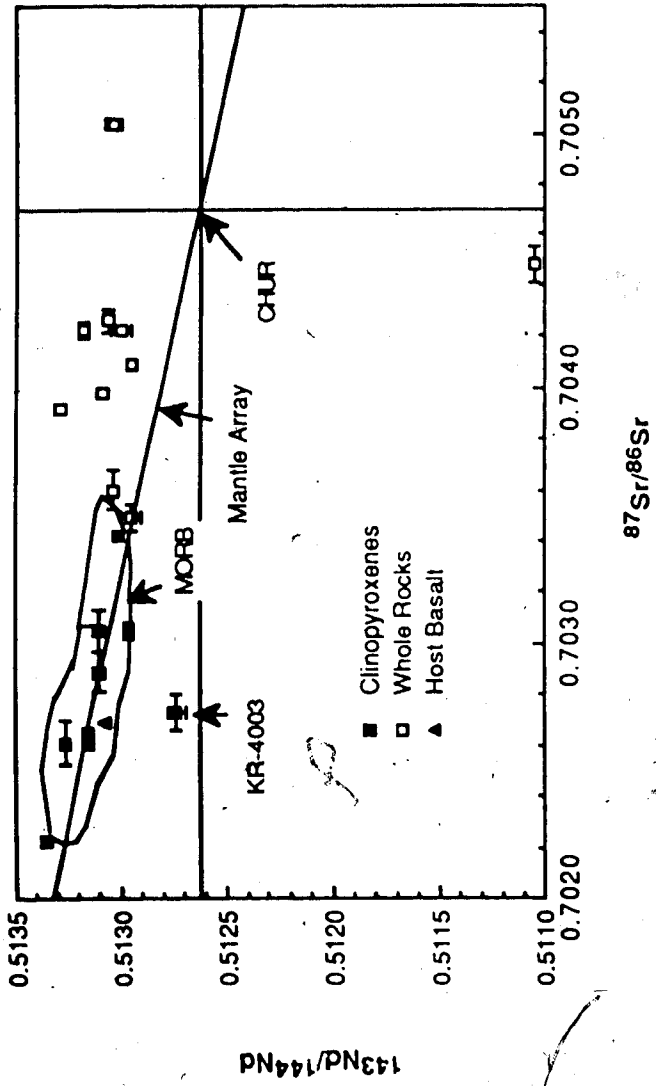


Fig. 11. Nd - Sr isotope diagram for clinopyroxenes and whole rocks of ultramafic xenoliths and host basanitoid from West Kettle River. Also plotted for comparison is the range for MORB (Zindler and Hart, 1986) and the mantle array (Faure, 1986). Error bars are derived from  $2\sigma$  standard deviations.

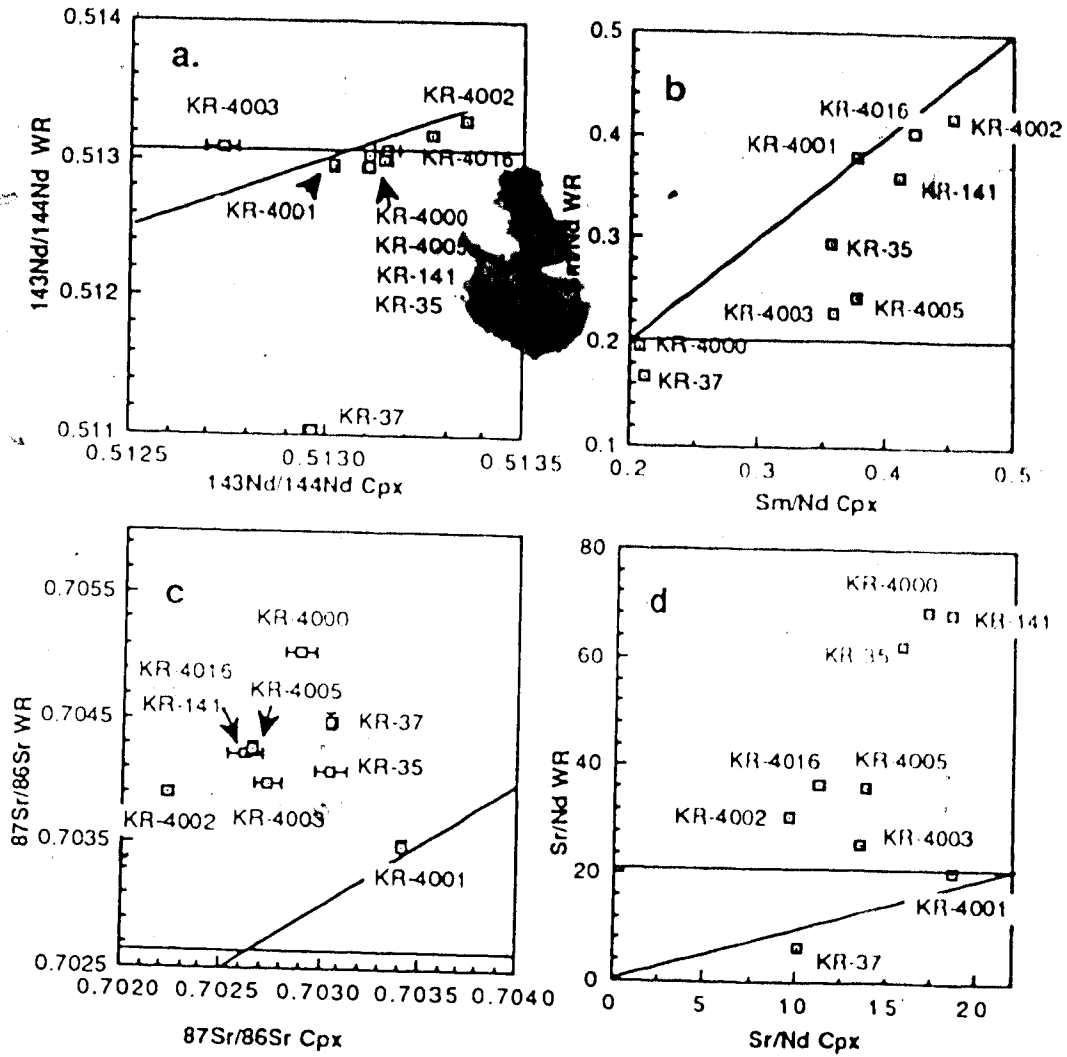


Fig. 12. Comparison of the  $^{143}\text{Nd}/^{144}\text{Nd}$  (a),  $\text{Sm}/\text{Nd}$  (b),  $^{87}\text{Sr}/^{86}\text{Sr}$  (c) and  $\text{Sr}/\text{Nd}$  (d) ratios between the whole rocks and clinopyroxenes for ultramafic xenoliths from West Kettle River. The horizontal line represents the composition of the host basaltoid. The slope line represents identical ratios between the whole rocks and clinopyroxenes (slope = 1). Host basalt contamination would result in the xenoliths falling between these two lines.

analysis (Sun, 1985) and a  $^{143}\text{Nd}/^{144}\text{Nd}$  ratio of 0.51308 (Table 8). It therefore falls within the range of the clinopyroxenes in the Nd - Sr isotope plot (Fig. 11).

## 2.. Problem of inter-mineral isotope equilibrium

Since over 80 % of the Sr and REE in the mineral phases of anhydrous mantle xenoliths are concentrated in clinopyroxenes (Zindler and Jagoutz, 1988; Stosch, 1982), the isotope compositions of clinopyroxenes are identical with those of the clean whole rocks (free from secondary contaminations), as long as significant isotopic disequilibrium among the coexisting minerals is lacking.

The question of inter-mineral isotope equilibrium in mantle xenoliths has received much attention since the 1970s (see reviews in Zindler and Jagoutz, 1988; Stosch et al., 1986). In the earlier studies, large isotope differences among the coexisting minerals were documented and were interpreted as resulting from radiogenic growth of Sr and Nd (Paul, 1971; Kudo et al., 1972; Stueber and Ikramuddin, 1974; Burwell, 1975; Dasch and Green, 1975). It was later recognized that these results were biased by the ubiquitous secondary contaminations (eg. Zindler and Jagoutz, 1988). More recent data on mantle xenoliths from diverse localities, such as Kilbourne Hole, New Mexico (Jagoutz et al., 1980), Peridot Mesa, Arizona (Zindler and Jagoutz, 1988), Tariat Depression, Mongolia (Stosch et al., 1986), South Africa (Richardson et al., 1985) and Malaita, Solomon Island (Rubenstone and Zindler, in prep.), demonstrated that inter-mineral Sr and Nd isotope equilibrium is generally attained for anhydrous ultramafic xenoliths. Experimental determinations of Sr and Sm diffusion rates (Sneeringer et al., 1984) indicate that these elements diffuse fast enough, at temperatures in excess of 1050°C, to keep pace with the radiogenic growth and therefore to maintain inter-mineral isotope equilibrium in a closed system (Zindler and Jagoutz, 1988). Stosch et al. (1986) suggest that this conclusion could be extended to temperatures as low as 950°C. It seems that isotope equilibrium between coexisting minerals in mantle xenoliths is the rule, rather than the exception.

The problem of inter-mineral isotope equilibrium for West Kettle River xenoliths may be evaluated through comparison of the whole rock and clinopyroxene data for those xenoliths that were least affected by secondary phases. KR-4001 is the only sample investigated in which the bulk of the Sr, Sm and Nd are contributed by the



major mineral phases. The nearly identical  $^{143}\text{Nd}/^{144}\text{Nd}$  and  $^{87}\text{Sr}/^{86}\text{Sr}$  ratios between its whole rock and clinopyroxene (Fig. 11, 12a,c) indicate apparent inter-mineral isotope equilibrium.

Direct measurements on the constituent clinopyroxenes, orthopyroxenes and olivines of ultramafic xenoliths from West Kettle River and similar localities in south-central British Columbia (Sun, 1985), on the contrary, have shown inter-mineral Sr isotope disequilibrium, which were interpreted as radiogenic growth of Sr. If this argument is valid, the Sr isotopic ratios of the clinopyroxenes would not be representative of those of the clean whole rocks. However, the averages of the calculated Sr partition coefficients for olivine/cclinopyroxene and orthopyroxene/cclinopyroxene in these xenoliths (Table 10) are about 15 and 35 times higher than those from Zindler and Jagoutz (1988). The coexisting minerals in these xenoliths are apparently out of chemical (Sr) equilibrium. Incomplete removal of the secondary phases (which occur as inclusions or interstitially), rather than radiogenic growth, may be responsible for the apparent Sr isotope disequilibrium in these xenoliths. These results cannot therefore disapprove the assumption of inter-mineral isotopic diffusive equilibrium. Since clinopyroxene has the highest Sr and REE abundances, it is least affected by the secondary contaminants among the coexisting minerals. With the assumption of inter-mineral isotope equilibrium, the Sr and Nd isotope ratios of the clinopyroxenes should be closest to, if not identical with, the values indigenous to the original mantle sources (whole rocks) (Stosch et al., 1980).

### 3. Sources of the secondary phases

The isotopic characteristics of the secondary phases in the ultramafic xenoliths can be inferred through comparison between the Sr and Nd isotopic systems of the clinopyroxenes (which are assumed to be identical to those of the clean whole rocks) and the measured whole rocks (Fig. 12a-d). These results, together with mass balance calculations and bulk REE data (Chapter V), may allow us to identify the sources of the secondary phases.

One possible source for the secondary phases is ground water contamination. The characteristics of the ground water may be established from the weathered xenolith (harzburgite KR-37). Its whole rock REE pattern has been shown to be distinctly

Table 10. Sr partition coefficients calculated for ultramafic xenoliths from south-central British Columbia (Data from Sun, 1985)

	Opx/Cpx	OI/Cpx
BM11	0.190	0.644
BM16	0.039	0.0446
BM55	0.0224	0.0078
KR35	0.0167	0.00664
KR2	0.0447	0.012
JL18	0.0176	0.00972
JL15	0.0508	0.00598
JL14	0.0392	0.0194
JL1	0.0367	0.0045
LL1	0.0297	0.0081
LL14	0.0472	0.0295
Average	0.0456	0.0182
Zindler & Jagoutz (1988)	0.00274	0.000522

BM = Big Timothy Mountains; KR = West Kettle River;  
 JL = Jacques Lake; LL = Lassie Lake; Also for comparison  
 are the average Sr partition coefficients obtained by  
 Zindler and Jagoutz (1988)

different from the other xenoliths by its strong negative Eu anomaly (Chapter V). Fig. 12a indicates that KR-37 also distinguishes itself in its markedly low whole rock  $^{143}\text{Nd}/^{144}\text{Nd}$  ratio relative to that of its clinopyroxene, a feature that is not demonstrated by the fresh xenoliths. One uncleaned olivine fraction from KR-37 gives a similarly low  $^{143}\text{Nd}/^{144}\text{Nd}$  (Table 9). Since clean olivine contains negligible amounts of Sr and Nd (Stosch, 1982; Zindler and Jagoutz, 1988), the isotope ratios of this uncleaned olivine largely reflect that of the secondary phases. The  $^{87}\text{Sr}/^{86}\text{Sr}$  of the whole rock and two uncleaned olivines of KR-37 are all significantly higher than the clinopyroxene (Table 8, 9; Fig. 12c). If these features can be solely attributed to weathering, the ground water must have a very low  $^{143}\text{Nd}/^{144}\text{Nd}$  ratio ( $\leq 0.51104$ ) and high  $^{87}\text{Sr}/^{86}\text{Sr}$  ratio ( $\geq 0.7045$ ), which are consistent with the inference that the original source of the ground water precipitation (as interstitial phases in the weathered xenoliths) may be the nearby Precambrian gneisses (see Chapter V). Few isotope data on ground water have been reported. A caliche filling in a mantle xenolith from Peridot Mesa, Arizona gave a  $^{87}\text{Sr}/^{86}\text{Sr}$  ratio of 0.70571 and  $^{143}\text{Nd}/^{144}\text{Nd}$  of 0.502687 (Zindler and Jagoutz, 1988). A HCl leach from a whole rock xenolith from Kilbourne Hole, New Mexico, believed to be representative of the ground water contaminant, has a similarly high  $^{87}\text{Sr}/^{86}\text{Sr}$  ratio (0.7055), but higher  $^{143}\text{Nd}/^{144}\text{Nd}$  ratio (0.512971) (Jagoutz et al., 1980). If the compositions of the ground water are buffered by the surrounding rocks, regional variations in the isotopic ratios of the ground water are conceivable. The ground water in the vicinity of West Kettle River may be characterized by high Sr, low REE contents and high  $^{87}\text{Sr}/^{86}\text{Sr}$ , low Sm/Nd, low  $^{143}\text{Nd}/^{144}\text{Nd}$  ratios. If this inference is valid, mild ground water contamination on the ultramafic xenoliths may cause significant increase in the whole rock  $^{87}\text{Sr}/^{86}\text{Sr}$  ratios and little or slight decrease in the whole rock  $^{143}\text{Nd}/^{144}\text{Nd}$  ratios.

Lherzolite KR-141, KR-4002, KR-4016 contain the bulk of the whole rock Sm and Nd and less than half of the Sr in the major mineral phases (Fig. 9). Their whole rock  $^{143}\text{Nd}/^{144}\text{Nd}$  and Sm/Nd ratios are similar to, or slightly lower than, those of the constituent clinopyroxenes and whole rock  $^{87}\text{Sr}/^{86}\text{Sr}$  and Sr/Nd ratios much higher than the clinopyroxenes (Fig. 12a-d). The  $^{87}\text{Sr}/^{86}\text{Sr}$  of two uncleaned olivine fractions of KR-35, largely representative of the secondary phases, gave similarly high  $^{87}\text{Sr}/^{86}\text{Sr}$  ratios (Table 9). If the inferred ground water isotopic compositions

are valid, these features could be accounted for by ground water contamination. In fact, high  $^{87}\text{Sr}/^{86}\text{Sr}$  ratios characterize almost all the whole rocks and HCl leachates of mantle xenoliths from West Kettle River (also see Sun, 1985), despite of the more variable Nd isotope ratios (Fig. 12a,c). It is likely that ground water contamination is ubiquitous and is responsible for these high  $^{87}\text{Sr}/^{86}\text{Sr}$  ratios. Ground water contaminations have also been widely recognized for mantle xenoliths elsewhere (eg. Jagoutz et al., 1980; Zindler and Jagoutz, 1988).

The whole rock Sr and Nd isotope features of lherzolites KR-4005, KR-35 and harzburgite KR-4000 (Fig. 12a-d) can be similarly accounted for by ground water contamination. However, as discussed in chapter V, the secondary phases in these xenoliths contain a considerable amount of Nd (Fig. 9), which requires an additional Nd-rich source. Interaction with the host basalt or a metasomatic fluid, from a mantle source that is isotopically similar to the host basalt, can explain these features.

The whole rock Sr isotope of lherzolite KR-4003 is not unlike the other xenoliths and could be attributed to ground water contamination. However, this xenolith is distinct in terms of the Nd isotope composition of the secondary phases. A  $^{143}\text{Nd}/^{144}\text{Nd}$  ratio of 0.5135 or higher, similar to that of KR-4002 clinopyroxene, is required for the secondary phases in KR-4003, in order to account for the difference in the Nd isotope ratios between its whole rock and clinopyroxene (Fig. 12a), as well as to account for the Nd mass balance (Fig. 9). The overall whole rock Sr and Nd isotopes of KR-4003 could be explained by a very recent mantle metasomatism by a fluid from an isotopically depleted region, superimposed by ground water contamination. Alternatively a mantle metasomatic fluid with both high Sr and Nd isotopic ratios could also explain these data. However, considering the ubiquitous presence of ground water contamination, the first explanation is preferred. The abundant fluid inclusions in this xenolith may be related to this inferred mantle metasomatism.

In summary, only one sample (KR-4001) appears to have escaped significant secondary contamination. Ground water contamination seems to be ubiquitous and may have affected most of the xenoliths, causing significant increase in their whole rock  $^{87}\text{Sr}/^{86}\text{Sr}$  ratios. The effect of ground water contamination on the whole rock Nd isotopes and REE patterns is possibly minor, unless the xenoliths have been severely weathered (eg. KR-37). After the effect of the ground water contamination is

established, it is revealed that three of the xenoliths (KR-4000, KR-4005, KR-35) may have interacted with the host basalt or a metasomatic fluid that was derived from a mantle source isotopically similar to the host basalt, and one lherzolite (KR-4003) may have interacted with a metasomatic fluid from an isotopically more depleted mantle source. Since these secondary processes have only affected the whole rocks (resulting in the presence of the secondary interstitial or inclusion phases), but not the clinopyroxenes, the mantle evolution prior to these secondary processes can still be evaluated by study of the clean clinopyroxenes in the xenoliths.

## VII. Oxygen Isotope Geochemistry

Oxygen isotopes present another useful tracer to mantle processes. Oxygen comprises almost half of the mass of the mantle and variations in its isotopic composition can arise from different physical-chemical mechanisms than those causing variations in the trace elements and radiogenic isotopes (Kyser, 1986). Thermodynamic theory predicts that oxygen isotope fractionations between anhydrous silicates are small at high temperatures and vary as a function of temperature in a closed system (Kieffer, 1982). However, much greater  $^{18}\text{O}/^{16}\text{O}$  variations than theoretically expected were reported recently for mantle xenoliths from southwest U.S.A. and central Europe (Kyser et al., 1981). There is considerable debate over whether these variations have resulted from closed system fractionation or non-equilibrium metasomatic exchange with an external fluid (Kyser et al., 1981, 1982, 1986; Kyser, 1986; Gregory and Taylor, 1986a, b).

Five West Kettle River Group I spinel lherzolites were analyzed for oxygen isotope composition (Table 11). The  $\delta^{18}\text{O}$  of their constituent olivines ranges from 5.06 to 5.35; orthopyroxenes from 5.69 to 6.32; clinopyroxenes from 5.22 to 5.82 and whole rocks from 5.26 to 5.57. These values are within the range for similar mantle xenoliths elsewhere (Kyser et al., 1981; Harmon et al., 1987), but have much smaller variations (Fig. 13). The  $\delta^{18}\text{O}$  fractionation between coexisting minerals is generally small and has a relative  $\delta^{18}\text{O}$  enrichment sequence of Orthopyroxene > Clinopyroxene > Olivine (Table 11). Sample KR-35 differs from the other West Kettle River xenoliths in having large  $\Delta_{\text{opx-cpx}}$  (1.10) and  $\Delta_{\text{opx-ol}}$  (1.16), but very small  $\Delta_{\text{cpx-ol}}$  (0.06) (Table 11). Except for sample KR-35, the range defined by the West Kettle River xenoliths is 0.1 - 0.3 for  $\Delta_{\text{opx-cpx}}$ , 0.6 - 0.7 for  $\Delta_{\text{opx-ol}}$  and 0.4 - 0.5 for  $\Delta_{\text{cpx-ol}}$ .

The oxygen isotopes of West Kettle River ultramafic xenoliths are similar to those of the xenolith suite from Tariat Depression, Mongolia (Harmon et al., 1987), in that both have limited ranges of  $\delta^{18}\text{O}$  (Fig. 13) and similar relative  $\delta^{18}\text{O}$  enrichment. These xenoliths have possibly not been significantly affected by mantle metasomatic processes and their consistent relative  $\delta^{18}\text{O}$  enrichment sequence (Opx > Cpx > Ol) may reflect the equilibrium fractionation factors among these minerals. In

Table 11. Oxygen isotope data for ultramafic xenoliths from West Kettle River

Sample No.	$\delta^{18}O$ (‰ SMOW)			Fractionation (‰)			Temperature (°C)			
	OI	Opx	Cpx	WR	$\Delta cpx-ol$	$\Delta opx-ol$	$\Delta opx-cpx$	1	2	3
KR-35	5.16	6.32	5.22	5.56	0.06	1.16	1.10	987	1140	3378
KR-3017	5.35	5.98	5.71	5.57	0.36	0.63	0.27	916	1080	1218
KR-3020	5.06	5.77	5.57	5.26	0.51	0.71	0.20	937	1045	979
KR-3020B		5.93	5.82				0.11	899		
KR-3003		5.69								
KR-141		5.70	5.54				0.16	898		

\* Calculated whole rock  $\delta^{18}O$  based on mineral  $\delta^{18}O$  values and sample modal compositions (excluding spinel). 1.

1. Based on the two-pyroxene geothermometer (Wells, 1977);

2. Based on the empirical oxygen isotope geothermometer (Kyser et al., 1981);

3. Based on theoretically derived geothermometer (Kieffer, 1982).

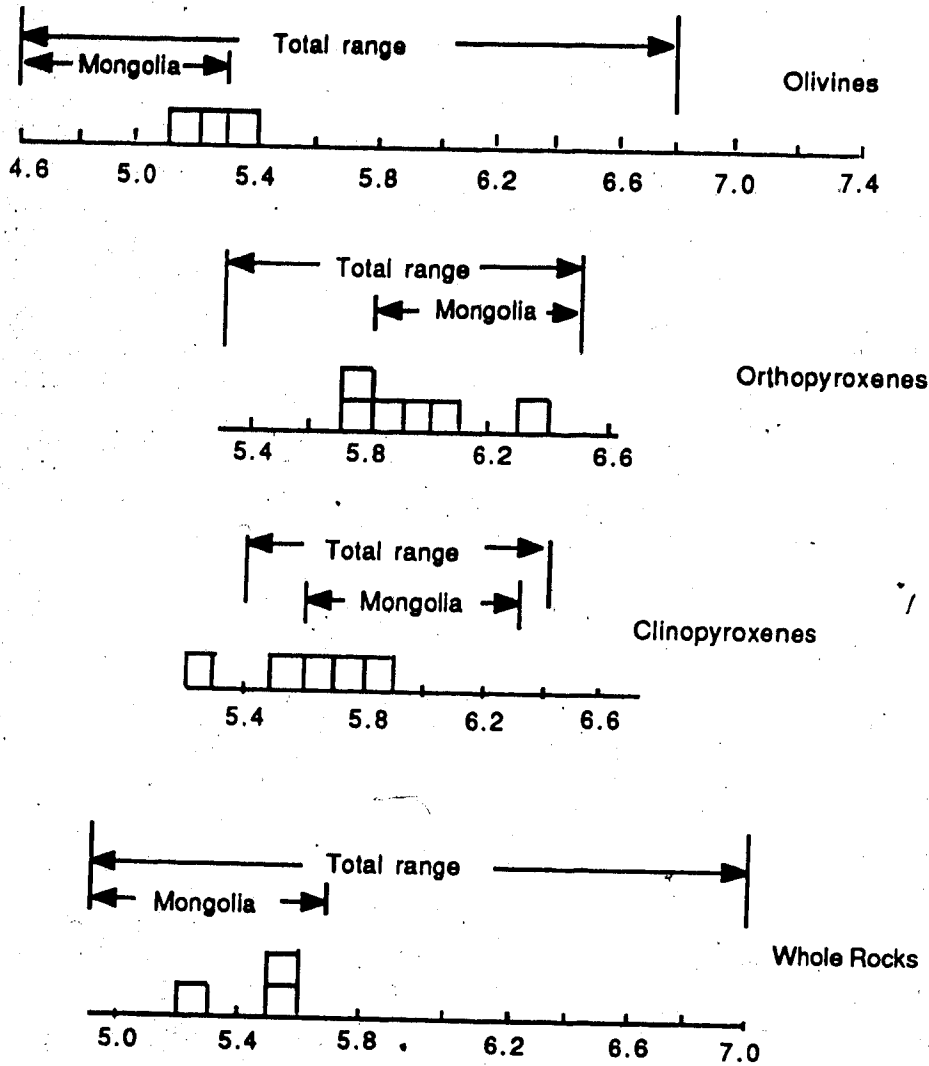


Fig. 13. Comparison of  $\delta^{18}\text{O}$  data for West Kettle River ultramafic xenoliths with the (total) range of the reported  $\delta^{18}\text{O}$  values for continental alkalic basalt-hosted ultramafic xenoliths worldwide (Kyser et al., 1981; Harmon et al., 1987). Also shown is the range for  $\delta^{18}\text{O}$  of ultramafic xenoliths from Tariat Depression, Mongolia (Harmon et al., 1987).



the  $\delta - \delta$  diagrams, all the West Kettle River xenoliths, except sample KR-35, fall close to an array parallel to the zero oxygen fractionation line ( $\Delta_{x-y} = 0$ ) (Fig. 14). Gregory and Taylor (1986 a, b) have demonstrated that such an array represents an isothermal equilibrium line, which is in accord with the limited temperature range (898-987°C) of these xenoliths (Table 11). Sample KR-35 plots off this array in these  $\delta - \delta$  diagrams (Fig. 14). Its large  $\Delta_{\text{opx-ol}}$  (1.16) suggests that the coexisting minerals may be out of oxygen isotope equilibrium (Kyser et al., 1981). KR-35 may have been subjected to a recent mantle metasomatism.

The clinopyroxene and orthopyroxene in an olivine websterite (KR-3020B) of a composite Group I xenolith has slightly higher  $\delta^{18}\text{O}$  values than the corresponding minerals in the host lherzolite (KR-3020) (Table 11). As discussed earlier, the websterite band very likely represents precipitates from a silicate melt (see chapter V). Its higher  $\delta^{18}\text{O}$  and smaller  $\Delta_{\text{opx-cpx}}$  than the host lherzolite may suggest that oxygen isotope equilibrium are not attained between the websterite and the host lherzolite. However, it should be noted that the differences in the oxygen isotopes are only marginally higher than the analytical uncertainties and are within the variations for the West Kettle River xenolith suite. Differences in their mineral compositions (Appendix IV) and element partition temperatures (Table 11) also seem to be within error. It cannot, therefore, be excluded that these differences in the oxygen isotope ratios may be only due to analytical uncertainties.

Plots of KR-3017 and KR-3020B on the  $\Delta_{\text{ol-cpx}}$  versus temperature diagram (Fig. 15) gives a temperature of 1200°C or higher by using Javoy (1977) and Mayeda et al. (1986)'s data and 1050-1100°C by using Kyser et al. (1981)'s empirical geothermometer. KR-35 is not plotted considering the possibility of its oxygen isotope disequilibrium. These oxygen isotope temperatures are higher than the element partition temperatures (ca. 900°C) (Table 11), possibly due to discrepancy in the calibration of the different geothermometers.

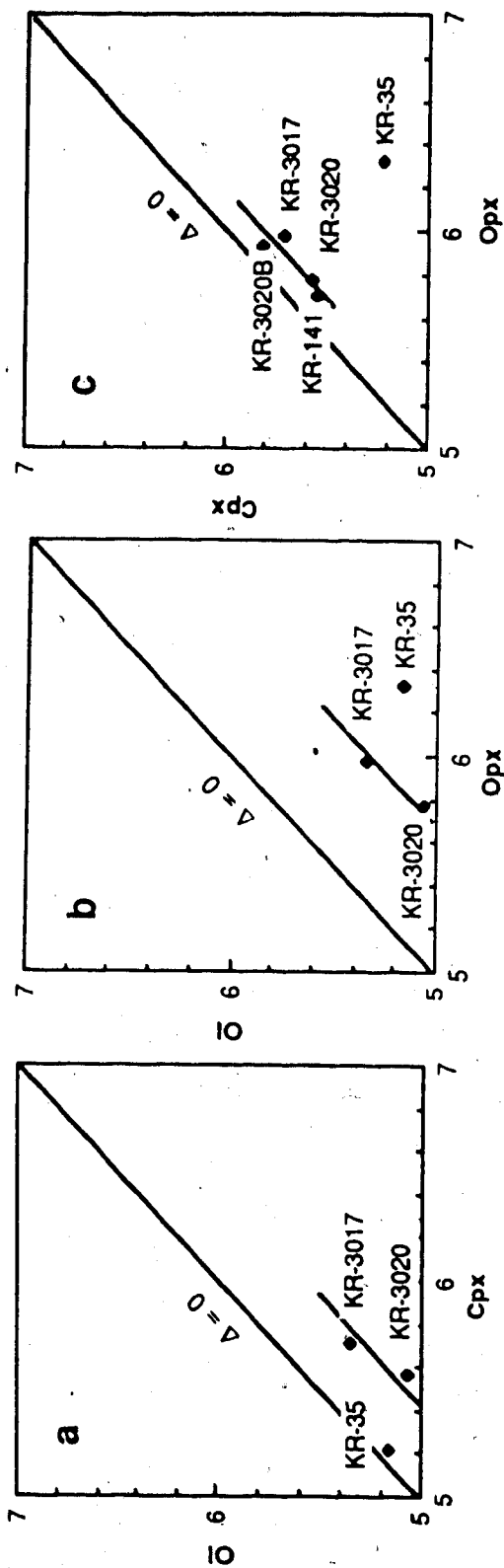


Fig. 14. Plot of (a)  $\delta^{180} \text{OI}$  (‰ SMOW) versus  $\delta^{180} \text{Cpx}$  (‰ SMOW); (b)  $\delta^{180} \text{OI}$  (‰ SMOW) versus  $\delta^{180} \text{Opx}$  (‰ SMOW) and (c)  $\delta^{180} \text{Cpx}$  (‰ SMOW) versus  $\delta^{180} \text{Opx}$  (‰ SMOW), for ultramafic xenoliths from West Kettle River.

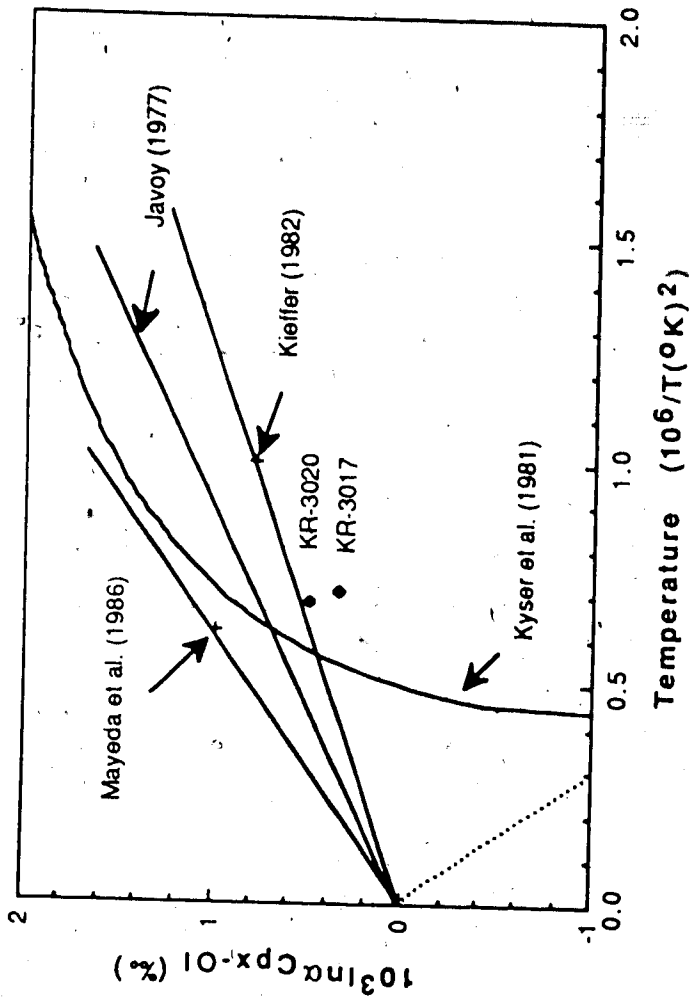


Fig. 15. Plot of clinopyroxene-olivine  $\delta^{18}\text{O}$  fractionation ( $10^3 \ln \alpha_{\text{Cpx-Ol}}$ ) as a function of temperature (Wells, 1977) ( $10^6/T(^\circ\text{K})^2$ ) for ultramafic xenoliths from West Kettle River. Together shown are the empirical fractionation curves of Javoy (1977) and Kyser et al. (1981), the 1000°K fractionation value calculated by Kieffer (1982) and the 1000°C fractionation value determined experimentally by Mayeda et al. (1986).

## VIII. Discussion

### 1. Chemical variations of the upper mantle beneath West Kettle River

#### (1) Undepleted upper mantle composition

The chemical and mineralogical variations of the Group I lherzolite and harzburgite xenoliths are very likely derived from variable degrees of partial melting of the upper mantle. The lherzolites with the highest CaO, Al<sub>2</sub>O<sub>3</sub> and lowest MgO and Mg/(Mg+Fe) are therefore closest to the primitive upper mantle composition. In Table 12 the chemical compositions of the three most fertile lherzolites from West Kettle River are compared with the estimated primitive upper mantle compositions, derived from the compositions of ultramafic xenoliths and/or partial melting model calculations (Ringwood, 1979; Jagoutz et al., 1979; Sun, 1982; Wanke, 1981; Palme and Nickel, 1985). Most of these estimated primitive upper mantle compositions are very similar to the pyrolite model of Ringwood (1979), except that derived by Palme and Nickel (1985), which has significantly lower MgO and higher CaO and Al<sub>2</sub>O<sub>3</sub> concentrations. The compositions of the fertile lherzolites from West Kettle River are very similar to that of the pyrolite and can therefore be assumed to represent the undepleted upper mantle composition beneath West Kettle River. The Mg/(Mg+Fe) ratios of these lherzolites (0.893) (Table 4) are, however, higher than that of the most primitive lherzolite (sample PA-15) from San Carlos, Arizona (0.881) (Frey and Prinz, 1978). High Mg/(Mg+Fe) ratios of these ultramafic xenoliths have been interpreted as evidence for the depleted nature of the upper mantle beneath south-central British Columbia (eg. Canil et al., in prep.). The similarity of the modal percentages of clinopyroxenes and the bulk CaO, Al<sub>2</sub>O<sub>3</sub> and MgO between the fertile lherzolites from both regions does not seem to agree with such an interpretation. Fig. 16 shows that the difference in Mg/(Mg+Fe) is not due to variable degrees of partial melting, but rather, is derived from the different FeO contents in the upper mantle beneath these two localities. Spinel lherzolites from Tariat Depression, Mongolia have comparable FeO contents to that of the West Kettle River xenoliths (Fig. 16). Preß et al. (1986) ascribe the variable Fe/Mg in different localities to the slight global heterogeneity of primitive upper mantle. Interestingly, the mantle xenoliths from Summit Lake, central British Columbia (Smith, 1986; Brearley et al., 1984) also

Table 12. Compositions of the fertile West Kettle River lherzolites compared to those estimated for the primitive upper mantle in the literature

	Primitive Upper mantle					Fertile KR Xenoliths		
	1	2	3	4	5	4001	4003	4005
SiO <sub>2</sub>	46.2	45.1	45.1	44.5	45.1	44.92	44.80	44.85
TiO <sub>2</sub>	0.23	0.22	0.2	0.22	0.22	0.08	0.17	0.15
Al <sub>2</sub> O <sub>3</sub>	4.75	4.14	3.3	4.31	3.97	3.51	4.26	4.02
Cr <sub>2</sub> O <sub>3</sub>	0.43	0.45	0.4	0.39	0.46	0.43	0.40	0.39
FeO	7.70	7.82	8.0	8.37	7.82	7.80	8.03	8.05
NiO	0.23	0.27	--	0.25	0.27	0.24	0.23	0.25
MnO	0.13	0.13	0.15	0.14	0.13	0.13	0.14	0.14
MgO	35.5	38.0	38.1	38.0	38.3	37.75	37.50	37.86
CaO	4.36	3.54	3.1	3.50	3.5	3.38	3.46	3.36
Na <sub>2</sub> O	0.40	0.36	0.4	0.40	0.33	0.00	0.20	0.15

1. Palme and Nickel (1985)
2. Wanke (1981)
3. Ringwood (1979)
4. Sun (1982)
5. Jagoutz et al. (1979)

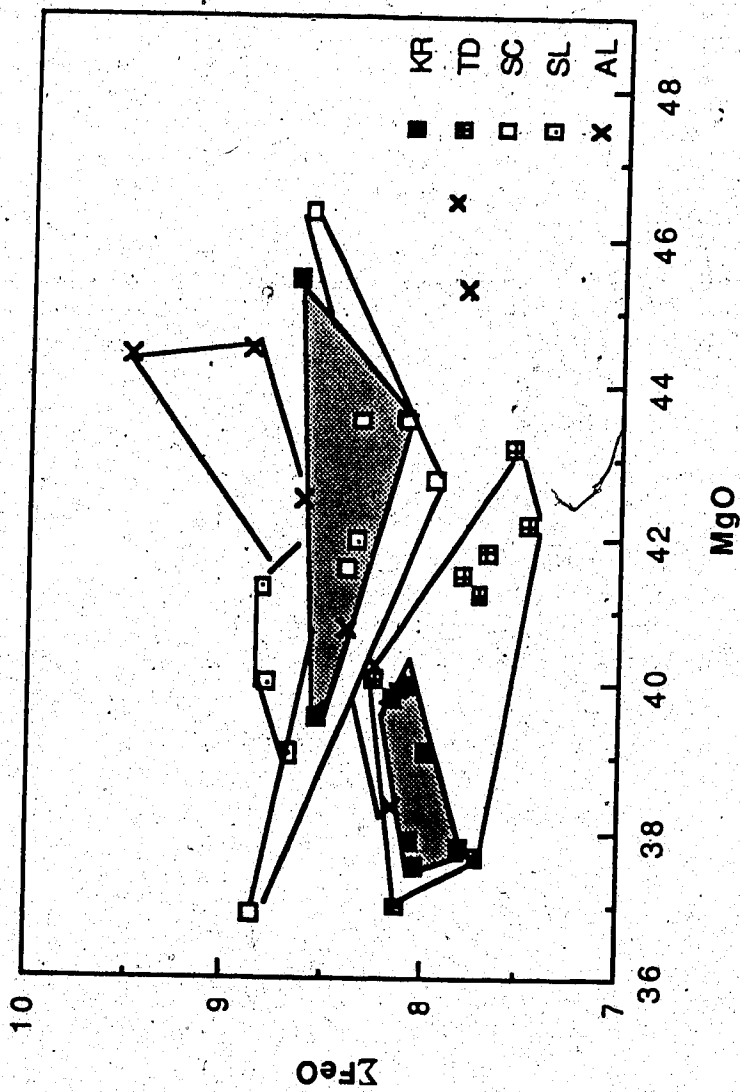


Fig. 16. Total Fe as FeO versus MgO for Group I peridotites from West Kettle River (KR), Summit Lake (British Columbia) (SL), Tariat Depression (Mongolia) (TD), San Carlos (U.S.A.) (SC) and Alligator Lake (Yukon) (AL).

has high FeO contents, similar to those of the San Carlos xenoliths (Fig. 16). Variation of the FeO contents in the upper mantle beneath south-central British Columbia has also been observed from the mineral compositions of the xenolith suites in different localities (Canil et al., in prep.). If the interpretation of Preß et al. (1986) is valid, the primitive upper mantle beneath south-central British Columbia must have been heterogeneous in FeO content. Alternatively, the higher FeO contents in the ultramafic xenoliths from San Carlos and Summit Lake may be a consequence of more extensive reaction with Fe-rich silicate melts in the upper mantle. A possible example of melt-xenolith reaction is presented by ultramafic xenoliths from Alligator, Yukon (Francis, 1987), which have FeO contents traversing the range of both the San Carlos and Mongolia xenolith suites (Fig. 16). The compositional variations of these lherzolites are toward the Fe-rich harzburgites, rather than Mg rich harzburgites (Fig. 16). Francis (1987) suggests that the composition of the upper mantle represents an important buffer for magmas migrating towards the Earth's surface. In this sense, the majority of the West Kettle River xenoliths may have less interacted with silicate melts than the Summit Lake and San Carlos xenoliths. Three of the West Kettle River xenoliths (two harzburgites and one lherzolite) have comparable FeO contents to the San Carlos and Summit Lake xenolith suites (Fig. 16) and, as will be discussed later, may have been metasomatized by silicate melts migrating in the upper mantle.

#### (2) Compositions of the melts equilibrated with mantle xenoliths

There have been some attempts to model the compositions of the melts that equilibrated with the peridotite xenoliths (eg. Nickel and Green, 1984; Francis, 1987). The numerous melting experiment results both on synthesized and natural peridotites at various pressures and temperatures (eg. Fujii and Scarfe, 1982b; Mysen and Kushiro, 1977; Takahashi, 1984) provide us with a guideline. It has been well established that at lower pressures (10 - 25 Kb), melting of anhydrous pyrolite will produce alkaline basalt or tholeiite melts leaving a lherzolite residue with lower degrees of partial melting, and produce tholeiite melt and harzburgite residues, with higher degrees of partial melting. At elevated pressure (>25 Kb), the melts will become increasingly more MgO-rich (picrite or komatiite), leaving a lherzolite or harzburgite residue (eg., Takahashi and Kushiro, 1983). Assuming a batch melting model, it can be demonstrated that the lherzolite and harzburgites from West Kettle

Table 13. Mantle source compositions calculated from the compositions of West Kettle River xenoliths and various melts, assuming a batch melting model. (X = degree of partial melting)

	Tholeiite Model <sup>2</sup>		Picrite Model <sup>3</sup>		Basanite Model <sup>4</sup>		Modal Melt <sup>5</sup>
	KR-4002 X = 5.8	KR-4000 X = 23.8	KR-4002 X = 9.2	KR-4000 X = 28.7	KR-4002 X = 5.2	KR-4000 X = 21.7	KR-4000 X = 22.3
SiO <sub>2</sub>	44.85	45.09	44.9	44.55	45.09	44.82	51.6
TiO <sub>2</sub>	0.15	0.14	0.15	0.21	0.26	0.71	0.33
Al <sub>2</sub> O <sub>3</sub>	4.04	4.21	4.26	4.78	4.14	4.33	12.9
FeO	8.03	7.92	7.97	8.4	8.18	9.33	5.83
CaO	3.46	3.46	3.43	3.6	3.18	2.59	13.17
Na <sub>2</sub> O	0.20	0.08	0.12	0.5	0.20	0.85	0.62

1 Primitive upper mantle composition estimated from the three most fertile West Kettle River xenoliths (Table 12)

2 Composition of the primary MORB of Donaldson and Brown (1977) are used in the calculation;

3 Composition of the model picrite of Nickel and Green (1984) are used;

4 Composition of the West Kettle River host basanitoid (Table 2) are used.

5 Calculated composition of the melt in equilibrium with a residue with the composition of harzburgite KR-4000, assuming  $F_{Oj} = 90.8$ , source composition = KRPUM, partition of Fe/Mg between olivine and melt = 0.3; Batch melting model is used in the calculation.



River could be either equilibrated with a tholeiite or picrite melt (Table 13) by 6-9% and 24-29% degrees of partial melting respectively. A basanite cannot be in equilibrium with the harzburgite residues, otherwise a very high  $\text{TiO}_2$  content (~1%) is required in the source rock (Nickel and Green, 1986), but it could be equilibrated with a lherzolite residue by 5% of partial melting (Table 13). A constant melt composition, as suggested for peridotite xenoliths from Victoria (Nickel and Green, 1984) and Mongolia (Preß et al., 1986), is not necessary for the West Kettle River harzburgites and lherzolites, because of the large scattering of their compositions in the oxides vs.  $\text{Mg}/(\text{Mg}+\text{Fe})$  plots (Fig. 4). Derivation of the melt compositions from the xenoliths themselves is hampered by the fact that they have experienced subsolidus recrystallization and therefore their mineral chemistry and thermal state are not necessarily the same as those during the melting event (Francis, 1987). The only preserved information about the chemical state during partial melting is the bulk composition of the residues represented by the whole rock compositions of the xenoliths. Following the approach of Francis (1987), the composition of the melt in equilibrium with the West Kettle River harzburgites may be estimated under the assumption that the  $\text{Fe}/\text{Mg}$  of the olivines has survived the subsolidus metamorphism. Assuming a  $\text{Mg}/(\text{Mg}+\text{Fe})$  of 0.91 for the olivine in KR-4000, a  $\text{Mg}/(\text{Mg}+\text{Fe})$  exchange coefficient of 0.3 between the melt and the olivine (Roeder and Emstie, 1970) and a source composition as the average of the three most fertile lherzolites, a tholeiite melt with  $\text{MgO}$  of 8% and  $\text{CaO}$ , 10% (Table 13) can be derived for harzburgite KR-4000. Francis (1987), however, obtained a picrite melt for the harzburgite xenoliths from Alligator, Yukon. As noticed from its transition element pattern, KR-4000 may have been metasomatized by a fluid of high Ti and Fe content. Higher  $\text{Mg}/(\text{Mg}+\text{Fe})$  in the olivine would yield a higher  $\text{MgO}$  in the calculated melt. Further complications for the estimation of the melt composition based on the xenoliths are imposed by the possibility of multiple melting events and involvement of  $\text{H}_2\text{O}-\text{CO}_2$  in the source rocks.

### (3) Ca/Al problem

Information from the ultramafic xenoliths in alkali basalts and kimberlites can only constrain the composition of the upper mantle (eg. Jagoutz et al., 1979). Most refractory (non-volatile) lithophile element abundance ratios (eg.,  $\text{Ti}/\text{Y}$ ,  $\text{Ti}/\text{Sc}$ ,

Sc/Yb) in the estimated primitive upper mantle compositions are close to chondritic, which has been argued as evidence for the lack of significant intramantle chemical fractionation (eg. Zindler and Hart, 1984). A notorious exception to this generalization is the non-chondritic Ca/Al ratio in some mantle-derived samples. This was first recognized in komatiites, which can be divided into two types: Al-depleted (Ca/Al ratio is 1.2 times of chondritic ratio) and Al-undepleted (Ca/Al ratio is close to chondrites)(eg. Sun and Nesbitt, 1978; Nesbitt et al., 1979). The Al-depleted komatiites have been interpreted by either garnet fractional crystallization or mechanical separation at high temperatures (eg., Green, 1975; Sun and Nesbitt, 1978; Arndt, 1986) or by a non-chondritic upper mantle composition due to fractionation of garnet or perovskite into the lower mantle (eg., Herzberg and O'Hara, 1985). Palme and Nickel (1985) recently compiled data for lherzolite xenoliths from many localities and concluded that the mantle xenoliths have consistently higher Ca/Al ratio (about 15% higher) than chondrites. Based on these data, they suggest that this high Ca/Al ratio is characteristic of the upper mantle and is possibly due to fractionation of garnet into the lower mantle (Palme and Nickel, 1985). However, the generalization of this conclusion was questioned by MacDonough and Sun (in prep.), who noticed many samples as exceptions (see Sun, 1987). Preß et al. (1986) reported that the Ca/Al ratios for xenoliths from Mongolia vary considerably and the average is much lower than both the chondritic and those compiled by Palme and Nickel (1985).

The Ca/Al ratios of the ten West Kettle River xenoliths have a considerable range from 0.6 to 1.3 (Fig. 17). These results present further examples of the variability of Ca/Al in mantle xenoliths.

The factors and processes that affect the Ca/Al ratios of the mantle xenoliths have to be assessed in order to ascertain the characteristics of the primitive upper mantle. The small sample size, coarse grain size and local modal heterogeneity of the mantle xenoliths may contribute to the sampling bias (eg., Ringwood, 1975; Zindler and Hart, 1986) and add variability to the Ca/Al ratios, particularly in harzburgites. Another factor is the fractionation of the Ca/Al ratios during partial melting. Fig. 18 demonstrates that the Ca/Al ratio of the silicate melts are sensitive to the melting conditions (temperature and pressure). Since most lherzolites and harzburgites have experienced partial melting to some extent, this factor has to be taken into

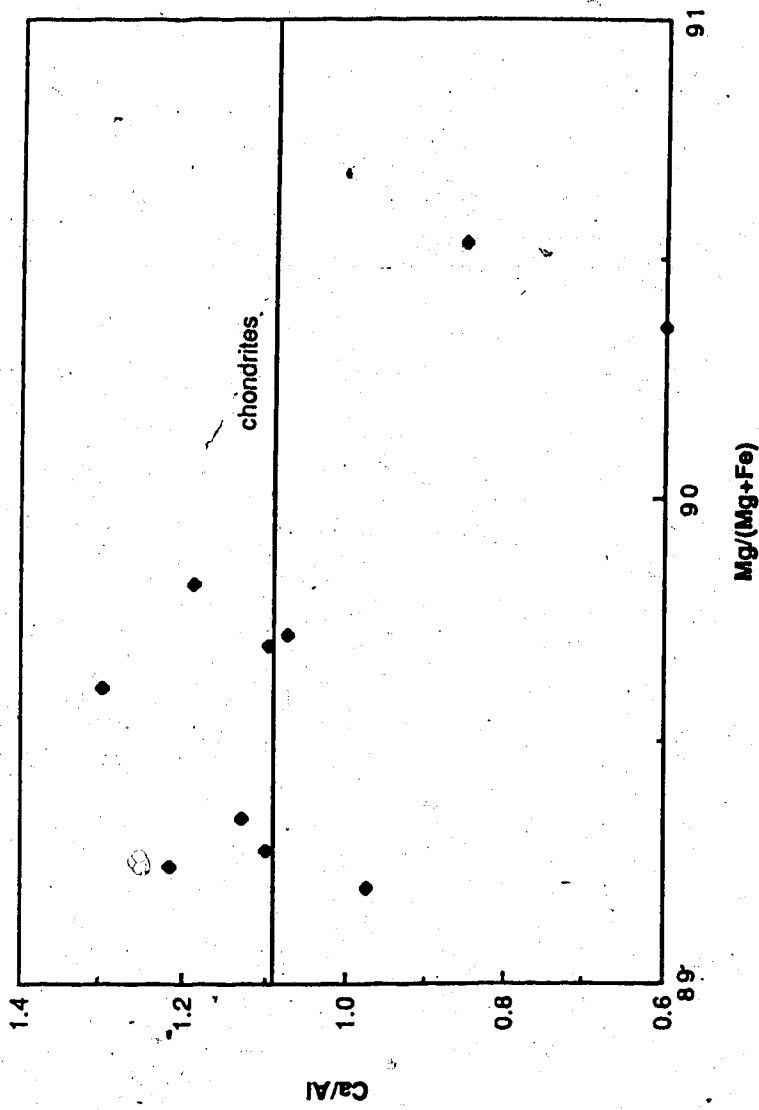


Fig. 17. Ca/Al (wt.) versus bulk Mg/(Mg+Fe) for ultramafic xenoliths from West Kettle River. The two harzburgites have the highest Mg/(Mg+Fe), but lowest Ca/Al.

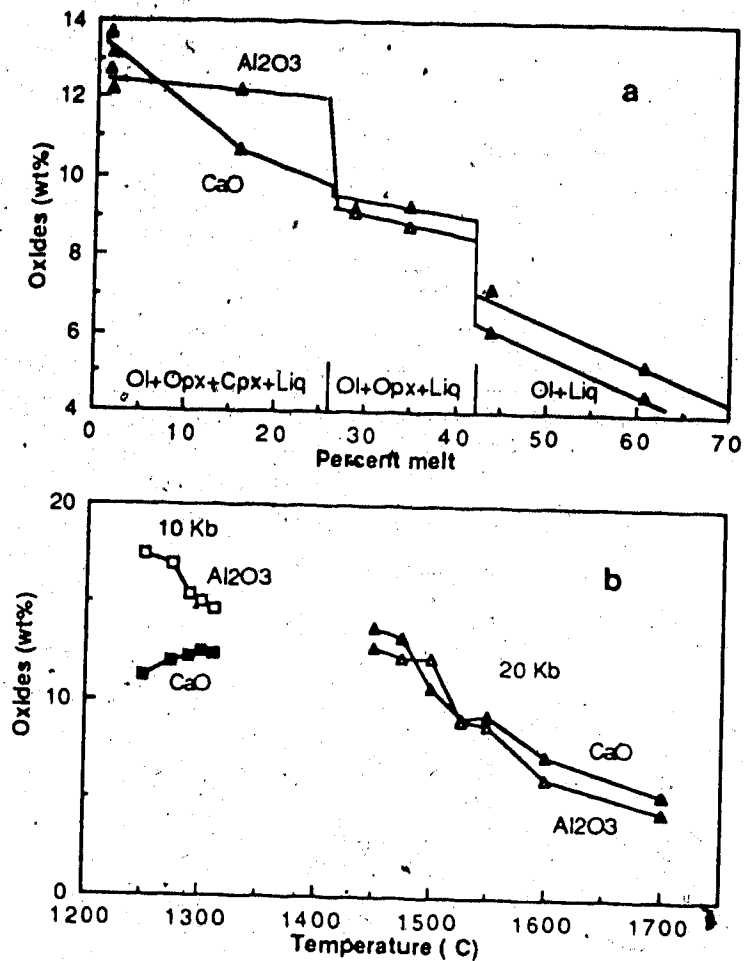


Fig. 18. (a) CaO and Al<sub>2</sub>O<sub>3</sub> concentrations in the melts as a function of degrees of partial melting at 20 Kb (adapted from Mysen and Kushiro, 1977). The starting material is a garnet peridotite xenolith from a Lesotho kimberlite (Mysen and Kushiro, 1977). Mineral assemblages describe coexisting phases in melting intervals. Noteworthy is the change of Ca/Al with degrees of melting.

(b). CaO and Al<sub>2</sub>O<sub>3</sub> concentrations of melts at 10 Kb and 20 Kb as a function of melting temperature (°C) (Compiled from Mysen and Kushiro, 1977; Fujii and Scarfe, 1985). The starting material for experiment at 10 Kb is a synthetic peridotite (Fujii and Scarfe, 1985) and data for 20 Kb experiment is the same as (a). Notice the variation of Ca/Al of the melt with both temperature and pressure.

consideration. The low Ca/Al ratios in the two harzburgites may be ascribed to extraction of melts of high Ca/Al ratios.

A third factor that deserves attention is the interaction of mantle xenoliths with silicate melts. Francis (1987) has shown that this process can effectively change the Ca/Al ratios of both the melts and the xenoliths involved. Again, the Ca/Al ratios of the resultant melts may vary as a function of pressure due to the variable stability of each mineral phase in the silicate melts at different pressures (Brearley and Scarfe, 1986).

Considering all these complications, it is suggested that Ca/Al ratios of the mantle xenoliths are very likely unrepresentative of those of the primitive upper mantle and caution should be taken in interpreting these data.

## 2. Evolution of the upper mantle beneath West Kettle River

### (1) Multiple mantle depletion and enrichment events

The clinopyroxenes in all the lherzolites but one (KR-4003) have Nd and Sr isotope compositions similar to MORB (Fig. 11) and their Nd model ages range from 1.5 - 3.6 Ga (Table 12). The  $^{143}\text{Nd}/^{144}\text{Nd}$  of these clinopyroxenes are correlated with the  $^{147}\text{Sm}/^{144}\text{Nd}$  and a reference Nd isochron with an age of 0.75 Ga and initial  $\epsilon_{\text{Nd}}$  of +6 can be drawn through them (Fig. 19). The 'uncontaminated' whole rocks of these lherzolites all display LREE depletion patterns (Fig. 7d). The isotopic variations and REE patterns in these lherzolites can be accounted for by a two stage melting model. The Nd model ages of 1.5 - 3.6 Ga may record a period between the initial and final melt extraction events due to the slightly greater incompatibility of Nd compared with Sm in a peridotite - melt system. The Nd isochron age (0.75 Ga) may date the second depletion event. In principle, multiple melt extraction would result in a residual peridotite with older Sr model ages than Nd, due to the much greater incompatibility of Rb than Sr, Sm and Nd (Stosch and Lugmair, 1986). The Sr model ages for these lherzolites cannot be estimated due to the lack of reliable Rb data. Nevertheless, the minimum Sr model ages (Table 14), can be derived with  $\text{Rb}/\text{Sr} = 0$  and they are indeed greater than the Nd model ages, as expected, for some of the lherzolites.

Lherzolite KR-35 may have had a more complex history than suggested by this simple two-stage melting model. The coexisting minerals in KR-35 lack oxygen isotope equilibrium and both its whole rock and constituent minerals are anomalously

Table 12: Nd and Sr Model Ages (Ga) for Mantle Xenoliths From West Kettle River.

Sample	$T_{Nd}^1$	$T_{min. Sr}^2$
KR-35	3.63	1.24
KR-37	(-)	1.19
KR-141	1.52	1.59
KR-4000	(-)	1.37
KR-4001	1.78	0.86
KR-4002	1.39	1.96
KR-4003	0.72	1.45
KR-4005	2.38	1.64
KR-4016	1.63	1.62

<sup>1</sup> Nd model age calculated with  $\lambda(^{147}\text{Sm}) = 6.54 \times 10^{-12}$ ,  $^{147}\text{Sm}/^{144}\text{Nd} = 0.1967$  (CHUR),  $^{143}\text{Nd}/^{144}\text{Nd} = 0.512638$  (CHUR).

<sup>2</sup> Minimum Sr model age calculated with  $\text{Rb}/\text{Sr} = 0$ ,  $\lambda(^{87}\text{Rb}) = 1.42 \times 10^{-11}$  (CHUR),  $^{87}\text{Rb}/^{86}\text{Sr} = 0.0816$  (CHUR),  $^{87}\text{Sr}/^{86}\text{Sr} = 0.7047$  (CHUR).

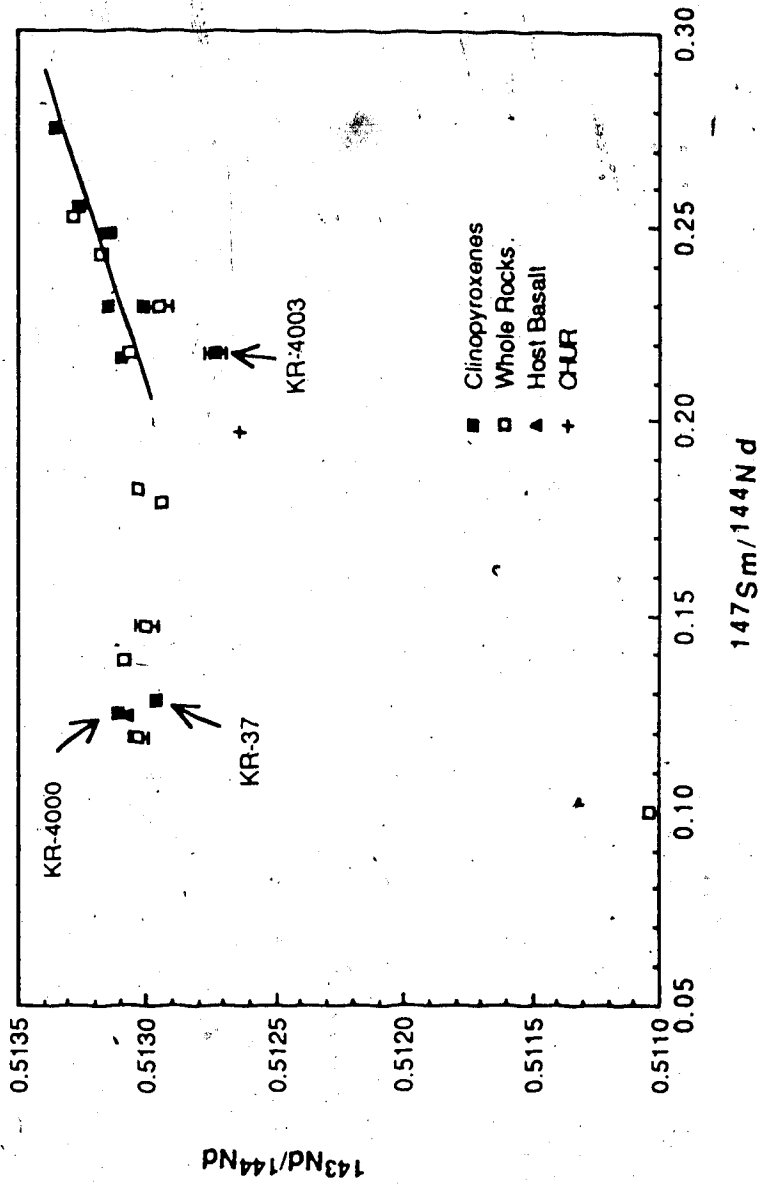


Fig. 19. Sm-Nd evolution diagram for clinopyroxenes and whole rocks of ultramafic xenoliths from West Kettle River. Error bars are derived from 2  $\sigma$  standard deviations.

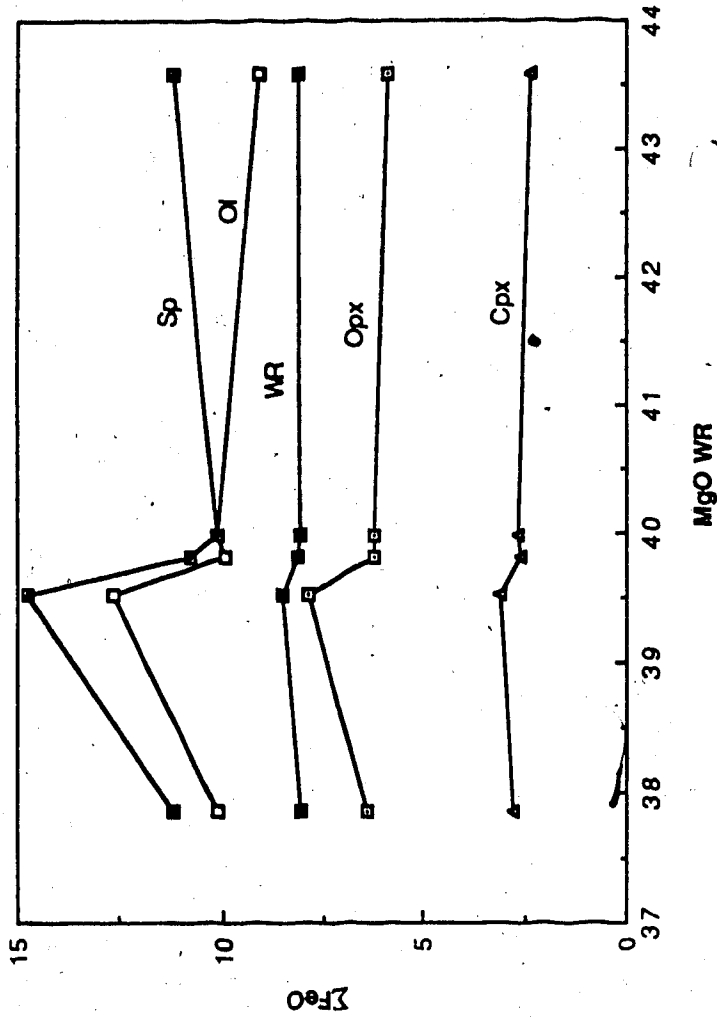
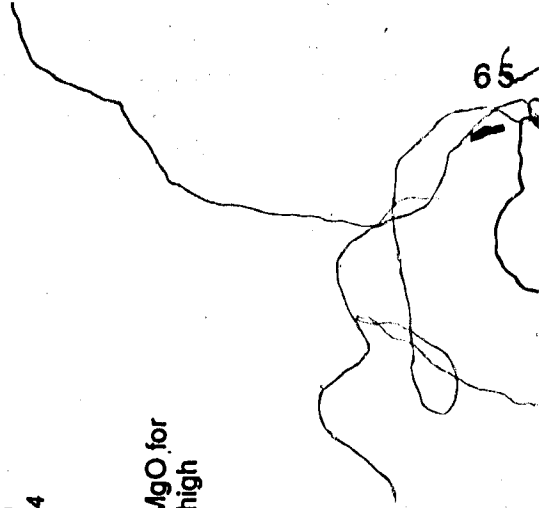


Fig. 20. Total Fe as FeO of whole rock and constituent minerals versus bulk MgO for ultramafic xenoliths from West Kettle River. Sample KR-35 has anomalously high FeO. Data in Appendix IV.





high in FeO contents compared with the other lherzolites (Fig. 16, 20). If these two features are related to each other, KR-35 may have experienced incomplete reaction with a silicate melt in the upper mantle. No chemical zoning were observed in the constituent minerals in KR-35. This may be a result of the large uncertainties in the probe analyses (see Appendix IV). It is controversial whether the oxygen diffusion rate is greater than those of the cations (Harmon et al., 1986; Dowty, 1980; Freer, 1981). If oxygen diffuses faster than cations as suggested by Harmon et al. (1986), it is possible that the Sr and Nd isotopes of the coexisting minerals in KR-35 are out of equilibrium, too. It follows that the Sr and Nd isotope systems of its whole rocks and clinopyroxenes could both have recorded this process. The mantle metasomatism, inferred from the whole rock data, might have been responsible for the oxygen isotope disequilibrium and high FeO content. As discussed in chapter V, this metasomatic fluid (silicate melt) has possibly been derived from an isotopically depleted source, similar to that of the host basalt. However, the effect of this metasomatic fluid on the Sm-Nd isotope system of the clinopyroxene may be minimal, considering that the Sm/Nd ratio of its clinopyroxene is very similar to the clinopyroxenes in the other xenoliths, but is much higher than its whole rock.

The  $^{143}\text{Nd}/^{144}\text{Nd}$  and  $^{87}\text{Sr}/^{86}\text{Sr}$  ratios of the two harzburgites are similar to the isotopically depleted lherzolites (Fig. 11). However, their Sm/Nd ratios are decoupled from the  $^{143}\text{Nd}/^{144}\text{Nd}$  and are lower than CHUR (Fig. 19). The 'uncontaminated' whole rocks of these two harzburgites are both LREE enriched (Fig. 7d). LREE enrichment in harzburgite xenoliths are very common and could be explained by the model of Frey and Green (1974), in which a partial melting event controls the major elements, and a subsequent enrichment or cryptic metasomatism (Dawson, 1984) introduces incompatible trace elements into the rocks, without markedly affecting the major element compositions. The decoupling of the  $^{143}\text{Nd}/^{144}\text{Nd}$  and Sm/Nd implies that the LREE enrichment may have occurred very recently and the metasomatic fluids have similar Sr and Nd isotope compositions to those of the clinopyroxene. The metasomatic fluids responsible for these two harzburgites are very likely silicate melts, similar to that inferred for lherzolite KR-35, because the bulk compositions of both harzburgites are characterized by high FeO (Fig. 16) and KR-4000 also has anomalously high  $\text{TiO}_2$  content (Fig. 6).

The clinopyroxene of one lherzolite, KR-4003, has similar  $^{87}\text{Sr}/^{86}\text{Sr}$  and  $^{147}\text{Sm}/^{144}\text{Nd}$ , but lower  $^{143}\text{Nd}/^{144}\text{Nd}$ , compared with the other lherzolites, and plots to the left of the mantle array in the Nd - Sr isotope diagram (Fig. 11). Its Nd model age (0.72 Ga) is lower than both its Sr model age (>1.45 Ga) and the Nd model ages of the clinopyroxenes in the other lherzolites (Table 14). The 'uncontaminated' whole rock of KR-4003 has a convex-upwards REE pattern (Fig. 7d). A more complex model involving both depletion and enrichment events has to be invoked in order to account for these isotopic and geochemical features. A possible interpretation is as follows:

- (1) A depletion event prior to 1.5 Ga ago, similar to the other lherzolites;
- (2) A metasomatism which decreased its Sm/Nd ratio but did not significantly change its Rb/Sr ratio;
- (3) A second depletion event which raised its Sm/Nd ratio to the present value above CHUR.

The timing of the mantle enrichment event and the second depletion event cannot be constrained. Nevertheless, sufficient time has to be allowed between the enrichment and subsequent depletion for  $^{143}\text{Nd}/^{144}\text{Nd}$  to respond to the decreased  $^{147}\text{Sm}/^{144}\text{Nd}$ . The isotope pattern of such enrichment (shifts to the left of the mantle array) has been observed in mantle xenoliths elsewhere and in continental volcanic rocks from several extensional environments (Zindler and Jagoutz, 1988; Menzies and Wass, 1983; Hawkesworth et al., 1984). This pattern may be associated with melt or melt-related fluid migration in the upper mantle (Hawkesworth et al., 1984).

More recent mantle metasomatism has been recorded by the whole rocks of KR-4003, and the Nd isotope composition of this metasomatic fluid was inferred to be depleted similar to that of the KR-4002 clinopyroxene (see discussion in Chapter VI).

Briefly, the Group I lherzolites and harzburgites from West Kettle River may have experienced at least two stages of melt extraction. Interactions with episodes of silicate melt or  $\text{CO}_2\text{-H}_2\text{O}$  rich fluids over a span of time are exhibited by some of these xenoliths. The isotopic compositions for most of these inferred metasomatic agents are similar to MORB.

Migration of melt in the upper mantle is also directly demonstrated by the occurrence of Group I websterites and Group II clinopyroxenes (either as discrete xenoliths or as bands and patches in Group I lherzolites). One olivine websterite

(KR-3020B), separated from its host lherzolite in a composite Group I xenolith was analyzed and gave a  $^{143}\text{Nd}/^{144}\text{Nd}$  ratio of 0.51304 and  $^{87}\text{Sr}/^{86}\text{Sr}$  of 0.7036 (Table 8). These values may represent the upper limit of  $^{87}\text{Sr}/^{86}\text{Sr}$  and lower limit of  $^{143}\text{Nd}/^{144}\text{Nd}$  for its 'uncontaminated' whole rock, due to the possibility of ground water contamination. Nevertheless, the MORB-like isotope signature is clearly demonstrated. The silicate melt, from which it segregated, may have been derived from an isotopically MORB-like mantle source.

The metasomatic fluids and melts could have come from sources different from the xenoliths themselves, and therefore may provide insight into the isotopic nature of the upper mantle below the xenolith source region. Their MORB-like isotopic characteristics, together with evidence from the clinopyroxenes, suggest that MORB-like mantle component is volumetrically significant and has played an important role in the magmatism in this region. The West Kettle River host basalt has similar Sr and Nd isotope ratios to the clinopyroxenes in the West Kettle River xenoliths (Fig. 11) and may therefore have been derived from such a MORB-like mantle source.

## (2) Models for the upper mantle evolution

Seismological results indicate that the lithosphere in the vicinity of West Kettle River is 40 - 50 Km thick with the mantle portion of the lithosphere approximately 15 - 20 Km thick (Wickens, 1977). The depth of equilibration for West Kettle River xenoliths cannot be accurately constrained due to lack of reliable geobarometers, but was found to be within the range of 30-60 Km (Fujii and Scarfe, 1982a). The actual depth interval of the West Kettle River xenoliths must be more restricted (possibly <10 Km) considering their very narrow temperature range (Fujii and Scarfe, 1982a). Derivation of these xenoliths from the thin mantle portion of the lithosphere is therefore suggested.

There is a great tendency to associate the mantle event possibly recorded by the Nd and Sr modal ages of mantle xenoliths with the formation of the overlying crust by igneous differentiation, particularly when these data match the ages of overlying crustal rocks (eg. Cohen et al., 1984; Stosch et al., 1986).

West Kettle River lavas are located in a region where the Terrane I of upper Paleozoic to mid-Mesozoic oceanic volcanic and sedimentary rocks were accreted to the western margin of the ancient Cordillera continental craton (Monger and Price,

1979; Monger et al., 1982). There are few constraints on whether the lithospheric mantle beneath West Kettle River is part of the accreted Terrane I, or whether it represents that underlying the ancient continental crust (Smith, 1986). In light of the above tectonic scenarios, three models may be offered for the evolution of the upper mantle beneath West Kettle River:

(a) The upper mantle represented by these xenoliths might have been associated with the old Cordilleran craton, instead of the oceanic crust of Terrane I. The initial melting event suggested by the Nd model ages may be related to the formation and stabilization of the ancient continental craton in the Archean through early Proterozoic (>1.5 Ga). Since the Nd model ages have been reset by a later depletion event, there is an ambiguity about the exact age of the initial depletion event. The Nd isochron defined by the depleted lherzolites may be related to Proterozoic volcanics in this region (Monger et al., 1982).

This model implies that the overlying crust was derived from a primitive upper mantle. However, there is increasing evidence from the isotopic study of crustal rocks, that the upper mantle was already isotopically depleted in Archean times (Stosch et al., 1986).

(b) Alternatively, the Nd model age may reflect global continental crustal formation and mantle differentiation in the asthenosphere. The isotopic similarity between MORB and mantle xenoliths from West Kettle River and many other localities, and the frequency of Proterozoic or Archean Nd model ages in these xenoliths (Stosch et al., 1986) support this model. The similar oxidation states for West Kettle River mantle xenoliths and MORB glasses (Canil et al., in prep.) lends further credibility for the argument of involvement of these xenoliths in the asthenosphere. The mantle section represented by the xenoliths might have been incorporated into the lithosphere later (possibly 0.75 Ga ago) during the formation of the overlying oceanic crust, which was subsequently accreted to North America in the Jurassic (Monger et al., 1982). The compositions of these xenoliths range from depleted harzburgites to undepleted lherzolites (Table 4), suggesting that the upper mantle beneath West Kettle River includes rocks similar to the MORB sources as well as those representing residues after MORB extraction.

(c) A third possibility is that these xenoliths had been part of the asthenosphere until they were brought up by the host basalt, as is the model for the xenoliths from

Kilbourne Hole, New Mexico (Roden et al., 1988), a tectonically similar locality (Gough, 1986). However, the available data, as discussed earlier, is more in favor of a lithospheric instead of asthenospheric origin for these xenoliths.

The second model is preferred over the other two, although neither of them can be conclusively excluded.

During and/or after the incorporation of the xenolith source mantle into the lithosphere, the upper mantle has episodically interacted with silicate melts and  $\text{CO}_2\text{-H}_2\text{O}$  rich fluids, which are possibly related to the late Tertiary volcanism in southern British Columbia, triggered by mantle upflow in this region (Gough, 1986).

### 3. Constraints on the source characteristics of volcanism in south-central B.C.

Since the tectonic setting for south-central British Columbia starting from the Miocene has been inferred to be very similar to its present tectonic regime, the Miocene through present volcanism in this region may have been derived from similar mantle sources (Souther, 1977). Information from the mantle xenoliths can therefore be used to place constraints on the source characteristics of these volcanic rocks.

Only limited isotope data are available for mantle xenolith clinopyroxenes from the other localities in south-central B.C.. Clinopyroxenes in seven of the eight previously analyzed mantle xenoliths from Jacques Lake, Big Timothy Mountain, Lassie Lake in south-central B.C. (Sun, 1985) have comparable  $^{87}\text{Sr}/^{86}\text{Sr}$  to those from West Kettle River. The Sr and Nd isotopes of one clinopyroxene, separated from a composite Group I xenolith from Rayfield River (Smith, 1986), is similar to the West Kettle River xenoliths (Fig. 21).

The Nd and Sr isotopic ratios of the late Tertiary Chilcotin plateau basalts from south-central B.C. (Smith, 1986), Quaternary alkaline basalts from the Wells Gray Provincial Park (Metcalf, 1987), host basalts of mantle xenoliths from West Kettle River (this study), Summit Lake and Rayfield River (Smith, 1986), along with clinopyroxenes in mantle xenoliths from West Kettle River (this study) and Summit Lake (Smith, 1986) are plotted in Fig. 22. These basalts and clinopyroxenes form a well defined trend. The clinopyroxenes lie on the more depleted end of this trend and partly overlap with the basalt range. The isotopic compositions of these basalts could be interpreted as resulting from mixing between a depleted component represented by the clinopyroxenes and enriched component(s), as suggested by Metcalfe (1987) and

Smith (1986). The host basalts of West Kettle River and Rayfield River xenoliths have very similar Sr and Nd isotope ratios (Fig. 22) and may have been least affected by the enriched components (Fig. 22). The late Tertiary Chilcotin plateau basalt and Quaternary alkaline basalts from the Wells Gray Provincial Park span a wide range in the Nd - Sr isotope plot (Fig. 22) and suggest variable proportions of the depleted and enriched component(s) in their mantle sources. The host basalt for mantle xenoliths from Summit Lake is by far the most enriched (Fig. 22) and a significant amount of enriched component(s) might have been involved in its mantle source. It would be interesting to determine whether such enriched isotope characteristics are also recorded in the mantle xenoliths from Summit Lake. However, so far only whole rock isotope data are available for these xenoliths (Smith, 1986). Although they are generally more enriched than the fresh whole rock xenoliths from West Kettle River (Fig. 21), caution should be taken in interpreting these data because of the possible secondary contaminations, particularly ground water contamination, on the whole rock isotope systems.

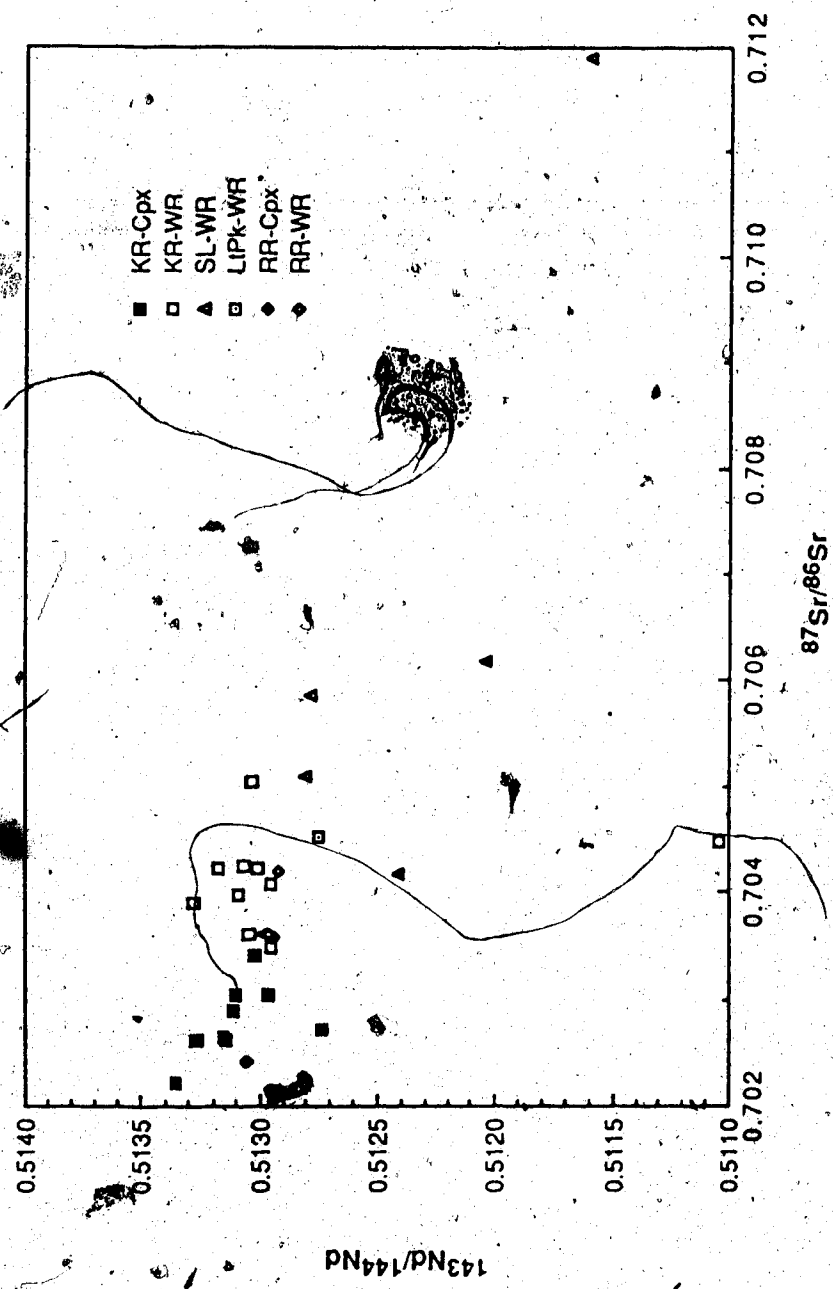


Fig. 21. Nd-Sr isotope diagram for ultramafic xenoliths from south-central British Columbia. Cpx = clinopyroxenes, WR = whole rocks; KR = West Kettle River; SL = Summit Lake; RR = Rayfield River; LL = Lightning Peak.

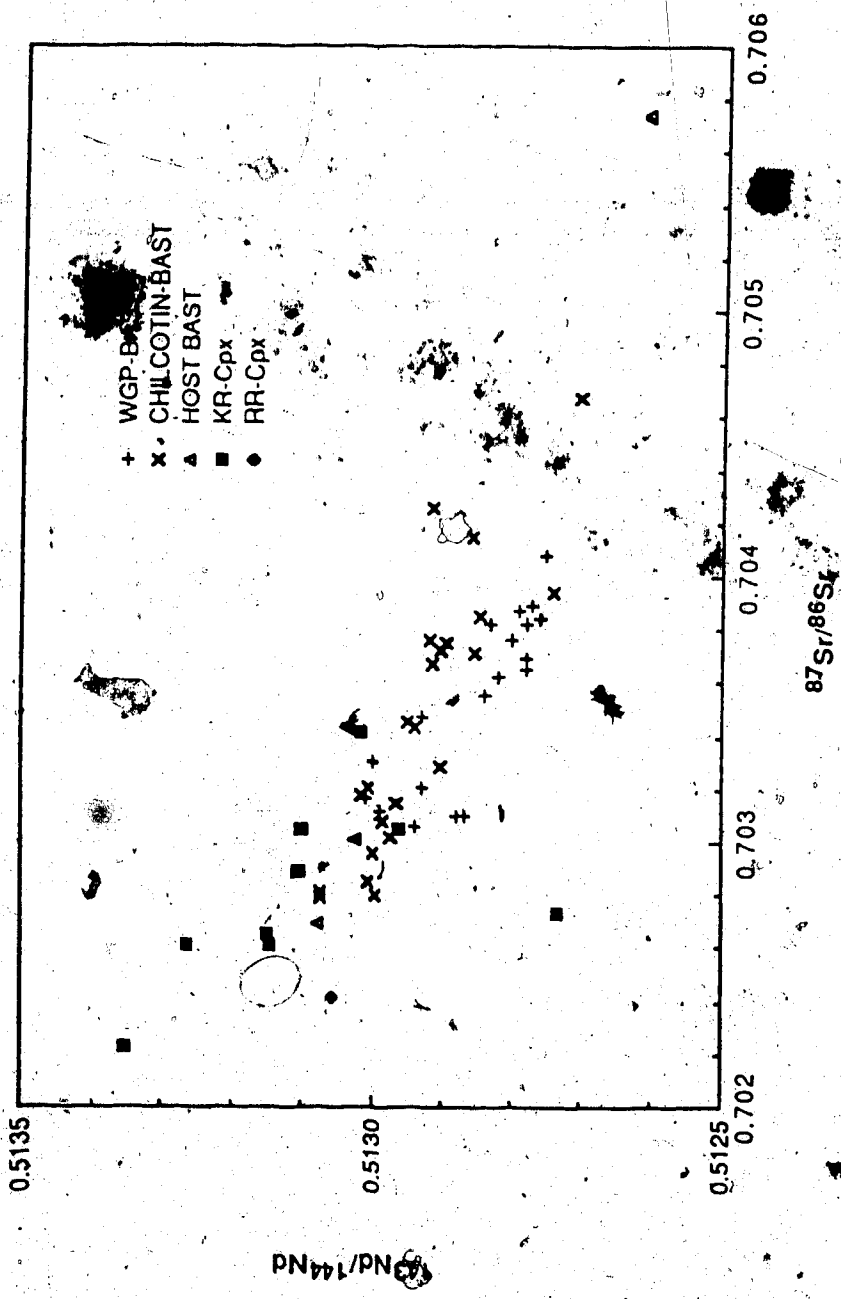


Fig. 22. Nd-Sr isotope diagram for ultramafic xenolith clinopyroxenes and Miocene to recent volcanics from south-central B.C.. BAST = Basalts; Host BAST = host basalts from West Kettle River (the most depleted one), Summit Lake (the most enriched) and Rayfield River (the one in between); WGP = Wells Gray Park; CHILCOTIN = Chilcotin plateau basalts (Smith, 1986); Other symbols same as in Fig. 21.



## IX. Summary and Conclusions

Systematic geochemical and Sr, Nd and O isotopic studies for ultramafic xenoliths from a Pliocene basanitoid flow at West Kettle River, British Columbia, have provided important information concerning the nature and evolution of the upper mantle beneath southern British Columbia. Three general conclusions may be drawn:

### 1. Mineralogical and chemical heterogeneity of the upper mantle

The mineralogy of the West Kettle River mantle xenoliths, including both Group I and II xenoliths, Major and considerable trace element concentrations of the bulk Group I lherzolites and harzburgites are systematically and are inferred to be largely controlled by partial melting processes. The composition of the most fertile lherzolites from West Kettle River are very similar to those estimated for the primitive upper mantle (eg. Ringwood, 1979). The harzburgites may be considered as residues after partial melting of these undepleted lherzolite source rocks. The compositions of the melts generated from the partial melting cannot be accurately determined because of the subsequent subsolidus recrystallization and interaction with migrating melts in the upper mantle, but may be estimated to be tholeiitic or picritic, possibly related to MORB generation. Melt migration and crystallization in the upper mantle were recorded by the occurrence of Group I websterites and Group II pyroxenites either as discrete xenoliths or as bands and patches in the host Group I lherzolites. Interaction of mantle xenoliths with silicate melts in the upper mantle is also reflected by the high FeO contents (and possibly  $\text{TiO}_2$ ) in some of the harzburgites and lherzolites. The majority of the West Kettle River lherzolites have lower FeO than xenolith suites from Summit Lake and San Carlos, which have comparable FeO contents only to the relatively Fe-rich West Kettle River xenoliths. The difference in FeO contents from these localities may be either due to global heterogeneity of the primitive upper mantle or interaction of the upper mantle rocks with migrating melts in the upper mantle.

### 2. Timing of mantle depletion and enrichment

Nd and Sr isotope ratios of the clinopyroxenes in all but one of the lherzolites and

harzburgites ( $^{143}\text{Nd}/^{144}\text{Nd} = 0.51296 - 0.51335$ ,  $^{87}\text{Sr}/^{86}\text{Sr} = 0.70223 - 0.70342$ ) are similar to MORB. The clinopyroxenes in these lherzolites give Nd model ages of 1.5 to 3.6 Ga and they are close to a reference Nd isochron with an age of 0.75 Ga and initial  $\epsilon_{\text{Nd}}$  of +6 in the Sm-Nd evolution diagram. These isotopic data can be interpreted by a two stage melting model. One of these lherzolites is out of inter-mineral oxygen isotope equilibrium, possibly indicating recent interaction with a silicate melt. Sm/Nd of the harzburgites ( $< \text{CHUR}$ ) are decoupled from their  $^{143}\text{Nd}/^{144}\text{Nd}$ , suggesting a recent mantle metasomatism. Because these metasomatized xenoliths all have higher FeO contents than the isotopically depleted lherzolites, the metasomatic agents can be inferred to be a silicate melt rather than a  $\text{CO}_2\text{-H}_2\text{O}$  rich fluid. The clinopyroxene of one other lherzolite has similar  $^{87}\text{Sr}/^{86}\text{Sr}$  and Sm/Nd to the isotopically depleted lherzolites, but is more enriched in  $^{143}\text{Nd}/^{144}\text{Nd}$  (0.51273), implying a more complex history involving a mantle enrichment subsequent to initial partial melting, and followed by a second melting event.

The effects of ground water contamination on the Sr and Nd isotope systems of whole rock xenoliths from West Kettle River are established by studying a severely weathered sample. The Sr isotopes of most of the West Kettle River xenoliths have been markedly affected by ground water contamination. The effect of ground water contamination on the whole rock Nd isotopes is significant only when the xenoliths are seriously weathered. After the vest of ground water contamination is removed, it is demonstrated that more recent mantle metasomatism may have affected some of the whole rock xenoliths. Mantle metasomatism at various times are also recorded by the REE patterns of the whole rock xenoliths, which are otherwise LREE depleted.

### 3. Evolution of the upper mantle and magmatism in south-central British Columbia

The Sr and Nd isotopic characteristics of the West Kettle River mantle xenoliths can be interpreted by a model in which southern British Columbia is underlain by an oceanic lithospheric mantle that was accreted by Terrane I of the Canadian Cordillera in mid-Jurassic. The Nd model ages of 1.5-3.6 Ga may reflect global continental crustal formation and were recorded in the xenoliths while they were part of the convecting asthenosphere. The Nd isochron age of 0.75 Ga may date the time of formation of the overlying oceanic crusts, which were subsequently accreted to the

Western margin of the ancient Cordillera continental craton during mid-Jurassic. The possible multiple mantle metasomatism recorded by the mantle xenoliths may be related to the Miocene to Recent volcanism in this region. Isotopic compositions of the metasomatic fluids and melts, inferred to have interacted with the West Kettle River xenoliths, are mostly depleted, similar to those of the depleted clinopyroxenes. This testifies that an isotopically MORB-like mantle component is volumetrically important and played an important role in the magmatism in West Kettle River. The West Kettle River host basanitoid may have been derived from such a MORB-like source region. The isotopic compositions of the Miocene to Recent volcanism in south-central British Columbia may be interpreted as mixing of such a MORB-like component, in various proportions, with more enriched mantle components.

## IX. Bibliography

AAGAARD P. (1974) Rare earth elements adsorption on clay minerals. *Bull. Groupe franc. Argiles*. XXVI, 193-199.

ARNDT N. T. (1986) Komatiites: A dirty window to the Archean mantle. *Episodes*. 3, 3-7.

ALLEGRE C. J., JAVOY M. and MICHARD G. (1968) Etude de la distribution et de l'abondance des éléments de transition dans l'écorce terrestre, comparée à celles des terres rares. In *Origin and Distribution of the Elements* (ed. L. H. Ahrens) pp. 913-928. Pergamon.

BEVER M. L. (1983) Regional stratigraphy and age of Chilcote Group basalts, south-central British Columbia. *Can. J. Earth Sci.* 20, 515-524.

BOUGAULT H. and FLECHIAN R. (1974) Rift valley in the Atlantic Ocean near 36°50'N: petrology and geochemistry of basaltic rocks. *Earth Planet. Sci. Lett.* 24, 249-261.

BOYNTON W. V. (1981) Cosmochemistry of the rare earth elements: meteorite studies. In *Rare Earth Element Geochemistry* (ed. P. HENDERSON), pp. 63-114. Elsevier.

BREARLEY M. and SCARFE C. M. (1986) Dissolution rates of upper mantle minerals in an alkali basalt melt at high pressure: An experimental study and implications for ultramafic xenolith survival. *J. Petrol.* 27, 1157-1182.

BREARLEY M., SCARFE C. M. and FUJII T. (1984) The petrology of ultramafic xenoliths from Summit lake, near Prince George, British Columbia. *Contrib. Mineral. Petrol.* 88, 53-63.

BURWELL A. D. M. (1975) Rb-Sr isotope geochemistry of lherzolites and their constituent minerals from Victoria, Australia. *Earth Planet. Sci. Lett.* 28, 69-78.

BVSP, (Basaltic Volcanism Study Project) (1981) *Basaltic volcanism on the terrestrial planets*. Pergamon, New York, N.Y. pp. 282-310.

CANIL D., BREARLEY M. and SCARFE C. M. (1987) Petrology of ultramafic xenoliths from Rayfield River, south-central British Columbia. *Can. J. Earth Sci.* 24, 1679-1687.

CANIL D., VIRGO D. and SCARFE C. M. (in prep.) Oxidation state of spinel lherzolite xenoliths from British Columbia.

CLAYTON R. N. and MAYEDA T. K. (1963) The use of bromine pentafluoride in the extraction of oxygen from oxides and silicates for isotopic analysis. *Geochim. Cosmochim. Acta* 27, 43-52.

COHEN R. S., O'NIONS R. K. and DAWSON J. B. (1984) Isotope geochemistry of xenoliths from East Africa: Implications for development of mantle reservoirs and their interaction. *Earth Planet. Sci. Lett.* 68, 209-220.

COLBY J. W. (1972) Tutorial Notes. Proceedgs. 7th Nat. Conf. Electron Probe Anal.

- CONEY P. J., JONES D. L. and MONGER J. W. H. (1980) Cordillera suspect terranes. *Nature*. 288, 329-333.
- CROCK J. G., LICHTER F. E., RIDDLE G. O. and BEECH G. L. (1986) Separation and preconcentration of the rare-earth elements and yttrium from geological materials by ion-exchange and sequential acid elution. *Talanta*. 7, 601-606.
- CULLERS R. L., CHAUDHURI S., ARNOLD B., LEE M. and WOLF C. W. JR. (1975) Rare earth distributions in clay minerals and in the clay-sized fraction of the Lower Permian Havensville and Eskridge shales of Kansas and Oklahoma. *Geochim. Cosmochim. Acta* 39, 1691-1703.
- DASCH E. J. and GREEN D. H. (1975) Strontium isotope geochemistry of lherzolite inclusions and host basaltic rocks, Victoria, Australia. *Am. J. Sci.* 275, 461-469.
- DAWSON J. B. (1984) Contrasting types of upper-mantle metasomatism? In *Kimberlites II. The mantle and Crust - Mantle Relationships* (ed. J. KORNPROBST), pp. 289-294. Elsevier.
- DONALDSON C. H. and BROWN R. W. (1977) Refractory megacrysts and magnesium-rich melt inclusions within spinel in oceanic tholeiites: indicators of magma mixing and parental magma composition. *Earth Planet. Sci. Lett.* 37, 81-89.
- DOSSO L. and MURTHY V. R. (1980) A Nd isotopic study of the Kerguelen islands: inferences on enriched oceanic mantle sources. *Earth Planet. Sci. Lett.* 48, 268-276.
- DOWNES H. and DUPUY D. (1987) Textural, isotopic and REE variations in spinel peridotite xenoliths, Massif Central, France. *Earth Planet. Sci. Lett.* 85, 121-135.
- DOWTY E. (1980) Crystal-chemical factors affecting the mobility of ions in minerals. *Am. Mineral.* 65, 174-182.
- DYPRVIK H. and BRUNNELL A. O. (1976) Rare elements in Lower Paleozoic epicontinental and eugeosynclinal sediments from the Oslo and Trondheim regions. *Sedimentology*. 23, 363-378.
- FAURE G. (1986) Principles of isotope geology. John Wiley & Sons, Inc.
- FRANCIS D. (1987) Mantle-melt interaction recorded in spinel lherzolite xenoliths from the Alligator Lake volcanic complex, Yukon, Canada. *J. Petrol.* 28, 569-597.
- FREER R. (1981) Diffusion in silicate minerals and glasses: a data digest and guide to the literature. *Contrib. Mineral. Petrol.* 76, 440-454.
- FREY F. A. (1984) Rare earth element abundances in upper mantle rocks. In *Rare Earth Element Geochemistry* (ed. P. HENDERSON), pp. 153-203. Elsevier.
- FREY F. A. and GREEN D. H. (1974) The mineralogy, geochemistry and origin of lherzolite inclusions in Victoria basanites. *Geochim. Cosmochim. Acta* 38, 1023-1059.

- FREY F. A., GREEN D. H. and ROY S. D. (1978) Integrated models of basalt petrogenesis: a study of basalt tholeiites to olivine melilitites from south eastern Australia utilizing geochemical and experimental petrological data. *J. Petrol.* 19, 463-513.
- FREY F. A. and PRINZ M. (1978) Ultramafic inclusions from San Carlos, Arizona: Petrologic and geochemical data bearing on their petrogenesis. *Earth Planet. sci. lett.* 38, 129-176.
- FUJII T. and SCARFE C. M. (1982a) Petrology of ultramafic nodules from West Kettle River, near Kelowna, southern British Columbia. *Contrib. Mineral. Petrol.* 80, 297-306.
- FUJII T. and SCARFE C. M. (1982b) Composition of liquids coexisting with spinel lherzolite at 10 Kbar and the genesis of MORBs. *Contrib. Mineral. Petrol.* 90, 18-28.
- GOUGH D. I. (1986) Mantle upflow tectonics in the Canadian Cordillera. *J. Geophys. Res.* 91, 1909-1919.
- GREEN D. H. (1975) Genesis of Archean peridotite magmas and constraints on Archean geothermal gradients and tectonics. *Geol.* 3, 15-18.
- GREGORY R. T. and TAYLOR H. P. Jr (1986a) Possible non-equilibrium oxygen isotope effects in mantle nodules; an alternative to the Kyser- O'Neil-Carmichael  $^{18}\text{O}/^{16}\text{O}$  geothermometer. *Contrib. Mineral. Petrol.* 93, 114-119.
- GREGORY R. T. and TAYLOR H. P. Jr (1986b) Non-equilibrium, metasomatic  $^{18}\text{O}/^{16}\text{O}$  effects in upper mantle mineral assemblages. *Contrib. Mineral. Petrol.* 93, 124-135.
- HARMON R. S., KEMPTON P. D., STOSCH H.-G., HOEFS J., KOVALENKO V. I. and EONOV D. (1987)  $^{18}\text{O}/^{16}\text{O}$  ratios in anhydrous spinel lherzolite xenoliths from the Shavaryn-Tsaram volcano, Mongolia. *Earth Planet. Sci. Lett.* 81, 193-202.
- HART S. R. and DAVIS K. E. (1978) Nickel partitioning between olivine and silicate melts. *Earth Planet. Sci. Lett.* 40, 203-219.
- HART S. R. and ZINDLER A. (1986) In search of a bulk-Earth composition. *Chem. Geol.* 57, 247-267.
- HAWKESWORTH C. J., ERLANK A. J., MARSH J. S., MENZIES M. A. and CALSTEREN P. van (1983) Evolution of the continental lithosphere: Evidence from volcanics and xenoliths in Southern Africa. In *Continental Basalts and Mantle Xenoliths* (eds. C. J. HAWKESWORTH and M. J. NORRY), pp. 111-138. Shiver.
- HAWKESWORTH C. J., ROGERS N. W., CALSTEREN P. W. C. van and MENZIES M. A. (1984) Mantle enrichment processes. *Nature.* 311, 331-335.
- HERZBERG C. T. and O'HARA M. J. (1985) Origin of mantle peridotite and komatiite by partial melting. *J. Geophys. Res.* 12, 541-544.
- HUMPHRIS S. E. (1984) The mobility of the rare earth elements in the crust. In *Rare*

*Earth Element Geochemistry* (ed. P. HENDERSON), pp. 317-342. Elsevier.

IRVING A. J. (1980) Petrology and geochemistry of composite ultramafic xenoliths in alkalic basalts and implications for magmatic processes within the mantle. *Am. J. Sci.* **280A**, 389-426.

IRVING A. J. and GREEN D. H. (1976) Geochemistry and petrogenesis of the Newer Basalts of Victoria and South Australia. *J. Geol. Soc. Aust.* **23**, 45-66.

JAGOUTZ E., CARLSON R. W. and LUGMAIR G. W. (1980) Equilibrated Nd-unequilibrated Sr isotopes in mantle xenoliths. *Nature* **286**, 708-710.

JAGOUTZ E., PALME H., BADDENHAUSEN H., BLUM K., CENDALES M., DREIBUS G., SPETTEL B., LORENZ V. and WANKE H. (1979) The abundances of major, minor and trace elements in the earth's mantle as derived from primitive ultramafic nodules. *Proc. Lunar Planet. Sci. Conf. 10th.* pp. 2031-2050.

JAVOY M. (1977) Stable isotopes and geothermometry. *J. Geol. Soc. London* **133**, 609-636.

KAY R. W. and GAST P. W. (1973) The rare earth content and the origin of alkali-rich basalts. *J. Geol.* **81**, 653-682.

KAY R. W. and HUBBARD N. J. (1978) Trace elements in ocean ridge basalts. *Earth Planet. Sci. Lett.* **38**, 95-116.

KEASLER K. M. and LOVELAND W. D. (1982) Rare earth element concentrations in some Pacific Northwest rivers. *Earth Planet. Sci. Lett.* **61**, 68-72.

KEMPTON P. D., MENZIES M. A. and DUNGAN M. A. (1984) Petrography, petrology and geochemistry of xenoliths and megacrysts from the Geronimo volcanic field, southeastern Arizona. In *Kimberlites II. The mantle and Crust - Mantle Relationships* (ed. J. KORNPROBST), pp. 71-84. Elsevier.

KIEFFER S. W. (1982) Thermodynamics and lattice vibrations of minerals: 5. Applications to phase equilibria, isotopic fractionation, and high pressure thermodynamic properties. *Rev. Geophys. Space Phys.* **20**, 827-849.

KUDO A. M., BROOKINS D. G. and LAUGHLIN A. W. (1978) Sr isotopic disequilibrium in lherzolites from the Puerco Necks, New Mexico. *Earth Planet. Sci. Lett.* **15**, 291-295.

KURAT G., PALME H., SPETTEL B., BADDENHAUSEN H., HOFMEISER H., PALME C. and WANKE H. (1980) Geochemistry of ultramafic xenoliths from Kapfenstein, Austria: evidence for a variety of upper mantle processes. *Geochim. Cosmochim. Acta* **44**, 45-60.

KYSER T. K. (1986) Stable isotope variations in the mantle. In: *Stable Isotopes in High Temperature Geological Processes* (eds. J. W. VALLEY, H. P. TAYLOR, JR. and J. R. O'NEIL) *Rev. Mineral.* **16**, 141-164.

KYSER T. K., O'NEIL J. R. and CARMICHAEL I. S. E. (1981) Oxygen isotope

thermometry of basic lavas and mantle nodules. *Contrib. Mineral. Petrol.* 77, 11-23.

KYSER T. K., O'NEIL J. R. and CARMICHAEL I. S. E. (1982) Genetic relations among basic lavas and ultramafic nodules: evidence from oxygen isotope compositions. *Contrib. Mineral. Petrol.* 81, 88-102.

KYSER T. K., O'NEIL J. R. and CARMICHAEL I. S. E. (1986) Reply to "Possible non-equilibrium oxygen isotope effects in mantle nodules, an alternative to the Kyser-O'Neil-Carmichael  $^{18}\text{O}/^{16}\text{O}$  geothermometer". *Contrib. Mineral. Petrol.* 93, 120-123.

MAALØE S. and AOKI K. -I. (1981) The major element composition of the upper mantle estimated from the composition of lherzolites. *Contrib. Mineral. Petrol.* 63, 161-173.

MAYEDA T. K., GOLDSMITH J. R. and CLAYTON R. N. (1986) Oxygen isotope fractionation at high temperature. *Terra Cognita* 6, 261.

MCDONOUGH W. F. and SUN S.-S. (in prep.) The Earth's primitive mantle composition.

MENZIES M. (1983) Mantle ultramafic xenoliths in alkaline magmas: evidence for mantle heterogeneity modified by magmatic activity. In *Continental Basalts and Mantle Xenoliths*, eds. C. J. HAWKESWORTH and M. J. NORRY, pp. 92-110. Shiver.

MENZIES M. and WASS S.-Y. (1983)  $\text{CO}_2$ - and LREE-rich mantle below eastern Australia: a REE and isotopic study of alkaline magmas and apatite-rich mantle xenoliths from the Southern Highlands Province, Australia. *Earth Planet. Sci. Lett.* 65, 287-302.

MERCIER J. C. and NICOLAS A. (1975) Textures and fabrics of upper mantle peridotites as illustrated by xenoliths from basalts. *J. Petrol.* 16, 454-487.

METCALFE P. (1987) Petrogenesis of alkaline lavas from Wells Gray Provincial Park and constraints on the subCordillera upper mantle. Ph.D. thesis. Univ. of Alberta. 395 pp.

MILNE, W. G., ROGERS G. C., RIDDIHOUGH R. P., MCMECHAN G. A., and HYNDMAN R. D. (1978) Seismicity of western Canada. *Can. J. Earth Sci.* 15, 1170-1193.

MONGER J. W. H., PRICE R. A. and TEMPELMAN-KLUIT D. J. (1982) Tectonic accretion and the origin of the two major metamorphic and plutonic belts in the Canadian Cordillera. *Geol.* 10, 70-75.

MONGER J. W. H. and PRICE R. A. (1979) Geodynamic evolution of the Canadian Cordillera--Progress and problems. *Can. J. Earth Sci.* 16, 770-791.

MYSEN B. O. and KUSHIRO I. (1977) Compositional variations of coexisting phases with degree of melting of peridotites in the upper mantle. *Am. Mineral.* 62, 843-865.

NESBITT H. W. (1979) Mobility and fractionation of rare earth elements during weathering of a granodiorite. *Nature.* 279, 206-210.



- NESBITT R. W., SUN S.-S. and PURVIS A. C. (1979) Komatiites: Geochemistry and petrogenesis. *Can. Mineral.* **17**, 165-186.
- NICHOLLS J., STOUT M. Z. and FEISINGER D. W. (1982) Petrologic variations in Quaternary volcanic rocks, British Columbia, and the nature of the underlying mantle. *Contrib. Mineral. Petrol.* **79**, 201-218.
- NICKEL K. G. and GREEN D. H. (1984) The nature of the uppermost mantle beneath Victoria, Australia as deduced from ultramafic xenoliths. In *Kimberlites II. The mantle and Crust - Mantle Relationships* (ed. J. KORNPROBST), pp. 161-178. Elsevier.
- PALME H. and NICKEL K. G. (1985) Ca/Al ratio and composition of the upper mantle. *Geochim. Cosmochim. Acta* **49**, 2123-2132.
- PAUL D. K. (1971) Strontium isotope studies on ultramafic inclusions from Dreiser Weiher, Eifel, Germany. *Contrib. Mineral. Petrol.* **34**, 22-28.
- PREß S., WITT G., SECK H. A., IONOV D. and KOVALÉNKO V. I. (1986) Spinel peridotite xenoliths from the Tariat Depression, Mongolia. I: Major element chemistry and mineralogy of a primitive mantle xenolith suite. *Geochim. Cosmochim. Acta* **50**, 2587-2599.
- RICHARDSON S. H., ERLANK A. J. and HART S. T. (1985) Kimberlite-borne garnet peridotite xenoliths from old enriched subcontinental lithosphere. *Earth Planet. Sci. Lett.* **75**, 116-128.
- RIDDIHOUGH R. P. and HYNDMAN R. D. (1976) Canada's active western margin: the case for subduction. *Geosci. Can.* **3**, 269-278.
- RINGWOOD A. E. (1975) Composition and petrology of the Earth's mantle. 618 pp. MacGraw-Hill.
- RINGWOOD A. E. (1979) Origin of the Earth and Moon. Springer-Verlag.
- RODEN M. F., IRVING A. J. and MURTHY V. R. (1988) Isotopic and trace element composition of the upper mantle beneath a young continental rift: results from Kilbourne Hole, New Mexico. *Geochim. Cosmochim. Acta* **52**, 461-473.
- ROEDER P. and EMSLIE R. F. (1970) Olivine-liquid equilibrium. *Contrib. Mineral. Petrol.* **29**, 275-289.
- ROSS J. V. (1983) The nature and rheology of the Cordilleran upper mantle of British Columbia: Inferences from peridotite xenoliths. *Tectonophys.* **100**, 321-357.
- ROY S., FREY F. A. and GREEN D. H. (1975) Models for alkaline basalt petrogenesis. *EOS* **56**, 463.
- RUBENSTONE J. L. and ZINDLER A. (in prep.) Isotopic variations in the sub-Pacific mantle: Inferences from Malaita peridotites.
- SCHIEBER J. (1986) Stratigraphic control of rare-earth pattern types in

mid-Proterozoic sediments of the belt supergroup, Montana, U.S.A.: Implications for basin analysis. *Chem. Geol.* **54**, 135-148.

SMITH A. D. (1986) Isotopic and geochemical studies of Terrane 1, south-central British Columbia. Ph.D. thesis, University of Alberta, Edmonton, Alberta.

SNEERINGER M., HART S. R. and SHIMIZU N. (1984) Strontium and samarium diffusion in diopside. *Geochim. Cosmochim. Acta* **48**, 1589-1608.

SOUTHER J. G. (1977) Volcanism and tectonic environments in the Canadian Cordillera--A second look. *Geol. Assoc. Can., Spec. Pap.* **16**, 3-24.

STOSCH H. G. (1982). Rare earth element partitioning between minerals from anhydrous spinel peridotite xenoliths. *Geochim. Cosmochim. Acta* **46**, 793-811.

STOSCH H. J. and LUGMAIR G. W. (1986) Trace element and Sr and Nd isotopic geochemistry of peridotite xenoliths from the Eifel (West Germany) and their bearing on the evolution of the subcontinental lithosphere. *Earth. Planet. sci. lett.* **80**, 281-298.

STOSCH H. J., LUGMAIR G. W. and KOVALENKO V.I. (1986) Spinel peridotite xenoliths from the Tariat Depression, Mongolia. II: Geochemistry and Nd and Sr isotopic composition and their implications for the evolution of the subcontinental lithosphere. *Geochim. Cosmochim. Acta* **50**, 2601-2614.

STOSCH H. J. and SECK H. A. (1980) Geochemistry and mineralogy of two spinel peridotite suites from Dreiser Weiher, West Germany. *Geochim. Cosmochim. Acta* **44**, 457-470.

STUEBER A. M. and IKRAMUDDIN M. (1974) Rb, Sr and the isotopic composition of strontium in ultramafic nodule minerals and host basalts. *Geochim. Cosmochim. Acta* **38**, 207-216.

SUN M. (1985) Sr isotopic study of ultramafic nodules from Neogene alkaline lavas of British Columbia, Canada and Josephine peridotites, southwestern Oregon, U.S.A. M.Sc. thesis. Univ. of British Columbia. 132 pp.

SUN S.-S. (1982) Chemical composition and origin of the Earth's mantle. *Geochim. Cosmochim. Acta* **46**, 179-193.

SUN S.-S. (1987) Chemical composition of Archean komatiites: implications for early history of the Earth and mantle evolution. *J. Volcanology Geotherm. Res.* **32**, 67-82.

SUN S.-S. and HANSON G. U. (1975) Origin of Ross Island basanitoids and limitations upon the heterogeneity of mantle sources for alkali basalts and nephelinites. *Contrib. Mineral. Petrol.* **52**, 77-106.

SUN S.-S. and Nesbitt R. W. (1978) Petrogenesis of Archean ultrabasic and basic volcanics: evidence from rare earth elements. *Contrib. Mineral. Petrol.* **65**, 301-325.

TAKAHASHI E. (1986) Melting of a dry peridotite KLB-1 up to 14 GPa: implications

on the origin of peridotitic upper mantle. *J. Geophys. Res.* **91**, 9367-9382.

TAKAHASHI E. and KUSHIRO I. (1983) Melting of a dry peridotite at high pressures and basalt magma genesis. *Am. Mineral.* **68**, 859-879.

WANKE H. (1981) Constitution of the terrestrial planets. *Phil. Trans. Roy. Soc. London* **A303**, 287-302.

WASS S. Y. (1980) Geochemistry and origin of xenolith-bearing and related alkali basaltic rocks from the Southern Highlands, New South Wales, Australia. *Am. J. Sci.* **280A**, 639-666.

WELLS P. R. A. (1977) Pyroxene thermometry in simple and complex systems. *Contrib. Mineral. Petrol.* **68**, 129-139.

WICKENS A. J. (1977) The upper mantle of southern British Columbia. *Can. J. Earth Sci.* **14**, 1100-1115.

WILSHIRE H. G. and SHERVAIS J. W. (1975) Al augite and Cr diopside ultramafic xenoliths in basaltic rocks from western United States. *Phys. Chem. Earth* **9**, 257-272.

ZINDLER A. and JAGOUTZ E. (1988) Mantle cryptology. *Geochim. Cosmochim. Acta* **52**, 319-333.

ZINDLER A. and HART S. R. (1986) Chemical Geodynamics. *Ann. Rev. Earth Planet. Sci.* **14**, 493-571.

## XI. Appendix I: Sample Preparation

Samples used for ICAP-AES and Rb-Sr, Sm-Nd isotopic analyses were prepared as described below. Those used for oxygen isotope analysis were prepared separately and analyzed as described in Chapter VI.

### 1. Whole rock powders

The xenoliths studied range from 10 - 20 cm in diameter. Except KR-37, all are extremely fresh. KR-37 was chosen as a weathered sample to test the weathering effect on mantle xenoliths. It is fragile, with a yellow surface on the olivine grains and white-yellowish veinlets pervading grain boundaries and fractured surfaces. Although very fresh, the rest of the samples also contain a small amount of similar white-yellowish veinlets along fractured surfaces, and in case of KR-4000, along the grain boundaries too. Care was taken to remove any visible fractured or weathered surfaces. However, it is not unlikely that some veins filling in microfractures may have escaped observation and should therefore be kept in mind in interpreting the whole rock data.

Xenoliths were first sawn from their host basalts. An oil-cooled saw was employed in separating samples KR-35, KR-37 and KR-141. For the rest of the samples (prepared later), a water-cooled saw was deliberately used instead to avoid possible contamination from the coolant oil. The xenoliths were then broken up with a hammer and those pieces away from the contacts with the host basalt were selected and carefully ground to remove weathered or fractured surfaces. Following this step, two slightly different procedures were employed for samples sawn with different coolants.

For samples that were separated with the water-cooled saw, the pieces chosen were cleaned ultrasonically in 2X distilled water for 20 minutes and dried with ultrapure acetone. Particular caution was taken in cleaning those that were processed with the oil-cooled saw, in order to prevent any possible residual oil contamination. After further crushing to about 5 mm in a steel mortar, the chosen pieces were cooked in 2X distilled water at about 80°C for 30 minutes, ultrasonically cleaned in ultrapure acetone for 20 minutes and then dried with acetone.

About 50-100 grams of the clean sample was selected and crushed in a Plattner steel mortar to pass 16 mesh sieve and split. Approximately 10-20 grams were laid

out, furthered crushed in the steel mortar to pass 40 mesh sieve and then finely ground in an agate mortar. The agate mortar was cleaned with sand, distilled water and ultrapure acetone before grinding, but with acetone only between samples.

## 2. Clinopyroxenes

After crushing with a steel mortar, the 40 - 60 mesh fraction of the xenoliths was used for separation of clinopyroxenes because this fraction contains essentially monomineralic clinopyroxenes of relatively large grain size. Clinopyroxene was preconcentrated using a Franz magnetic separator, then carefully picked under a binocular microscope two to three times to remove any other mineral grains as well as clinopyroxene grains with surface impurities or fluid/solid inclusions. It was then cleaned ultrasonically with 5 - 8 ml 2.5 N HCl in a 10 ml silica beaker for 20 minutes, rinsed with a sufficient amount of water and dried on a hot plate under a fume hood for about 5 minutes. The HCl leachate was yellow-greenish in color. Following the leaching procedure, the clinopyroxene was re-picked twice to ensure no visible impurities, then further reduced to pass a 80 mesh sieve and the very fine powders washed off by distilled water. Two more examinations under the binocular microscope ensured that the clinopyroxene was free from any visible impurities. Finally it was ultrasonically cleaned in 2.5 N HCl in the 10 ml silica beaker for another 10 minutes, then again rinsed with water and dried on the hot plate. This time the HCl leachate was colorless. Clinopyroxene at this stage was believed to be at least 99.95% pure. It was now finely ground in an agate mortar. Before the sample grinding, the agate mortar was rinsed with 7 N nitric acid followed by Nanopure water and ultrapure acetone. It was then cleaned by successively grinding sand and a small amount of clinopyroxene sample, and was finally rinsed with ultrapure acetone. Between samples, the agate mortar was rinsed with 7 N nitric acid followed by Nanopure water and ultrapure acetone.

## 3. Basalt powder

One fresh host basalt sample, containing the least amount of xenoliths and xenocrysts, was chosen and rock powders prepared.

After reducing the sample to 1 cm chips with a hammer, those with no visible xenoliths/xenocrysts were carefully selected. The chips were then cleaned

ultrasonically in 2X distilled water for 20 minutes and dried with acetone. Two fractions of this basalt sample were prepared. One (KRBAL-1) was ground in an aluminum shatter box, the other (KRBWC-1) in a tungsten carbide shatter box.

## XII. Appendix II: Procedures For Major and Trace Element Analyses With ICAP-AES

The major and trace element concentrations were determined by inductively-coupled argon plasma atomic-emission spectrometry (ICAP-AES) at the Department of Geological Sciences, University of Washington.

Nanopure H<sub>2</sub>O and reagent grade HF, HNO<sub>3</sub>, HCl, HClO<sub>4</sub> and NaOH were used for the sample decomposition and REE and Y separation.

### 1. Major element analysis

Lithium metaborate fusion technique was employed for sample decomposition. The samples and lithium metaborate (LiBO<sub>2</sub>) flux were oven-dried for at least three hours at 105°C and then cooled down in a desiccator for 20 minutes. About 0.1000 gm sample and 0.70 gm LiBO<sub>2</sub> (7:1 flux to sample ratio) were mixed and fused in a graphite crucible in a furnace at 1050°C for 20 minutes. The molten bead was dissolved in 50 ml 4% HNO<sub>3</sub> in a plastic beaker on a stirplate. The solution was then quantitatively transferred into a 100 ml volumetric flask and 5 ml of 1500 ppm La internal standard added before diluted to the mark with Nanopure water. 20 ml of this fusion solution was pipetted for Si and Mg analysis. It was further diluted to 100 ml with Nanopure H<sub>2</sub>O after addition of 5 ml of 200 ppm Y internal standard. The rest of the solution was saved for the determination of the other major elements (Ti, Al, Fe, Ca, Mn, Cr). Results were corrected against USGS standard PCC-1 for Si and Mg analysis and against a basalt sample (BHVO) of known composition for the rest of the major elements.

### 2. Trace element analysis (excluding REE and Y)

The same rock powers as those used for major element analysis (oven-dried) were employed for trace element analysis. Samples were decomposed by a hydrofluoric/perchloric acid dissolution technique. To maintain a constant dissolved solid content in the solution after HF attack, 0.50 gm of sample was weighed for ultramafic xenoliths and 0.65 gm for the host basanitoid ( Fig. 23).

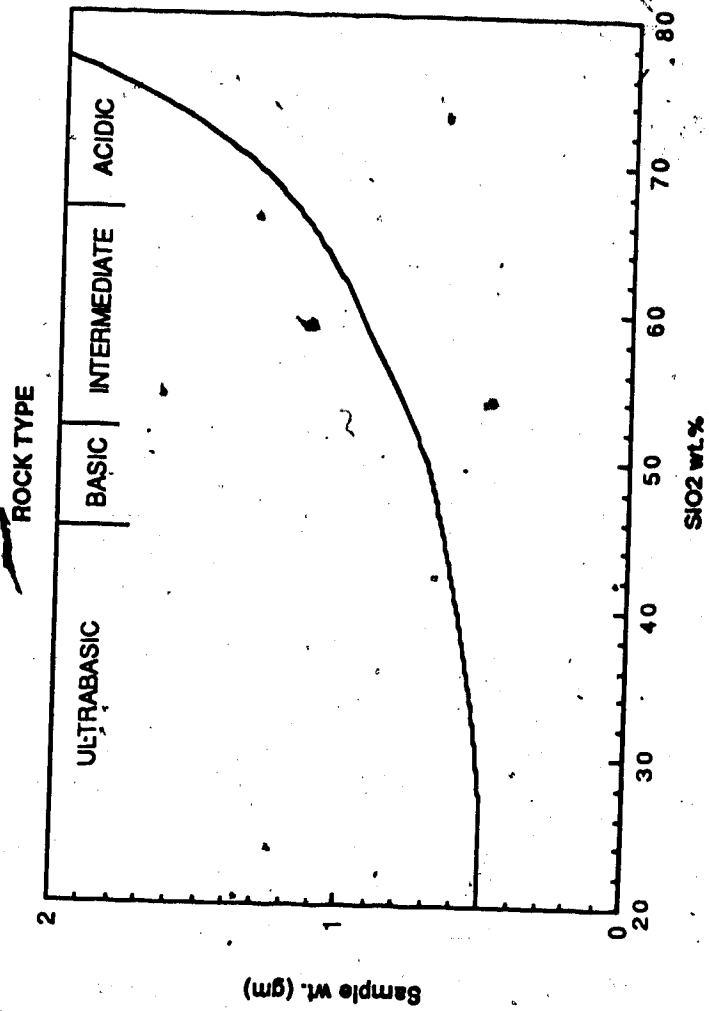


Fig. 23. Relationship between sample weight and SiO<sub>2</sub> content for trace element analysis with ICAP-AES



A mixture of 5 ml concentrated  $\text{HNO}_3$  and 10 ml HF was added to the sample in a teflon beaker, which was then allowed to stand cold overnight in the fume hood with a teflon lid on. The following day the solution was evaporated to complete dryness on a hot plate at medium setting and then treated with 5 ml concentrated  $\text{HClO}_4$  for three or more times until the free  $\text{F}^-$  was all removed. Sample was then dissolved in 30 ml 6.2 N HCl. Undigested spinel was broken down through a mini-fusion technique:

A special Buchner funnel with a filter membrane and suction filtrator was employed to filter the clear solution into a 100 ml plastic flask containing 1 ml boric acid. After transferred into a silver crucible, the membrane was washed with 5 drops of chloroform, then ashed in a small furnace at  $800^\circ\text{C}$  for 7 minutes. The residue was then fused with 2-4 pellets of NaOH in a furnace for 20 minutes and the fusion product dissolved in 50% HCl. The solution was then quantitatively transferred into the flask containing the rest of the sample.

5 ml 200 ppm Lu internal standard was added before the sample solution was diluted to 100 ml with Nanopure water. 15 ml of the solution was pipetted into a dry 125 ml polybottle for storage. 5 ml trace element spike solution and 5 ml 30 ppm Lu/acid solution was added to the remaining solution, which was then diluted to 100 ml with Nanopure water and stored in a dry polybottle. The concentrations of the trace elements were determined by analyzing the blank, the unspiked solution and the spiked solution.

### 3. REE and Y analysis

#### (1) Sample dissolution

The dissolution technique employed for the REE and Y analysis was adapted from that for trace element analysis. Effort was made to achieve a small volume for the sample solution (20 - 30 ml), before loaded onto the cation exchange column. The sample was decomposed with a mixture of 10 ml concentrated HF, 2 ml concentrated  $\text{HNO}_3$  and 3 ml concentrated  $\text{HClO}_4$  in a teflon beaker at room temperature overnight and then treated with 5 ml concentrated  $\text{HClO}_4$  two to three times. During the  $\text{HClO}_4$  treatment, care was taken to increase the temperature of the hot plate step by step so that the acid worked most efficiently. The residue was taken up in 5 ml 1 N HCl. At this stage, unattacked spinel and some other insoluble materials remained and the

solution was therefore filtered and residue fused with NaOH as in the trace element analysis. The fused residue was dissolved in appropriate amount of 1 N and 6 N HCl so that the acidity of the solution was close to 1 N. The resultant solution was subsequently filtered into the flask containing the rest of the sample solution. Filtration at this stage was considered necessary because small amount of spinel residue normally persisted, which contained very little REE and Y, but may cause clogging of the resin if loaded onto the ion exchange column. At all stages of transferring, only 1 N HCl was used for rinsing and the volume of the rinsing solution always kept minimum. The volume of the final solution was within 30 ml and was ready to be loaded onto the column. A small volume of sample solution was important in order to minimize the interferences on REE from Mg, Fe and Cr in ultramafic xenoliths.

#### (2) Cation exchange separation

The cation exchange method is very similar to that described by Crock et al. (1986). 10-30 ml of sample solution was loaded, followed by rinsing with 1 N HCl (total volume of 50 ml, including the sample solution); The resin was then eluted with 50 ml 2 N HCl, followed by 50 ml of 2 N HNO<sub>3</sub>. Subsequent elution with 50 ml of 6 N nitric acid, followed by 50 ml of 8 N nitric acid were collected in a Erlenmeyer flask for REE and Y determination. The columns were regenerated by cleaning with 100 ml of 8 N HNO<sub>3</sub>, resettled with Nanopure water and then equilibrated with 1 N HCl. The sample, after evaporated to dryness, was stored in the flask covered with parafilm until the ICAP-AES run.

The sample was dissolved in 1 ml of 10% HNO<sub>3</sub> containing Cd internal standard for the ICAP-AES run. Reduction of the solution volume from 5 ml in the routine procedure to 1 ml for analysis of ultramafic xenoliths was critical in order to achieve a reasonable signal to background ratio.

### XIII. Appendix III: Procedures for Rb-Sr and Sm-Nd Isotopic Analyses

#### 1. Sample decomposition

An aliquot of 0.05-0.20 gm of clinopyroxene separates or 0.5-1.0 gm of whole rock powders was weighed and mixed spike solutions of  $^{87}\text{Rb}$ - $^{84}\text{Sr}$  and  $^{149}\text{Sm}$  -  $^{145}\text{Nd}$  added prior to sample dissolution for isotope dilution analysis (ID). The isotope ratio measurements (IR) were carried out on a separate aliquot of the same sample.

The sample was digested overnight in a mixture of concentrated hydrofluoric and nitric acids in a screw-capped teflon vessel on the hot plate at approximately  $100^{\circ}\text{C}$ . After evaporation to dryness, it was treated with nitric acid at least three times to remove the fluorides. The residue was then taken up in 1:1  $\text{HNO}_3$  and heated on the hot plate in the capped teflon vessel for about 20 minutes to achieve a clear solution. Next, the solution was evaporated to half of its original volume. For the clinopyroxene samples, it was now ready for  $\text{Ba}(\text{NO}_3)_2$  co-precipitation. For the whole rock samples, the solution still contained unattacked spinel residue, for which two alternative procedures were employed:

For the whole rock powders of KR-35, KR-37 and KR-141, analyzed during the early stage of the project, the spinel residue was digested with 6 N HCl in a high pressure teflon bomb in an oven at about  $150^{\circ}\text{C}$  for three days, then treated with nitric acid and recombined with the rest of the sample solution.

For the rest of the samples analyzed, the small amounts of spinel were simply ignored and the residue discarded. The contents of REE and other incompatible elements in these spinel residues were considered negligible. In order to avoid possible residual REE - bearing fluorides, the nitric acid solution was boiled in a silica tube above a burner, then centrifuged and the residue discarded.

The initial separation of Sr was done by  $\text{Ba}(\text{NO}_3)_2$  co-precipitation: The concentrated nitric solution was transferred into a centrifuge tube containing 2-5 drops of saturated  $\text{Ba}(\text{NO}_3)_2$  solution and stirred with a teflon rod. Strontium was quantitatively retained in the  $\text{Ba}(\text{NO}_3)_2$  precipitate along with barium, leaving magnesium, calcium, iron and REE in the supernatant liquid. After standing for about

20 minutes, the solution was centrifuged and the supernatant liquid saved in a clean silica tube for the REE. A prolonged precipitation was avoided so as not to crystallize  $\text{Mg}(\text{NO}_3)_2$  from the solution, which would seriously interfere with  $\text{Ba}(\text{NO}_3)_2$  co-precipitation. The precipitate was then dissolved in a minimum amount of water and transferred into a smaller centrifuge tube, where  $\text{Ba}(\text{NO}_3)_2$  co-precipitation was repeated by addition of concentrated nitric acid. Following centrifuging and discarding of the supernatant liquid, the precipitate was dissolved in 0.25 ml 1.0 N HCl and ready for the first Sr column.

To separate the REE, the supernatant liquid from the first Ba co-precipitation was diluted with water and the  $\text{R}_2\text{O}_3$  elements precipitated by addition of ammonia drop by drop until the pH was close to 7. After centrifuging and discarding the supernatant, the precipitate was dissolved in 6 N HCl and the  $\text{R}_2\text{O}_3$  precipitation procedure was repeated one more time. The final precipitate was dissolved in 6 N HCl of approximately equal volume to achieve a hydrochloric solution close to 2.3 normality, which was ready for the first Sm-Nd column.

## 2. Ion-exchange separation

Two cation exchange columns were employed for the Sr separation:

Sr column 1: This was a teflon column containing 0.5 gm of Dowex 50W-X8, 100 mesh cation exchange resin cleaned with 6 N HCl, rinsed with Nanopure water and then equilibrated with 1 N HCl. After the sample in 0.25 ml 1.0 N HCl was loaded onto the column, the resin was eluted with 1.0 N HCl in three 0.25 ml portions, one 1.00 ml portion and four 2.00 ml portions successively to remove Rb. Sr was then collected in 2.5 ml 2.3 N HCl, leaving Ba in the resin. After evaporation to dryness, the sample was passed through the same column for a second time to ensure a thorough separation of Sr from Rb and Ba.

After separation through the first Sr column twice, a small but significant amount of Rb from the reagents still persisted in the Sr concentrates. This was largely removed by purification through a second capillary column.

Sr column 2: This was the same column used as the fourth Sm-Nd column, which contained fresh Dowex 50W-X8, 100 mesh cation exchange resin of 1 mm in diameter and 12.3 cm in length below a loading reservoir. After equilibrating the resin with 1.0

N HCl, the sample was loaded onto the resin in 0.05 ml 1.0 N HCl. The resin was then washed with three fractions of 0.05 ml 1.0 N HCl, followed by elution with 1 fraction of 0.20 ml 1.0 N HCl and one fraction of 0.25 ml 2.3 N HCl. Sr was subsequently collected in 0.30 ml 2.3 N HCl. The final residue after evaporation of this solution contained very little alkali and was ready for loading onto the mass spectrometer filament.

The procedures for the separation of Sm and Nd were adapted from those outlined by Dosso and Murthy (1980) and involved four cation exchange columns:

Sm-Nd column 1: This column was packed with Dowex 50W-X8, 100 mesh cation exchange resin of 6.0 mm diameter and 21.4 cm length. The resin was cleaned with 6 N HCl, resettled with water and then equilibrated with 2.3 N HCl before the sample solution was loaded. Elution with 80 ml 2.3 N HCl removed major elements, such as Fe, Mg, Ca, Sr. REE were then collected as a group in 55 ml 2.3 N HCl. This solution was then evaporated to dryness and the residue treated with one drop of nitric acid to collect in one spot. Just before being loaded onto the second Sm-Nd column, the sample was taken up in one drop of 0.2 M methylactic acid (MLA) adjusted to a pH value of  $4.43 \pm 0.01$  with ammonia.

Sm-Nd column 2: This column contained Dowex 50W-X8, 100 mesh cation exchange resin of 3 mm diameter and 34.3 cm length and was designed to purify Sm and Nd. The resin was first cleaned with 6 N HCl, resettled with water, and equilibrated to 0.2 M MLA adjusted to a pH of  $4.43 \pm 0.01$  with ammonia. Following the loading of the sample solution, the resin was eluted with 0.2 M MLA. The 10-20 ml fraction was collected for Sm and the 39-69 ml fraction for Nd.

Sm-Nd column 3: This column, 3 mm in diameter, contained a length of 8.0 cm of Dowex 50W-X8, 100 mesh cation exchange resin cleaned with 6 N HCl, resettled in water and then equilibrated to 0.1 N HCl. Before loading onto the column, the solution containing Sm or Nd (collected from the second Sm-Nd column) was mixed with an appropriate amount of 6 N HCl to adjust the pH to 0.5 - 1.0. Alternatively, the solution collected from the second Sm-Nd column could be evaporated to dryness and loaded onto the column in 1.5 N HCl, although a poorer Sm or Nd yield might result due to incomplete dissolution of the residue. The column was then rinsed with 0.1 N HCl three times, followed by elution with 8 ml 2.3 N HCl, which completely removed the MLA and ammonium salts. Sm or Nd was then collected in 20 ml 6 N HCl and the sample

solution evaporated to dryness.

Sm-Nd column 4: 1 mm in diameter with 12.3 cm of Dowex 50W-X8, 100 mesh fresh cation exchange resin equilibrated to 2.3 N HCl. This column was designed to remove alkali from the Sm or Nd concentrate. The sample was loaded onto the resin in a minimum amount of 2.3 N HCl and 0.80 ml of 2.3 N HCl was then eluted through the column in small fractions to remove soluble alkali. Subsequently Sm or Nd was collected in 1.6 ml 6 N HCl, which was evaporated to dryness and ready for loading onto the mass spectrometer filament.

### 3. Mass spectrometry

The Sr sample was loaded onto the side filament of a double rhenium filament assembly in 2.3 N or 6 N HCl as chloride, dried at low current in air and then heated very briefly at higher current. Sm or Nd was loaded onto a double rhenium filament in concentrated or 1:1 HNO<sub>3</sub>, gently heated at low current followed by a dull red glow to convert to oxide. All the <sup>143</sup>Nd / <sup>144</sup>Nd ratios (Nd-IR's) and most of the <sup>87</sup>Sr/<sup>86</sup>Sr ratios (Sr-IR's) were determined on a VG 354 mass spectrometer; While most of the spiked samples (Sr, Sm, or Nd -ID's) and some of the <sup>87</sup>Sr/<sup>86</sup>Sr ratios (Sr-IR's) were determined on a Micromass 30 mass spectrometer. All <sup>143</sup>Nd / <sup>144</sup>Nd ratios were normalized to <sup>144</sup>Nd / <sup>146</sup>Nd = 0.7219 and <sup>87</sup>Sr/<sup>86</sup>Sr ratios to <sup>86</sup>Sr/<sup>88</sup>Sr = 0.1194.

Precision and reproducibility were established from repeated analyses of the N.B.S. SRM 987 standard for <sup>87</sup>Sr/<sup>86</sup>Sr (Table 15) and the La Jolla standard for <sup>143</sup>Nd / <sup>144</sup>Nd through the entire study (Table 16). Eight analyses of the La Jolla standard on the VG 354 mass spectrometer gave a weighted mean for <sup>143</sup>Nd / <sup>144</sup>Nd of  $0.511855 \pm 2$  (2  $\sigma$ ). Six analyses of the N.B.S. SRM 987 standard on the VG 354 mass spectrometer defined a weighted mean for <sup>87</sup>Sr/<sup>86</sup>Sr of  $0.71025 \pm 3$  (2  $\sigma$ ). No corrections against these standards were attempted for the <sup>87</sup>Sr/<sup>86</sup>Sr and <sup>143</sup>Nd / <sup>144</sup>Nd measurements.

### 4. Reagents and blanks

2X distilled HNO<sub>3</sub>, 2X distilled HCl and 1X distilled HF were used for the isotope separation procedure. 3X distilled water was used before the lab was moved into a new

Table 15:  $^{87}\text{Sr}/^{86}\text{Sr}$  measurements of N.B.S.  
SRM 987 strontium standard

No.	Date	$^{87}\text{Sr}/^{86}\text{Sr}$ ( $2\sigma$ error)
1	Oct. 1, 1987	$0.71028 \pm 6$
2	Nov. 19, 1987	$0.71029 \pm 1$
3	Dec. 31, 1987	$0.71027 \pm 6$
4	Jan. 19, 1988	$0.71027 \pm 2$
5	Apr. 25, 1988	$0.71023 \pm 1$
6	May 13, 1988	$0.71024 \pm 1$

Table 16:  $^{143}\text{Nd}/^{144}\text{Nd}$  measurements of La Jolla  
neodymium standard

No.	Date	$^{143}\text{Nd}/^{144}\text{Nd}$ ( $2\sigma$ error)
1	Sept. 5, 1987	$0.511858 \pm 10$
2	Nov. 21, 1987	$0.511855 \pm 6$
3	Jan. 23, 1988	$0.511855 \pm 13$
4	Feb. 9, 1988	$0.511850 \pm 11$
5	Mar. 8, 1988	$0.511858 \pm 7$
6	Mar. 30, 1988	$0.511853 \pm 11$
7	Apr. 25, 1988	$0.511851 \pm 6$
8	May 14, 1988	$0.511857 \pm 7$

space in ESC in June, 1988, while Nanopure water was utilized after the move.

$\text{Ba}(\text{NO}_3)_2$  used for Sr separation was purified from reagent grade salt by passing through a large cation exchange column several times until the Sr blank came down to a satisfactory level (81.6 ppb Sr in  $\text{Ba}(\text{NO}_3)_2$  crystals). Reagent grade MLA was used prior to Sept. 30, 1988, but was purified afterwards through the same cation exchange column used for  $\text{Ba}(\text{NO}_3)_2$ . The MLA purification significantly reduced the total procedure blanks for Sm and Nd, which is evidenced through a comparison of Blank 8 with Blanks 1 and 4 (Table 17). A total procedure reagent blanks of 0.026 ng and 0.34 ng for Sm and Nd respectively, determined on a mixture of HF,  $\text{HNO}_3$ , HCl and MLA, was achieved after this MLA purification (Table 18). It is worth mentioning that only Blank 8 represents the true Sm and Nd blanks after the purified MLA was employed. Blanks 6, 7 were biased because of poor Sm and Nd yields caused by the omitting of the third Sm-Nd column. The poor Sm and Nd yields also resulted in failures of almost all the Sm-Nd determinations on the ultramafic xenolith samples, with which Blanks 6 and 7 were analyzed.

The average Sr blank through this study was 4.03 ng. Before September, 1988, the average blanks for Sm and Nd were 0.84 ng and 11.20 ng respectively. Subsequently, the blank was reduced to 0.09 ng for Sm and 1.26 ng for Nd. The blanks for Sr, Sm and Nd were considered insignificant and blank corrections therefore not made.

The Rb blanks were surprisingly high (10 -52 ng) throughout the study. Considering the very low Rb contents in mantle xenoliths, blank corrections on these Rb concentrations are simply too high to be reliable and the Rb data therefore ignored.



Table 17: Sm, Nd and Sr total blanks

No.	DATE	Sm (ng)	Nd (ng)	Sr (ng)
1	Jan. 14, 1987	0.71	10.48	
2	Feb. 12, 1987			6.85
3	Mar. 24, 1987			2.85
4	May 18, 1987	0.96	11.93	
5	Sept. 15, 1987	1.07 <sup>1</sup>		3.96
6	Sept. 30, 1987	0.076 <sup>1,2</sup>	9.66 <sup>1,2</sup>	1.18
7	Jan. 13, 1988	0.17 <sup>1,2</sup>	4.78 <sup>1,2</sup>	
8	April 8, 1988	0.090 <sup>1,2</sup>	1.26 <sup>1,2</sup>	5.32

<sup>1</sup> These values are biased from the actual blanks because of poor Sm and Nd yields as a result of the omitting of the third Sm-Nd column.

<sup>2</sup> Purified MLA was used for the Sm and Nd separation; otherwise, the reagent grade MLA was used.

Table 18: Reagent blanks

Date	Reagent	Sm (ng/g)	Nd (ng/g)	Rb (pg/g)	Sr (pg/g)
Summer, 1984	1X HNO <sub>3</sub>			5.9	18.2
Summer, 1984	2X HNO <sub>3</sub>				2.93
Aug., 1987	2X HCl			0.083	2.42
Aug., 1987	1X HF			0.17	1.21
June, 1987	Ba(NO <sub>3</sub> ) <sub>2</sub> crystals				81.6 X10 <sup>3</sup>
July, 1984	MLA <sup>1</sup>	0.78	2.47		
Oct., 1987	Sm-Nd procedure total reagents <sup>2</sup>	0.026 ng	0.34 ng		

<sup>1</sup> Data from A.D. Smith (1986), the rest from H. Baadsgaard (per. commun.);

<sup>2</sup> A mixture of 1X HF, 2X HCl, 2X HNO<sub>3</sub> and purified MLA in appropriate amounts to be representative of all the reagents used for Sm-Nd separation and purification.

#### XIV. Appendix IV Microprobe Analyses of Xenolith Minerals

Microprobe analyses of xenolith minerals were performed on an ARL SEMQ microprobe, using wavelength dispersive analysis (WDA), at the Department of Geology, University of Alberta. Operating conditions were 15 kV operating voltage, 10 nA probe current and 100 s counting times for the peak and 80 s for backgrounds. The raw data were processed with ZAF corrections using MAGIC IV (Colby, 1972).

The probe results are presented in Table 20. The typical reproducibility of the analyses is shown by the  $2\sigma$  errors of the repeated analyses of sample KR-3017 (Table 20). For some unknown reasons, the total percentages for some of these analyses are too high or low (Table 20). Repeated runs of the standard diopside (Table 19) indicate that the erratic totals are mainly due to the analyses of  $\text{SiO}_2$ , which were dedicated to a spectrometer of PET crystal. The  $\text{SiO}_2$  for the analyses with too high or low totals were therefore corrected, for the purpose of mass balance calculations, so that the totals are within 99 - 110 %. Data corrected this way are considered acceptable for mass balance calculations. However, the uncertainties are too large for detection of chemical variations within mineral grains.

Table 19. Repeated probe analyses of standard diopside (Wakefield, Quebec)

	1	2	3	4	5	6	7	8	9
$\text{TiO}_2$	0.08	0.06	0.00	0.11	0.12	0.09	0.10	0.05	0.02
$\text{SiO}_2$	55.36	55.25	55.06	55.02	54.37	53.57	54.57	53.06	51.49
$\text{MgO}$	18.63	18.56	18.73	18.68	18.94	18.92	18.74	19.00	18.91
$\text{CaO}$	25.73	25.80	25.75	25.84	25.76	25.59	25.59	25.46	25.60
Total		99.68	99.54	99.66	99.19	98.17	99.00	97.57	96.02

1. Standard values;

2-9. Analyses during this study.

Table 20. Microprobe analyses for xenolith minerals

Cpx	SiO <sub>2</sub>	TiO <sub>2</sub>	Al <sub>2</sub> O <sub>3</sub>	Cr <sub>2</sub> O <sub>3</sub>	MgO	FeO	MnO	NO	CaO	Na <sub>2</sub> O	Total
KR-3017	52.94	0.28	5.34	1.59	15.45	2.41	0.06	0.04	19.93	2.02	100.06
	51.82	0.31	5.33	1.64	15.08	2.47	0.07	0.04	20.14	1.97	98.88
	52.12	0.70	5.40	1.68	15.22	2.53	0.05	0.06	19.96	2.46	100.18
	53.08	0.22	5.25	1.62	15.19	2.56	0.08	0.13	19.76	2.11	100.00
	52.71	0.23	5.20	1.48	15.41	2.71	0.02	0.04	19.39	2.24	99.42
	53.97	0.21	4.97	1.37	15.74	2.59	0.08	0.03	19.48	2.07	100.52
	52.77	0.20	5.16	1.48	15.38	2.60	0.05	0.03	19.80	2.15	99.63
	53.64	0.10	5.12	1.22	15.57	2.68	0.07	0.08	18.98	2.05	99.50
Av.	52.88	0.28	5.22	1.51	15.38	2.57	0.06	0.06	19.68	2.13	99.77
2σ	0.67	0.17	0.13	0.15	0.20	0.09	0.02	0.03	0.35	0.14	
KR-37	51.51	0.15	5.02	1.13	15.91	2.56	0.08	0.04	21.68	1.14	99.22
	54.12	0.13	4.37	0.88	16.50	2.36	0.06	0.04	21.92	1.03	101.42
	52.08	0.13	4.65	1.16	16.16	2.24	0.06	0.03	21.97	1.18	99.66
Av.	52.57	0.14	4.68	1.06	16.19	2.38	0.06	0.04	21.86	1.11	100.09
KR-35	53.03	0.59	6.73	0.73	15.86	3.20	0.09	0.00	19.44	1.64	101.30
	52.20	0.55	6.90	0.79	15.58	3.12	0.12	0.04	19.63	1.72	100.65
	52.89	0.58	7.09	0.81	15.00	3.01	0.04	0.05	19.91	1.79	101.28
Av.	52.71	0.57	6.91	0.78	15.52	3.11	0.08	0.03	19.66	1.72	101.09
KR-141	51.99	0.49	6.41	0.85	15.08	2.58	0.06	0.08	20.74	1.76	100.05
	52.22	0.49	6.48	0.87	15.10	2.66	0.10	0.08	20.72	1.79	100.52
	50.95	0.49	6.63	0.87	15.13	2.64	0.07	0.04	20.65	1.73	99.20
Av.	51.72	0.49	6.51	0.86	15.10	2.63	0.08	0.07	20.70	1.76	99.92
KR-4005	56.01	0.58	7.32	0.66	15.20	2.81	0.12	0.05	21.05	1.74	105.52
	55.25	0.58	7.16	0.66	14.90	2.86	0.05	0.02	21.36	1.70	104.54
	53.37	0.57	6.95	0.65	15.01	2.73	0.10	0.07	21.95	1.71	103.10
Av.	54.88	0.57	7.14	0.66	15.04	2.80	0.09	0.05	21.45	1.72	104.39
KR-4016	51.72	0.56	6.44	0.66	15.43	2.65	0.10	0.02	21.02	1.50	100.10
	51.89	0.58	6.68	0.71	15.51	2.63	0.08	0.01	21.22	1.50	100.79
	50.64	0.55	6.39	0.72	15.38	2.54	0.06	0.03	21.28	1.50	99.09
	51.39	0.49	6.63	0.64	16.64	2.90	0.08	0.03	20.76	1.47	101.04
	52.37	0.54	6.89	0.72	15.13	2.70	0.08	0.05	20.67	1.53	100.68
Av.	51.60	0.54	6.45	0.69	15.62	2.68	0.08	0.03	20.99	1.50	100.18
KR-3020	53.86	0.29	6.69	0.75	15.30	2.93	0.07	0.08	20.44	1.64	101.85
	54.53	0.26	6.00	0.71	15.58	2.76	0.05	0.04	20.75	1.55	102.24
	52.50	0.29	6.67	0.69	15.62	2.71	0.09	0.01	20.71	1.60	100.89
Av.	53.56	0.28	6.45	0.72	15.50	2.80	0.07	0.04	20.63	1.60	101.65
KR-3020B	50.97	0.32	7.69	0.59	15.33	2.73	0.06	0.04	20.55	1.72	100.01
	51.74	0.25	6.34	0.63	15.91	2.60	0.06	0.06	20.51	1.64	99.75
	51.73	0.26	6.86	0.58	15.69	2.38	0.10	0.06	20.73	1.64	100.03
Av.	51.81	0.27	6.21	0.58	15.28	2.58	0.05	0.06	21.04	1.48	99.36

Opx	SiO <sub>2</sub>	TiO <sub>2</sub>	Al <sub>2</sub> O <sub>3</sub>	Cr <sub>2</sub> O <sub>3</sub>	MgO	FeO	MnO	NO	CaO	Na <sub>2</sub> O	Total
KR-3017	56.84	0.05	2.88	0.47	34.24	6.02	0.14	0.10	0.61	0.15	101.49
	55.58	0.04	2.95	0.49	33.64	6.24	0.10	0.08	0.62	0.14	99.88
	57.13	0.02	2.85	0.44	34.15	5.98	0.13	0.12	0.65	0.17	101.63
	55.98	0.05	2.89	0.46	33.39	6.22	0.16	0.10	0.65	0.16	100.05
	54.64	0.05	3.10	0.44	33.84	6.10	0.14	0.10	0.62	0.14	99.17
Av.	56.03	0.04	2.93	0.46	33.85	6.11	0.13	0.10	0.63	0.15	100.43
2σ	0.89	0.01	0.09	0.02	0.32	0.10	0.02	0.01	0.02	0.01	
KR-37	55.67	0.04	3.54	0.43	33.92	5.95	0.13	0.07	0.58	0.09	100.33
	54.60	0.04	3.21	0.29	33.42	5.87	0.11	0.13	0.57	0.10	98.32
	54.85	0.04	3.66	0.42	33.11	5.81	0.10	0.09	0.62	0.08	98.78
	Av.	55.04	0.04	3.47	0.38	33.45	5.88	0.11	0.09	0.59	0.09
KR-35	57.65	0.08	4.22	0.28	32.02	8.00	0.15	0.06	0.59	0.16	103.21
	56.64	0.09	4.06	0.28	32.10	7.91	0.14	0.12	0.66	0.13	102.13
	51.48	0.25	4.40	0.31	31.44	8.11	0.14	0.15	0.90	0.14	97.31
	49.62	0.12	4.46	0.34	52.42	7.60	0.12	0.11	0.63	0.11	95.53
	Av.	53.85	0.13	4.28	0.30	32.00	7.90	0.14	0.11	0.70	0.13
KR-141	54.42	0.10	4.20	0.34	33.06	6.23	0.09	0.11	0.57	0.13	99.26
	54.54	0.08	4.16	0.30	32.96	6.08	0.12	0.12	0.61	0.12	99.10
	55.12	0.08	4.11	0.31	33.24	6.32	0.14	0.09	0.57	0.14	100.12
	54.71	0.09	4.03	0.30	33.30	6.25	0.14	0.10	0.56	0.11	99.59
	Av.	54.70	0.09	4.12	0.31	33.14	6.22	0.12	0.10	0.58	0.12
KR-4005	58.65	0.11	4.49	0.30	33.20	6.41	0.13	0.07	0.61	0.12	104.09
	58.15	0.08	4.31	0.26	33.38	6.56	0.08	0.08	0.68	0.12	103.70
	58.09	0.08	4.37	0.29	33.32	6.42	0.15	0.08	0.63	0.14	103.60
	56.67	0.09	4.36	0.27	33.69	6.36	0.14	0.11	0.66	0.13	102.47
	Av.	54.39	0.09	4.38	0.28	33.40	6.44	0.12	0.11	0.64	0.13
KR-4016	54.00	0.11	4.43	0.26	33.62	6.24	0.14	0.12	0.74	0.14	99.80
	53.25	0.13	4.75	0.32	34.45	6.25	0.14	0.11	0.62	0.14	100.15
	56.49	0.09	4.28	0.28	33.51	6.25	0.10	0.12	0.67	0.15	101.93
	Av.	54.58	0.11	4.49	0.29	33.86	6.25	0.13	0.12	0.68	0.14
KR-3020	55.38	0.07	4.44	0.27	34.11	6.32	0.12	0.07	0.60	0.12	101.50
	56.04	0.08	4.15	0.27	33.85	6.40	0.16	0.07	0.61	0.14	101.78
	55.92	0.06	4.37	0.28	33.80	6.37	0.11	0.09	0.60	0.13	101.72
	Av.	55.78	0.07	4.32	0.27	33.92	6.36	0.13	0.08	0.60	0.13
KR-3020B	54.49	0.05	4.29	0.16	34.06	6.26	0.14	0.11	0.57	0.00	100.13
	55.44	0.04	4.28	0.22	34.11	6.19	0.10	0.07	0.67	0.14	101.28
	53.84	0.06	4.79	0.32	34.14	6.28	0.13	0.09	0.59	0.14	100.38
	53.92	0.05	4.82	0.30	34.02	6.21	0.15	0.15	0.57	0.14	100.33
	54.15	0.06	4.50	0.31	34.08	6.15	0.15	0.06	0.64	0.13	100.23
	52.99	0.06	4.58	0.22	34.23	6.07	0.16	0.10	0.57	0.15	99.12
	Av.	54.14	0.05	4.54	0.26	34.11	6.19	0.14	0.10	0.60	0.12

Cl	SiO <sub>2</sub>	TiO <sub>2</sub>	Al <sub>2</sub> O <sub>3</sub>	Cr <sub>2</sub> O <sub>3</sub>	MgO	FeO	MnO	NO	CaO	Na <sub>2</sub> O	Total
KR-3017	41.02	0.00	0.08	0.00	49.32	9.94	0.12	0.38	0.05	0.02	100.91
	41.26	0.00	0.04	0.01	49.34	9.86	0.12	0.38	0.06	0.02	101.09
	40.44	0.00	0.08	0.06	49.97	9.84	0.12	0.33	0.05	0.00	100.89
Av.	41.24	0.00	0.06	0.02	49.54	9.88	0.12	0.36	0.05	0.01	101.28
KR-37	41.06	0.00	0.07	0.02	48.95	9.20	0.12	0.39	0.04	0.05	99.89
	40.17	0.00	0.08	0.00	49.53	8.93	0.12	0.32	0.04	0.03	99.22
	41.20	0.01	0.08	0.01	49.70	9.11	0.11	0.38	0.05	0.04	100.68
Av.	40.81	0.00	0.08	0.02	49.39	9.08	0.12	0.36	0.04	0.04	99.94
KR-35	41.42	0.01	0.09	0.00	47.95	12.51	0.18	0.34	0.11	0.04	102.64
	41.82	0.00	0.09	0.00	48.32	12.58	0.13	0.34	0.12	0.05	103.46
	38.51	0.00	0.13	0.03	46.99	12.90	0.12	0.33	0.14	0.02	99.17
Av.	40.58	0.00	0.10	0.01	47.75	12.66	0.15	0.34	0.13	0.04	101.76
KR-141	40.77	0.00	0.07	0.00	49.46	10.00	0.12	0.40	0.06	0.03	100.92
	41.30	0.00	0.11	0.04	49.32	10.02	0.15	0.35	0.10	0.06	101.45
	41.30	0.00	0.10	0.02	49.34	9.72	0.08	0.39	0.09	0.03	101.08
Av.	41.12	0.00	0.09	0.02	49.37	9.91	0.12	0.38	0.08	0.04	101.13
KR-4005	44.02	0.00	0.08	0.02	49.64	10.06	0.14	0.41	0.08	0.03	104.47
	44.02	0.00	0.07	0.00	49.55	10.18	0.12	0.38	0.10	0.06	104.48
	42.84	0.00	0.08	0.00	49.72	10.10	0.13	0.38	0.12	0.02	103.40
Av.	43.63	0.00	0.08	0.00	49.64	10.11	0.13	0.39	0.10	0.04	104.11
KR-4016	38.51	0.00	0.09	0.01	51.12	9.93	0.14	0.36	0.07	0.07	100.29
	39.94	0.00	0.06	0.00	50.75	9.96	0.10	0.39	0.07	0.05	101.34
	37.24	0.00	0.09	0.01	50.23	10.43	0.13	0.36	0.09	0.06	98.65
Av.	38.38	0.00	0.08	0.01	50.70	10.11	0.12	0.37	0.08	0.06	99.91
KR-3020	42.46	0.00	0.08	0.00	50.52	10.06	0.11	0.35	0.06	0.05	103.69
	42.53	0.01	0.09	0.00	50.22	10.14	0.10	0.36	0.09	0.04	103.58
	41.44	0.01	0.08	0.02	51.14	10.08	0.09	0.32	0.05	0.05	103.27
Av.	42.14	0.01	0.08	0.00	50.63	10.09	0.10	0.34	0.07	0.05	103.51
KR-3020B	40.93	0.00	0.07	0.01	51.16	9.62	0.12	0.32	0.10	0.06	102.40
	40.46	0.00	0.07	0.00	51.42	9.52	0.11	0.34	0.08	0.06	102.06
	40.62	0.01	0.13	0.03	51.68	9.30	0.08	0.38	0.09	0.04	102.36
Av.	40.67	0.00	0.09	0.01	51.42	9.48	0.10	0.35	0.09	0.05	102.27

Sp	SiO <sub>2</sub>	TiO <sub>2</sub>	Al <sub>2</sub> O <sub>3</sub>	Cr <sub>2</sub> O <sub>3</sub>	MgO	FeO	MnO	NO	CaO	Na <sub>2</sub> O	Total
KR-3017	0.08	0.05	38.85	29.86	17.78	13.51	0.14	0.24	0.00	0.00	100.51
	0.05	0.04	40.07	28.60	17.49	13.64	0.16	0.23	0.01	0.00	100.29
	0.10	0.06	38.40	30.12	17.86	13.62	0.16	0.22	0.01	0.00	100.52
	0.14	0.08	38.00	29.55	17.48	13.20	0.22	0.18	0.01	0.02	99.85
	0.07	0.05	38.77	29.04	17.26	13.30	0.14	0.17	0.01	0.00	99.83
	0.10	0.04	39.37	29.51	18.02	13.45	0.16	0.20	0.01	0.00	100.86
	0.08	0.05	39.53	28.37	17.46	13.87	0.14	0.25	0.01	0.00	99.76
Av.	0.09	0.05	39.00	29.29	17.62	13.51	0.16	0.21	0.01	0.00	99.94
2σ	0.03	0.08	0.65	0.60	0.25	0.21	0.03	0.03			
KR-37	0.07	0.05	50.49	17.73	19.41	11.37	0.13	0.27	0.00	0.00	99.52
	0.07	0.05	50.26	17.66	19.60	11.01	0.13	0.29	0.02	0.01	99.09
	0.05	0.04	49.27	17.58	19.47	10.99	0.16	0.32	0.01	0.01	97.89
	Av.*	0.07	0.05	50.38	17.70	19.50	11.19	0.13	0.28	0.01	0.00
KR-35	0.12	0.63	55.35	10.16	20.19	14.91	0.12	0.35	0.01	0.01	101.87
	0.15	0.64	55.82	9.53	20.30	14.66	0.10	0.34	0.00	0.01	101.57
	0.15	0.63	56.28	9.05	20.47	14.75	0.07	0.38	0.00	0.00	101.79
	Av.	0.14	0.63	55.82	9.58	20.32	14.77	0.10	0.35	0.00	0.01
KR-141	0.07	0.12	56.70	10.87	21.14	10.86	0.11	0.37	0.00	0.00	100.26
	0.07	0.17	56.27	11.00	21.05	10.84	0.10	0.32	0.00	0.01	99.83
	0.08	0.13	55.98	10.65	21.26	10.59	0.11	0.33	0.00	0.04	99.17
	Av.	0.07	0.14	56.32	10.84	21.15	10.76	0.10	0.34	0.00	0.02
KR-4005	0.08	0.19	60.77	8.16	21.78	11.12	0.08	0.37	0.00	0.00	102.57
	0.09	0.32	60.36	8.48	21.93	11.22	0.10	0.34	0.01	0.05	102.90
	0.11	0.39	59.77	8.32	21.90	11.26	0.09	0.38	0.01	0.00	102.23
	Av.	0.09	0.30	60.30	8.32	21.87	11.20	0.09	0.36	0.01	0.02
KR-4016	0.12	0.17	58.91	9.17	21.97	10.28	0.12	0.34	0.02	0.02	101.12
	0.09	0.13	59.27	9.32	22.03	9.91	0.09	0.35	0.01	0.02	101.23
	Av.	0.10	0.15	59.09	9.25	22.00	10.10	0.10	0.34	0.01	0.02
KR-3020	0.08	0.07	58.99	8.97	22.16	10.84	0.12	0.38	0.01	0.02	101.04
	0.10	0.05	58.47	8.80	22.18	10.66	0.10	0.36	0.01	0.03	100.74
	0.06	0.04	58.05	8.70	22.30	10.63	0.10	0.37	0.01	0.02	100.27
	Av.	0.08	0.05	58.50	8.82	22.21	10.51	0.11	0.37	0.01	0.02
KR-3020B	0.07	0.06	59.72	7.03	22.34	10.53	0.08	0.37	0.00	0.04	100.24
	0.09	0.19	60.12	6.81	22.38	10.73	0.08	0.39	0.01	0.04	100.84
	0.06	0.05	60.47	7.66	22.74	9.68	0.09	0.41	0.00	0.03	101.18
	0.13	0.04	58.38	8.91	23.08	10.21	0.22	0.33	0.00	0.03	101.34
	Av.	0.09	0.08	59.67	7.60	22.64	10.29	0.12	0.38	0.00	0.04

Av. = Average

\* Average of the first two analyses.